

Computational studies of surfactant self-assembly on nanostructured surfaces

by

Chetana Singh

A dissertation submitted in partial fulfillment
of the requirements for the degree of
Doctor of Philosophy
(Chemical Engineering and Scientific Computing)
in The University of Michigan
2010

Doctoral Committee:

Professor Sharon C. Glotzer, Chair

Professor Ronald G. Larson

Professor Robert M. Ziff

Professor Nicholas Kotov

Assistant Professor Anton Van der Ven

Associate Professor Francesco Stellacci, Massachusetts Institute of Technology

© Chetana Singh

All Rights Reserved

2010

For my parents, my sister and my husband

Acknowledgments

I thank my advisor Prof. Sharon Glotzer for providing me with the opportunities and resources to learn and to grow as a researcher. Your support, patience and guidance have been instrumental in my development as a graduate student. From the umpteen opportunities and platforms to showcase my research, financial support and mentorship to teaching me the skill of academic writing and the importance of having an outlook, I am grateful to you.

I thank my committee member, collaborator and co-author, Prof. Francesco Stellacci for invaluable discussions about experimental systems, novel phenomena and insightful suggestions that often helped me improve and revise my simulations. Your constant support has helped me learn a lot more beyond my immediate field of study.

I thank my committee members Prof. Ronald G. Larson, Prof. Robert M. Ziff, Prof. Nicholas A. Kotov and Prof. Anton Van der Ven for their time, useful suggestions and encouraging discussions. Prof. Larson and Prof. Ziff, I am grateful to you for providing crucial insights into the systems I'm simulating and for always being there to meet with me for discussions. Prof. Kotov and Prof. van der Ven, thank you for being excellent and attentive teachers and for always encouraging me.

I thank Dr. Mark Horsch, who was always there to boost my confidence as a new student. You have a wonderful intuition about the systems we study - thank for sharing that and for being an excellent mentor. Dr. Hao Jiang and Dr. Aaron Santos, your guidance and discussions have taught me more than many books. I am lucky to have worked with you on such great projects. I thank my colleagues in Prof. Stellacci's group SunMaG: Dr. Alicia Jackson, Jeffrey Kuna, Kislou Voitchovsky, Kosuke Kuwabara and Dr. Ying Hu, who I've had the good fortune to work and collaborate with.

I am thankful to Susan Hamlin, Mike Africa, Connie Bacus, Shelley Fellers, Claire O'Connor and Pam Derry for very efficient and prompt help and advice. I thank the team at Center for Advanced Computing for working tirelessly to make life easy for us. I thank the UofM for providing an endless selection of resources - between the poster printing at the Duderstadt to UM Virusbusters, I've used quite a few of them!

Raghu and Abhishek thank you for the extended coffee breaks, just one of the many

ways in which you've made these years memorable for me. Stephanie, thank you for always giving me sound advice, for your enthusiasm for Indian cooking and for introducing me to American candy! Thank you Mark, Steph, Aaron Santos, Kevin, Carolyn, Eric, Ryan, Aaron Keys and Michael, for editing and revising my written word on various occasions. I thank the newer members of the group - Trung, Amir, Eric, Carolyn (well, newer than me), Nguyen, Antonio, Ines, Daniel, Jaime, Bryan, Ryan and Pablo - your enthusiasm is contagious! Joshua, thank you for introducing me to the power of GPUs; I hope to use the HOOMD-DPD soon. Kevin, thank you for the food - your commitment is exemplary!

My dear family: my parents, Mrs. Manju and Prof. Bani Singh, my sister Priya and my husband Chun Lee, I am indebted to you for your love and constant support and foremost for your unwavering faith in me. I am blessed to have such a wonderful and caring family. Your expectations and dreams motivate me everyday and because of you this achievement is meaningful.

Table of Contents

Dedication	ii
Acknowledgments	iii
List of Figures	viii
List of Appendices	xvi
Abstract	xvii
Chapter 1 Introduction	1
1.1 Motivation	1
1.2 Objectives	3
1.3 Thesis organization	3
Chapter 2 Background	5
2.1 Surfactants and their self-assembly	5
2.2 Homoligand SAMs	6
2.2.1 Experimental studies of homoligand SAMs	6
2.2.2 Simulation studies of homoligand SAMs	7
2.3 Mixed SAMs	7
2.3.1 Experimental studies of mixed SAMs	9
2.3.2 Simulation studies of mixed SAMs	12
Chapter 3 Simulation model and method	13
3.1 Dissipative particle dynamics method	13
3.1.1 Soft and repulsive pair potential	14
3.1.2 Built-in Langevin Thermostat	15
3.1.3 Integration method	17
3.2 Simulation model	17
3.2.1 Surfactants	18
3.2.2 Substrate	19
3.2.3 Bulkiness	20
3.3 Validation	21

3.3.1	Phase separation in simple incompatible mixtures on cylindrical surfaces	21
3.3.2	Phase separation in block copolymers on spherical surfaces	22
3.4	Caveats	24
3.4.1	Temperature control	24
3.4.2	Three-dimensional density	25
3.4.3	Parameter limitations	26
3.5	DPD in soft matter simulations	26
Chapter 4	Striped spherical nanoparticles	28
4.1	Introduction	28
4.2	Energy and entropy in mixed SAMs	29
4.3	Simulations of SAMs on nanospheres	31
4.3.1	Effect of increasing chain length difference	31
4.4	Effect of increasing bulkiness difference	32
4.5	Effect of increasing surface coverage	33
4.6	Effect of substrate curvature	34
4.7	Comparison with atomistic simulations and experiments	36
4.8	Geometric scaling relation for stripe width	38
4.9	Summary	40
Chapter 5	Striped versus patchy pattern formation in phase-separating mixed SAMs on flat surfaces	42
5.1	Introduction	43
5.2	Contradicting experimental observations	43
5.3	Simulations of symmetric mixtures	44
5.3.1	Effect of length difference, surface coverage and degree of immiscibility	45
5.3.2	Effect of different starting configurations	46
5.4	Simulations of asymmetric mixtures	49
5.4.1	Varying relative composition and degree of immiscibility	49
5.4.2	Two-dimensional micelles as the equilibrium phase	50
5.4.3	Micelle ordering	51
5.4.4	Varying relative composition and length difference	53
5.4.5	Comparison of DPD results with experiments	53
5.4.6	Comparison with other phase-separating mixtures confined to flat surfaces	55
5.5	Summary	57
Chapter 6	Surfactant-coated nanowires and nanorods	59
6.1	Dependence on cylinder dimensions	59
6.1.1	Effect of cylinder radius	59
6.1.2	Effect of cylinder length	60
6.1.3	Effect of aspect ratio	61
6.2	Dependence on the properties of the surfactant mixture	63

6.2.1	Effect of increasing immiscibility	63
6.2.2	Effect of increasing length difference	63
6.2.3	Effect of increasing surface coverage	64
6.2.4	Helices	65
6.3	Exploiting substrate stress to modify nanoscale surface patterns	66
6.3.1	Introduction	66
6.3.2	Curvature induction in simulations	66
6.3.3	Curvature induction in experiments	68
6.3.4	Discussion	69
6.4	Unique alignment of stripes in experiments	70
6.5	Comparison with other phase-separating mixtures confined to cylindrical surfaces	70
6.6	Summary	72
Chapter 7 Interfacial properties of striped nanoparticles		73
7.1	Introduction	73
7.2	Experiments	75
7.3	Simulations	76
7.4	Two competing, molecular-level phenomena lead to non-monotonicity in the work of adhesion, W_{SL}	77
7.4.1	Cavitation	79
7.4.2	Confinement	79
7.5	Summary	82
Chapter 8 Conclusions and outlook		83
8.1	Contributions	83
8.2	Related projects	86
8.2.1	Ising-type model simulations as an alternative to DPD simulations	86
8.2.2	Quantifying cavitation (bridging) across hydrophobic domains	87
8.2.3	Ternary mixtures	88
8.2.4	Characterization of interface instability	90
8.3	Directions for future research	91
Appendices		94
Bibliography		112

List of Figures

Figure

1.1	Schematic representation of striped phase separation of octanethiol (yellow) and mercaptopropionic acid (red) surfactants on the surface of a gold nanoparticle (11).	2
1.2	A CdTe nanowire covered by SiO ₂ spikes giving it the appearance of a nanocentipede (14).	3
2.1	A drawing of a typical homoligand SAM describing surfactants adsorbed on a metal substrate (2).	6
2.2	Some of the mechanisms that have been proposed for phase separation in SAMs. The open and closed circles indicate the two different components adsorbing or adsorbed onto the surface (17).	8
2.3	Three possible scenarios that can arise in mixed SAMs with respect to phase separation of its components (8).	9
3.1	Left: A plot of the conservative force as a function of distance r_{ij} between particles i and j . Right: Definition of r_{ij}	16
3.2	A. A two-dimensional cartoon of the simulation set-up. The orange circle in the center represents a gold nanoparticle. Red and yellow circles make up the short and the long surfactant chains respectively. The entire set-up is simulated in a cubic or non-cubic box. B. A single surfactant chain on a spherical nanoparticle.	18
3.3	Two separate models implemented and tested to make one of the surfactants (yellow) bulkier than the other (red). A. The size of the tail end bead is increased to make it bulky. B. Additional beads are attached to the tail end bead to make it bulky.	21
3.4	Interface direction switches from A. horizontal to B. vertical, when length of a radius = 3σ ($2\pi R = 18.8$) is changed from 22.0 to 15.0, where R is the radius of the cylinder	22
3.5	Phase separation of block copolymers in which two immiscible segments are bonded together. Different images show evolution of the pattern in time leading to the formation of a striped phase in the end (78).	23

3.6	A. A two-dimensional cartoon of the set-up for simulating phase separation in block copolymers constrained to spherical surfaces. Red and yellow circles make up the immiscible segments of the block copolymer chains that are tied to each other. The simulation is carried out in a cubic box. B. A single block copolymer chain on a spherical surface. Each of the beads in the chain is tied to its neighbors by simple harmonic springs.	23
3.7	Two different views of the same simulated system showing striped patterns formed by phase separation in block copolymers constrained on a sphere. . .	24
3.8	The temperature profile of a DPD simulation showing a situation in which excellent temperature control was obtained by fine-tuning several parameters. The figure also shows the zoomed-in region of the temperature profile at the beginning of the simulation.	25
4.1	A. Completely separated configuration for a system of strongly immiscible surfactants with six beads each. B. and C. Free volume (shaded grey areas), available to long (yellow, six-bead) surfactant chains when arranged with short (red, four-bead) chains in B. completely separated and C. microphase separated striped states. The bead in the chain that is constrained to the surface is the head group and the rest of the chain is the tail of the surfactant. (142)	29
4.2	Free volume (grey region) available to a long (yellow) surfactant chain surrounded by A. two chains of the same length as itself. B. Two shorter (red) chains. The shaded area is larger when the neighbors are shorter. . . .	30
4.3	Free volume (grey region) available to a surfactant chain on surfaces of different curvatures. A. small nanoparticle, B. large nanoparticle, C. flat surface. (143)	31
4.4	Effect of length difference on phase separated patterns formed in mixtures of incompatible long (yellow) and short (red) surfactant chains on the surface of a sphere. The radius of the sphere is 5σ where diameter of one bead is σ . The red and yellow chains on top of each simulation snapshot indicate the number of beads in the surfactants used for that simulation. The systems simulated from left to right are denoted by m_n where m and n are the number of beads in the short and long surfactants respectively. A. 4_4, B. 4_6, C. 4_7, D. 4_8, E. 4_13. Some of the images have been taken from reference (101).	32
4.5	Effect of bulkiness difference on phase separated patterns formed in mixtures of incompatible surfactant chains on the surface of a sphere. The radius of the sphere is 5σ where diameter of one bead is σ . The red and yellow chains on top of each simulation snapshot indicate the number of beads in the surfactants used for that simulation. Some of the images have been taken from reference (101).	33
4.6	Effect of surface coverage on phase separated patterns formed in mixtures of incompatible long (yellow) and short (red) surfactant chains on the surface of a sphere. The radius of the sphere is 5σ where diameter of one bead is σ . Surface densities in number of beads per σ^2 are A. 4.0, B. 5.0, C. 6.0. . . .	34

4.7	Effect of nanoparticle size on phase separated patterns formed in mixtures of incompatible long (yellow) and short (red) surfactant chains on a surface. The short and long surfactants are four and seven beads in length respectively. The radii of curvature for the surfaces shown are A. 3σ , B. 5σ , C. 8σ , D. 10σ and E. infinite. σ is the diameter of a single bead. The snapshots are not shown to scale. Some of the images have been taken from reference (101).	35
4.8	Functionalization and polymerization of striped nanoparticles into chains (33).	36
4.9	Transmission electron microscopy (TEM) images of gold nanoparticles linked through mercaptoundecanoic acid linkers into chains (28).	36
4.10	Size distributions before and after chaining for three different sets of nanoparticles. Chains form only for nanoparticles in a certain size range. Bars represent actual data; lines are Gaussian fits. Simulation images at the bottom show the patterns expected in the different size regimes. (33)	37
4.11	(a) and (b) C4:C6 SAMs from atomistic simulations and experiment, respectively. The tail-end groups are identical, but the lengths differ. (c) and (d) Dodecanethiol/ Mercaptoundecanoic acid (C11:C12) SAMs from atomistic simulations and experiment, respectively. Here the tail-end groups differ somewhat in size and the tail lengths are nearly identical. (e) Atomistic simulation of mixture of equal-length (C3:C3) surfactants, with different tail-end groups. For atomistic snapshots, blue (dark) and yellow (light) beads are head groups of surfactants that are short (or contain -COOH) and long (or contain -CH ₃), respectively. In all cases, the head groups (-SH) are identical. (f) Variation of stripe width with the length of long surfactant in number of carbon atoms. The same trend is seen when stripe width is plotted against short surfactant length. The atomistic simulation data points are for equal-length surfactants. (101)	39
4.12	Images from atomistic simulations (left) and experiments (right) showing phase separated stripe-like patterns in SAMs on flat surfaces (101).	39
5.1	Experimental, STM images of striped and patchy phase separated patterns imaged in mixed SAMs on flat surfaces taken from references (19-21).	44
5.2	A. to C. Simulation snapshots of phase separation in symmetric ($\phi = 0.5$) mixtures at surface density of $\rho = 4.0$ of immiscible ($\Delta a = 15$) surfactants of various lengths of short and long surfactants, respectively. A. 4 and 4 (equal-length mixture), B. 4 and 9, C. 4 and 14. Snapshots from left to right show progression of phase separation in time. The number in the top right corner indicates the time step at which the snapshot was taken, where K refers to thousands and M refers to millions of time steps, D. Simulation snapshots of equilibrium patterns formed for unequal length surfactants (4, 13 beads long) with ρ of 3, 3.5 and 4, respectively, from left to right. E. Simulation snapshots of patterns formed for unequal length surfactants (4, 13 beads long) with Δa of 5, 10 and 20, respectively, from left to right. Red (dark) and yellow (light) beads represent short and long surfactant head groups, respectively. Surfactant tails have been removed for clarity. (121)	46

5.3	Simulation images of phase separation in symmetric mixtures ($\phi = 0.5$) of 4-bead (red) and 7-bead (yellow) surfactants starting from different initial patterns. A. and B.: Evolution starting from completely separated and uniformly mixed configurations, respectively. The number in the top right corner is the time step at which the snapshot was taken, where K refers to thousands and M to millions of time steps. C. to J.: Initial (left) and final (right) patterns. K. Phase separation in the system shown in B, continued after locally perturbing the system after 30 million time steps. The blue square indicates the perturbed configuration. Snapshots to the right of the blue square show evolution of the perturbed state. (121)	48
5.4	U (blue) and L (red) for different final patterns shown in Figs. 5.3A to J. (121)	49
5.5	Simulation snapshots of microphase separation in asymmetric mixtures of 4 bead (red) and 13 bead (yellow) surfactants for increasing fraction of long surfactants $\phi = 0.17, 0.20, 0.25, 0.33, 0.50, 0.67, 0.75, 0.80, 0.83$ (from left to right). A. $\Delta a = 5$; B. $\Delta a = 10$; C. $\Delta a = 15$; D. $\Delta a = 20$. (121)	50
5.6	L for patterns from Fig. 5.3D and an arbitrary striped pattern at $\phi = 0.83$ (enclosed in blue square). (121)	51
5.7	The figure shows, in tabular form, plots of the radial distribution functions (RDF), $g(r)$ of centers of mass of micelles shown in Fig. 5.5D and patches shown in Fig. 5.3B. The nearest neighbor micelle/patch coordination numbers were calculated by integrating over the first peak in $g(r)$ plots. The table also lists the average domain (patch/patch) size and the standard deviation in the domain size. The large standard deviation of the patch size distribution relative to standard deviations of the micelles indicates that the patches are non-equilibrium while micelles are equilibrium patterns. Note that the terms patch and micelle have been selected to mean kinetically-arrested, non-equilibrium islands versus equilibrium islands, respectively. Since the number of patches/system is small, we were only able to study order up to second nearest neighbors. Simulating larger systems is computationally expensive and was not undertaken. (121)	52
5.8	A. to H.: Equilibrium patterns formed by asymmetric and symmetric mixtures of surfactants with increasing length differences. A. to C.: $\Delta l < 3$. Complete phase separation is seen for all values of ϕ ; D. to H.: $\Delta l \geq 3$. All asymmetric mixtures with $\phi < 0.5$ form patches. Stripes are formed by all symmetric and asymmetric mixtures when $0.5 \leq \phi \leq 0.67$. For highly asymmetric mixtures with a majority of long surfactants ($\phi > 0.67$), stripes are formed for a very small range of $2 < \Delta l < 5$ while patches are formed for all larger values of Δl . As shown in Fig. 5.6, ordered, 2D micelles are entropically preferred over stripes for highly asymmetric mixtures with a majority of long surfactants. When Δl is large (> 4 beads), the gain in conformational entropy for long surfactants by forming patches is large. However when Δl is just sufficient for microphase separation ($2 < \Delta l < 5$), the conformational entropy gain for the long surfactants by forming micelles is small and stripes are energetically and entropically favored. (121)	54

5.9	STM images showing nanoscale domains in SAMs on flat surfaces. Surfactant combinations and approximate relative compositions obtained by image analysis are: A. and B. Hexanethiol and dodecanethiol, $\phi = 0.50$, B is the contrast image of the original STM image shown in A, C. Octanethiol and mercaptopropionic acid, $\phi = 0.26$, average domain size = 3.4 ± 0.4 nm, D. Butanethiol and nonanethiol, $\phi = 0.15$, average domain size = 6.1 ± 1.4 nm, E. Butanethiol and pentanethiol, $\phi = 0.22$, average domain size = 6.5 ± 1.5 nm, F. Octanethiol and 3-mercapto-1-propane sulfonic acid, $\phi = 0.24$, average domain size = 4.0 ± 0.9 nm. In the STM image, bright spots, dark/black spots and the background represent locations of long surfactants, etch pits and short surfactants, respectively. In the contrast image shown in B, blue, black and grey regions represent locations of the long surfactants, short surfactants and etch pits, respectively. (121)	56
6.1	Effect of cylinder radius on phase-separated pattern formed in mixtures of long (7-bead, yellow) and short (4-bead, red) surfactants grafted on a cylinder surface. The radii of the cylinders are A. 2σ , B. 3σ , C. 4σ , D. 5σ , E. 7σ , F. 9σ , G. 11σ , H. 13σ . (143)	60
6.2	Effect of cylinder length on phase-separated pattern formed in mixtures of long (7-bead, yellow) and short (4-bead, red) surfactants grafted on the cylinder surface. The lengths of the cylinders are A. 10σ , B. 15σ , C. 20σ , D. 25σ , E. 30σ , F. 35σ , G. 40σ , H. 45σ , I. 50σ . Radius of the cylinder is 5σ in all cases. (143)	61
6.3	Interface direction switches from A. horizontal to B. vertical, when length of a radius = 3σ ($2\pi \cdot \text{radius} = 18.8$) is changed from 22.0 to 15.0, for simple, incompatible binary mixtures guided by incompatibility alone rather than competing interactions.	62
6.4	Entropic considerations in A. vertical versus B. horizontal stripes. Red and yellow beads represent short and long surfactants respectively. The tails of the short surfactants have been removed for clarity. In the central stripe comprised of long surfactants, blue and black arrows represent the direction(s) in which the long surfactants can bend to take advantage of the cylinder curvature and neighboring short chains, respectively. The red arrow in A. represents the direction in which the long surfactants are crowded. (143)	62
6.5	Effect of surfactant immiscibility on phase-separated pattern formed in mixtures of long (7-bead, yellow) and short (4-bead, red) surfactants grafted on a cylindrical surface. The values of the repulsion parameter, Δa (larger Δa implies higher immiscibility) are: A. 3, B. 5, C. 10, D. 15, E. 20, F. 25. (143)	64
6.6	Effect of surfactant length difference on phase-separated pattern formed in mixtures of long (7-bead, yellow) and short (4-bead, red) surfactants grafted on a cylindrical surface. The systems simulated from left to right are denoted by m_n where m and n are the number of beads in the short and long surfactants respectively. A. 4_4, B. 4_6, C. 4_7, D. 4_9, E. 4_11, F. 4_13. (143)	64

6.7	A. Patchy pattern formed on a cylinder of radius 5σ and surface coverage of 5.0 particles per σ^2 . B. Unrolled view of the result shown in A.	65
6.8	Helical pattern formed by phase separation in SAMs.	65
6.9	Transfer of an arbitrary pattern from a flat surface onto a cylinder. A. Starting pattern on flat surface. B. Intermediate curved surface. C. Final pattern on cylindrical surface. (142)	67
6.10	Simulation procedure for curving a flat, surfactant-coated substrate. Snapshots, from left to right: phase separation of long (yellow) and short (red) surfactants on a flat substrate leading to the formation of the patchy pattern which is stable over many time steps (tails removed for clarity); a patch-covered cylinder obtained by rolling the patch-covered flat substrate; the remaining four snapshots show evolution of the patchy pattern on the surface of the cylinder - the cylinder has been un-rolled for better visualization of the changing pattern - the simulation is conducted on a cylindrical surface (tails removed for clarity). t and t' indicate time for the simulations on flat and cylindrical substrates respectively. τ is the time step used in both simulations (0.01 unit each). (142)	68
6.11	Experimental images, from left to right: A. STM image of a patchy pattern on flat substrate formed by octanethiol and mercaptopropionic acid surfactants; cartoon showing application of stress; and alignment and merging of patches after stressing. Dark and light regions indicate short and long surfactants respectively. B. STM image of aligning and merging patches obtained after stressing another surfactant system: octanethiol and methyl benzenethiol. (142)	69
6.12	STM current images of phase separating octanethiol and mercaptopropionic acid SAMs on gold nanorods showing an average stripe width of 0.85 nm. The images have been obtained at different scanning speeds varying from 0.17 $\mu\text{m/s}$ to 2.2 $\mu\text{m/s}$. (143)	71
7.1	Non-monotonic behavior of work of adhesion of striped nanoparticles coated with octanethiol (OT) and mercaptohexanol (MHol) with water solvent, obtained using contact angle measurements (blue) and AFM (red). (12) . . .	74
7.2	Linear and monotonic behavior of work of adhesion W_{SL} of flat surfaces coated with > 5 nm stripes of octanethiol (OT) and mercaptohexanol (MHol) with water solvent. The measured values of W_{SL} were obtained using contact angle measurements (blue) and AFM (red). (12)	75
7.3	Procedure for substrate preparation. For domains $> 5\text{nm}$, flat gold surfaces are immersed in a solution of the two surfactants. For domains $< 2\text{nm}$, striped gold nanoparticles are first prepared and then deposited layer-by-layer to form an extended flat surface. OT and MHol are shown in yellow and red, respectively. (12)	76

7.4	Surface patterns (head group positions) simulated with MD. The surfactant tails and surrounding water molecules have been removed. Grey and yellow beads are the headgroups of the hydrophobic (OT) and the hydrophilic (MHol) surfactants, respectively. A. to C. Janus particles with 33%, 50% and 67% MHol, respectively. D. to F. Striped nanoparticles with 33%, 50% and 67% MHol, respectively. Stripe widths of MHol (OT) for the striped nanoparticles are same as the experimental stripe widths: D. 0.6 (1.2) nm, E. 0.7 (0.7) nm, F. 1.2 (0.6) nm. (12)	78
7.5	Water number density near the striped nanoparticle surface as a function of the radial coordinate along the direction perpendicular to the stripes. Peaks and troughs represent the regions over OT and MHol, respectively. The white regions represent the depletion layer over OT domains, including the tail-end groups of the OT molecules. (12)	78
7.6	Striped nanoparticle coated with narrow hydrophobic (grey) and hydrophilic (yellow) stripes. Three bridge-like structures have been highlighted showing the participating hydrophilic chains that act as anchors and the water molecules that form the hydrogen-bonded network to complete the bridge. Rest of the water molecules have been removed for clarity. (12)	80
7.7	A water molecule shown confined in three directions in a molecular pocket formed over a hydrophilic domain (yellow) bordered by hydrophobic domains (grey). (12)	81
7.8	Local number densities n_{MHol}^W and n_{OT}^W of water molecules immediately above the hydrophilic (Left) and hydrophobic (Right) domains, respectively. The open and closed symbols indicate striped and Janus particles, respectively. (12)	81
8.1	A. A snapshot showing one of the several possible conformations for surfactants i and j when the head groups of the surfactants are separated by a distance r_{ij} . B. Plot of the avoidance probability $p(i \otimes j)$. Red circles denote measured probabilities while the solid black line shows the fitted function given by Equation 8.1, where $m = 0.56442$ and $\phi = 0.97332$. (120)	86
8.2	System configurations obtained as a function of tether length difference dL and strength of attraction ϵ . As observed in DPD and atomistic simulations, stripes are observed for sufficiently large dL provided ϵ is not too large. (120)	88
8.3	Output of the bridge identification code showing several hydrogen-bonded water bridges anchored at the hydrophilic (violet, green, blue and yellow) stripes and over the hydrophobic domains (removed for clarity). All other water molecules and surfactant chains have been removed for clarity. Different hydrophilic stripes are shown in different colors. Hydrogen bonds are shown by dashed lines.	89
8.4	Preliminary results for patterns formed in ternary SAMs. Both striped and patchy patterns are seen. Dark blue, red and light blue beads indicate head groups of longest, intermediate length and shortest surfactants, respectively. The patterns are preliminary and possibly not equilibrated.	89

8.5	A. Snapshots of time evolution of highly immiscible ($\Delta a = 30$) surfactants showing complete separation. B. Snapshots of time evolution of slightly immiscible ($\Delta a = 5$) surfactants showing formation of jagged stripe-like and patchy domains. Yellow and red beads represent long (7 beads) and short (4 beads) surfactants respectively. The number in the top right corner is the time step at which the snapshot was taken, where K refers to thousands of time steps. (121)	90
8.6	Plots of stripe widths as a function of the degree of immiscibility between the two surfactants for A. 4-bead and 9-bead surfactants and B. 4-bead and 12-bead surfactants. The short and long surfactants are shown in red and yellow respectively. The stripe widths for $\epsilon = 0.3$ for the two systems are 4.83 and 4.95 respectively. The plots have been obtained using the Ising-type model described in Section 8.2.1. Such a small difference in stripe width is difficult to capture using DPD.	92
8.7	Phase separated patterns formed in mixtures of 4-bead (red) and 13-bead (yellow) surfactants on cylinders of radius 5σ . A. $\phi = 0.20$ and B. $\phi = 0.80$	92

List of Appendices

Appendix

A	Constrained dynamics code	95
A.1	Spherical surfaces	95
A.2	Cylindrical surfaces	96
A.3	Flat surfaces	97
B	Bridge identification code	98
B.1	bridge.cpp	98
B.2	bridges.h	106
B.3	definitions.h	108

Abstract

The study of interactions between different types of molecules on, or near, surfaces and their subsequent self-assembly into patterns is an exciting and challenging area of research in chemical engineering. In particular, a self-assembled monolayer (SAM), formed by the adsorption of molecules on a surface, is an attractive system to model, modify and study surface properties. SAMs allow scientists to engineer surface properties by varying several independent parameters such as number, composition, length and arrangement of molecules on the surface. Research in this field has gained momentum due to an increased interest in nanostructured surfaces like nanoparticles, nanotubes, nanopores and more recently nanotetrapods, tetrahedrons, cones etc. Use of SAMs to coat these complicated nanoscale polyhedra provides a pathway to manipulate interparticle interactions via the surroundings. Phase-separated domains in SAMs can act as attractive, repulsive or reactive patches that influence interactions between particles and can act as precursors or catalytic sites during reactions. The ability to control the placement of attractive patches with directional interactions can help arrange the particles into higher order structures. The use of phase-separating SAMs to arrange sticky patches on a nanoscale particle is therefore a powerful method for assembling hierarchical structures from the bottom-up.

Using computer simulations we try to understand the factors that drive molecular self-assembly and phase separation on surfaces, and more specifically how the curvature of the surface at nanometer length scales affects the self-assembly. In this thesis, we describe results from dissipative particle dynamics simulations used to simulate phase separation and pattern formation in SAMs comprising of two incompatible species. We describe an entropic driving force, resulting from length or bulkiness difference between the co-adsorbed molecules, which leads to the formation of striped patterns and two-dimensional micelles in SAMs on nanospheres, nanocylinders and flat surfaces. We describe why Janus particles will form if the substrate has a sharp curvature. We explain how surface stress, arising from curvature, is important for formation of ordered stripes. We predict that phase separation in SAMs can be used as a useful tool to obtain ordered stripes on nanorods, and that the stripes

will always be rings around that circumference rather than form along the length of the cylinder. Our results on flat surfaces explain why kinetically arrested patches might form in experiments on flat surfaces. Our understanding of patterned substrates allows us to explain an unexpected, non-monotonic dependence of work of adhesion of striped nanoparticles on the compositions of surfactants on their surface.

In general, we study pattern formation in SAMs on nanospherical, nanocylindrical and flat surfaces as a function of substrate curvature, surface coverage, composition, immiscibility and length/bulkiness of adsorbed molecules. Results from these simulations have important applications in fields ranging from catalysis to biosensing.

Chapter 1

Introduction

1.1 Motivation

Due to their stability and ease of preparation, self-assembled monolayers (SAMs) (1; 2) have been studied extensively to engineer surface properties and to control and modify surface interactions (3–5). They have served as model systems to study a variety of surface phenomena including corrosion prevention, molecular recognition, electrode modification, and protein resistance (6–10). Mixed SAMs have applications in fields as diverse as nano-electronics, catalysis and sensing (11–15). Most of the available literature and results are for studies of SAMs on flat surfaces (7; 8; 10; 16–23). With the aid of powerful visualization techniques like scanning tunneling microscopy (STM) (24) and atomic force microscopy (AFM) (25), scientists can probe deeper and study properties of SAMs on an molecular level. Because of such advanced tools and techniques, we are now able to study SAMs formed on a variety of nanoscale surface geometries viz. spheres, tubes, cylinders and faceted shapes like cubes, tetrahedrons and tetrapods (26).

When SAMs on flat surfaces or nanoobjects are composed of only one type of molecules (homoligand SAMs), aspects of interest are the properties of the ligand-coated surface, as well as those of the ligand molecules themselves. Properties of the ligand-coated surface include contact angle, hydrophobicity or hydrophilicity and interactions with biomolecules (1; 2). Properties of ligand molecules include surface coverage, tilt angle and molecular orientation. When a SAM is comprised of more than one type of molecules (mixed SAM), especially molecules that are incompatible with each other, there are additional aspects that need to be addressed and characterized. These include phase separation and pattern formation within the SAM as a function of time, domain sizes and stability (7; 8; 10; 16–21). Interesting and unexpected trends have been revealed in recent years regarding properties of mixed SAMs on nanoobjects (11; 14; 27–30). For example, SAMs comprised of two incompatible ligands, e.g. mercaptopropionic acid and octanethiol on gold nanospheres, are expected to completely phase separate into macroscopic domains each containing one ligand

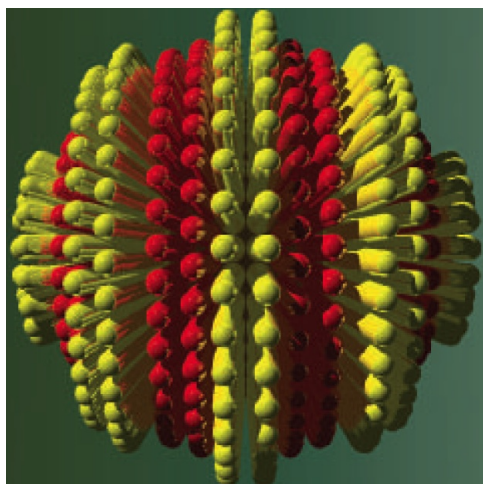


Figure 1.1 Schematic representation of striped phase separation of octanethiol (yellow) and mercaptopropionic acid (red) surfactants on the surface of a gold nanoparticle (11).

only. Instead, they microphase-separate into domains comprised of alternating stripes of the two ligands as shown in Figure 1.1 (11). Computer simulations of phase separation in SAMs on nanospheres can provide useful insight into the formation of these stripes. Providing explanations for recently observed phenomena using computer simulations is one of the primary motivating factors for our work.

Phase separated patterns in SAMs on nanoobjects are also important in the context of bottom-up, hierarchical self-assembly of novel materials (26; 31). Nanometer-scale domains formed by phase-separating, incompatible ligands on the surface of a nanoobject can act as attractive (sticky), repulsive or reactive patches that govern interactions of the nanoobject with its surroundings. These patchy nanoparticles (32) can act as nanobuilding blocks for formation of higher order structures as predicted by simulations earlier and recently confirmed by experiments. Domains on nanoobject surfaces can also act as precursors or catalytic sites for reactions (33). For example, phase separation in SAMs of two incompatible ligands (mercaptosuccinic acid and 3-mercaptopropyl trimethoxylane) on CdTe nanowires, leads to formation of 3-mercaptopropyl trimethoxylane nanoscale patches on the nanowires (14). When these patched nanowires are subsequently coated with SiO_2 , the patches act as preferred sites for deposition of SiO_2 and its subsequent growth into spikes. The resulting nanowires resemble nanocentipedes (Fig. 1.2). The key again lies in phase separation of ligands on a nanoobject surface. Studying mixed SAMs on nanoobjects is therefore an exciting and challenging area of research. The lack of information regarding general trends in pattern formation on nanospherical and nanocylindrical objects and their comparison with pattern formation on flat surfaces is another factor motivating our work.

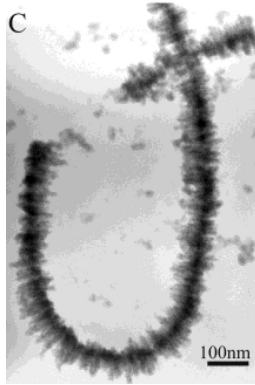


Figure 1.2 A CdTe nanowire covered by SiO_2 spikes giving it the appearance of a nanocentipede (14).

1.2 Objectives

Specific objectives of this work are

1. Adapting existing mesoscale models and methods to perform computer simulations of phase separation in grafted monolayers on simple surfaces such as spheres, cylinders and flat surfaces; developing simulation and analysis codes for the same.
2. Performing the simulations and obtaining and analyzing phase separated patterns on nanostructured and flat surfaces. Providing guidelines and design rules to obtain desired patterns in experiments.
3. Using simulation results to provide insight into unexplained phenomena observed in experiments. Collaborating with experimental groups to verify the guidelines provided through simulations and making qualitative comparisons with experimental results.

1.3 Thesis organization

This thesis is organized as follows.

Chapter 1 describes the motivation for and objectives of this work.

Chapter 2 provides the background and a detailed literature review of experimental and simulational studies performed on SAMs. This chapter includes a short description of homoligand SAMs followed by a detailed discussion of phase separation in mixed SAMs.

Chapter 3 provides the details of the simulation models and methods used in this work. The description includes polymer models, mesoscale dissipative particle dynamics (DPD) and constrained dynamics. A brief review of literature of successful use of these methods in studying phase separation in similar systems like block copolymers and polymer blends is

also included.

Chapter 4 describes the entropic driving force for phase separation in mixed monolayers containing surfactants with mismatched length and/or bulkiness. This chapter describes our results and predictions for SAMs on spherical surfaces. Corroborating experimental results are also provided.

Chapter 5 addresses long-standing issues regarding phase separation in mixed SAMs observed on flat surfaces. In this chapter we present simulation results that explain when and why disordered patches, ordered micelles and striped phases may be expected in experiments on mixed SAMs. This chapter includes a detailed discussion of kinetically-arrested patchy patterns that are often observed in experiments. Old and new experimental results for mixed SAMs on flat surfaces are also discussed in the light of these simulations. We describe pattern formation in symmetric as well as asymmetric mixtures. Finally we provide a comparison of patterns formed in mixed SAMs with those formed in similar systems like block copolymer melts and mixtures of incompatible point charges.

Chapter 6 discusses simulation results on cylindrical surfaces. Patterns on cylinders differ from those on flat and spherical surfaces in a variety of ways. Specifically, the patterns on cylinders are found to be abundant in stripes that were more ordered than those on flat surfaces and spheres. In this chapter we discuss the reasons behind these differences and show how curvature is essential to the formation of ordered stripes.

Chapter 7 describes our work on one of the properties of striped nanoparticles - their work of adhesion in water. The work of adhesion shows an unexpected, non-monotonic dependence on increase in the hydrophilic component of the SAM on its surface. Such behavior is against the traditional view of SAMs comprising of more than one component. We describe two molecular-level effects that compete with each other and combine to result in the non-monotonicity in work of adhesion, thus explaining the unusual behavior.

Chapter 8 summarizes the key observations and predictions from our work and provides directions for future research some of which are already being pursued in the group.

Chapter 2

Background

This chapter gives an introduction to surfactant systems in general and self-assembled monolayers (SAMs) in particular. Vast simulation and experimental literature is available on the formation and properties of SAMs. For the purpose of our discussion in this chapter, we have divided SAMs into two broad categories homoligand SAMs and mixed SAMs. We are most interested in studies of phase separation in mixed SAMs on nanoparticle surfaces. To understand the role of curvature in the phase separation process, we have extensively reviewed phase separation in mixed SAMs on flat surfaces as well. Also, since most of the experimental studies have been performed on flat surfaces, it is useful to keep flat surface observations in mind while studying phase separation on nanostructured surfaces.

2.1 Surfactants and their self-assembly

Surfactants (34; 35) are amphiphilic molecules that have solvent-loving and solvent-hating segments bonded to each other. In most surfactants, one of these sections is a long linear segment called the tail which is usually an 8-20 carbon atom hydrocarbon chain. The other is a bulky, globular part called the head. In solution, amphiphilic molecules form structures like spherical and cylindrical micelles, bilayers and vesicles (34; 35). All of these phases are formed by phase separation, wherein solvent-loving and solvent-hating parts of a molecule prefer to aggregate with their counterparts in neighboring molecules. More recently, it has been shown that novel patterns can be formed by surfactants aggregating near nanotubes by virtue of geometrical confinement alone. For example, the surfactant sodium dodecyl sulfate (SDS) is known to form hemicylindrical aggregates on flat graphite surfaces (36). However, when instead of a flat graphite surface, carbon nanotubes (CNTs) are used, the SDS molecules can arrange into rings, helices or double helices on the CNT surface depending on geometrical parameters (diameter and symmetry) of the CNT (37). Surfactants are also called ligands and stabilizers, when used in the preparation of nanoparticles to limit their growth and stabilize the nanoparticles in solution.

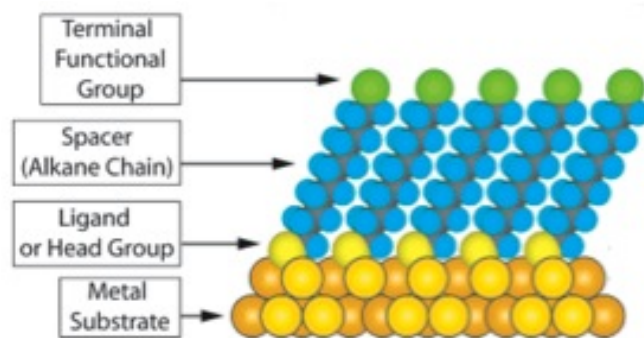


Figure 2.1 A drawing of a typical homoligand SAM describing surfactants adsorbed on a metal substrate (2).

2.2 Homoligand SAMs

Surfactant SAMs are formed when a surface is immersed in a solution of surfactant molecules and the solvent-hating segments of the amphiphiles adsorb to the surface through physisorption or chemisorption (1; 2). The first layer of adsorbed molecules then shields the surface from further adsorption thus forming a monolayer of molecules. The monolayers can be functionalized to allow for chemisorption of more layers on top of the monolayer forming a multilayer of molecules on the substrate (38; 39). SAMs and multilayers are dynamic systems in equilibrium with the surrounding solvent. When SAMs are composed of a single type of surfactant molecules, they are called homoligand SAMs. A simple cartoon describing homoligand SAMs is shown in Fig. 2.1 (2).

2.2.1 Experimental studies of homoligand SAMs

Recently, SAMs, specifically those comprised of thiols on coinage metals like gold, silver, copper etc., have been studied extensively due to their stability and the ease in which they can be used to modify surface properties (1; 2). They are also used as model systems for a variety of studies such as biomolecules-surface interactions, protein resistance, molecular recognition, corrosion prevention, catalysis, and electrode modification (6–10). Some of the important properties of homoligand SAMs are tilt and twist angles, surface coverage, solvent affinity and reactivity. Surfactant molecules in SAMs are known to tilt with respect to the surface normal. For example, monolayers of $\text{CH}_3(\text{CH}_2)_{15}\text{SH}$ on flat gold surfaces show a tilt angle of 28 to 40 degrees with the surface normal (4). This tilting occurs so as to maximize the van der Waals interactions between adjacent chains while maintaining the head lattice structure (40). For similar reasons, the surfactant chains also twist on the

surface. Surface coverage refers to the density of adsorbed ligands on the substrate. Factors that lead to increased surface coverage include greater affinity of the surfactant head or tail for the surface, lattice structure of the substrate and ability of the chains to tilt on the surface. For example, chemisorption leads to larger surface coverage as compared to physisorption (41). Chain length is also known to affect tilt angles and coverage of surfactants on a surface (5; 42). Tail-end groups of the surfactant chains determine key properties and functionality of a SAM e.g. its hydrophobicity or -philicity and the ability to form multilayers and interact with biomolecules, to name a few. Most other studies on flat surface SAMs have focused on the adsorption and arrangement of the surfactant heads on the surface (43–47). Experimental studies indicate that the surfactant head groups arrange in a $(\sqrt{3} \times \sqrt{3})R30^\circ$ two-dimensional triangular lattice (48).

2.2.2 Simulation studies of homoligand SAMs

Several simulation studies have been conducted on homoligand SAMs. Most of these were performed using atomistic molecular dynamic simulations and focused on obtaining tilt angles and chain conformations for comparison with experimental results (48–50). They have reported that the substrate-thiol interactions are important in replicating the correct tilt angles (48). The tilt angles obtained in molecular dynamics simulations were found to be in good agreement with experimentally observed tilt angles (48–50). Schmid et al have obtained phase diagrams for tilt angles as a function of temperature and molecular footprint using a simple idealized model in Monte Carlo simulations (40). Ghorai and Glotzer have recently studied homoligand SAMs of alkanethiols on the surface of a gold nanoparticle (50). In quantitative agreement with experimental observations, they found that the tilt angle for molecules on flat surfaces decreases with an increase in the temperature. They predicted that the crystallographic (51) and continuous (52) models are valid for arrangement of surfactants on a nanosphere at low and high temperatures respectively. They also found that longer thiol chains form more ordered coronas around a gold nanoparticle as compared to shorter thiols.

2.3 Mixed SAMs

SAMs comprised of more than one type of surfactant molecules are called mixed SAMs; binary, ternary, quaternary SAMs are, for example, comprised of two, three and four types of surfactant molecules, respectively. To date, the largest number of ligands that has been

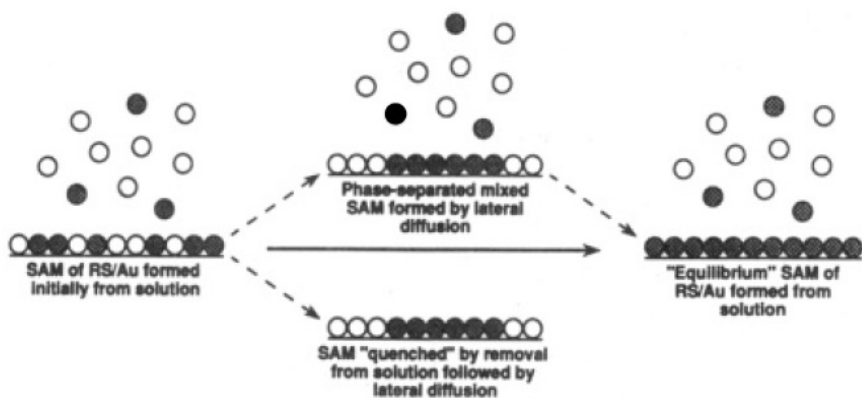


Figure 2.2 Some of the mechanisms that have been proposed for phase separation in SAMs. The open and closed circles indicate the two different components adsorbing or adsorbed onto the surface (17).

co-adsorbed on to a substrate is five (53). Phase separation in the co-adsorbed components is responsible for the wide range of applications of mixed SAMs. Most commonly studied mixed SAMs are binary SAMs comprised of two incompatible surfactants and these are the focus of this thesis. Binary mixed SAMs are often made by a one-step method in which the surface is immersed in a solution containing both surfactants. Both species simultaneously adsorb on the substrate and therefore compete with each other (16). The surfactants in a SAM immersed in a solution are always in dynamic equilibrium with the surfactants in the solution. If the substrate is left in the solution for a sufficiently long time, the competition between the two surfactants will finally result in the presence of only one surfactant on the surface forming a homoligand SAM. The surfactant that is less soluble in the SAM is the one that will form the SAM. Alternatively, a two-step method can be used in which the substrate is first immersed in a solution of the relatively more soluble surfactant, forming a homoligand SAM. This homoligand SAM is then immersed in a solution of the other surfactant, which has a relatively lower affinity for the solvent (therefore higher tendency to adsorb) and can place-exchange the previously adsorbed surfactants. Again, if the substrate is left in the solution sufficiently long (17), all of the more soluble surfactant will be replaced by the less soluble surfactant and again, a homoligand SAM will be obtained. Therefore, in order to obtain a mixed SAM with sufficient presence of both species, it is important to keep the immersion time short. The immersion time required to obtain a mixed SAM of the desired relative composition from a solution of a given composition has to be determined by trial and error.

Several mechanisms have been proposed for phase separation in SAMs, some of which are shown in Fig. 2.2. There is still disagreement over which mechanism best explains the

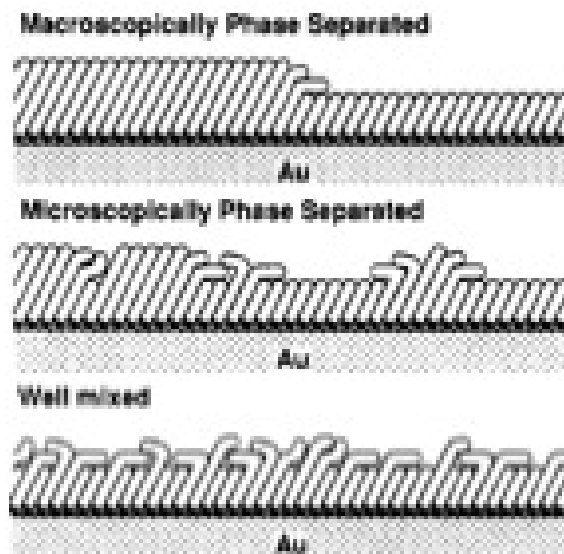


Figure 2.3 Three possible scenarios that can arise in mixed SAMs with respect to phase separation of its components (8).

phase separation process. As in any phase separation process, one of the three scenarios shown in Fig. 2.3 can occur. Macrophase separation is expected to occur in systems that are comprised of highly incompatible components, e.g. highly hydrophilic and highly hydrophobic components will macrophase separate in water. Macrophase separation is alternately called complete or bulk phase separation. Microphase separation occurs when there is a tendency to phase separate but incompatibility between the components is not large enough to result in complete phase separation. In this case, the two components phase separate into equilibrium, nanoscale or microscale domains. The third scenario is that the components are either barely incompatible or not incompatible at all, in which case they do not phase separate at all but instead stay well-mixed.

2.3.1 Experimental studies of mixed SAMs

On flat surfaces

The Whitesides and Weiss groups performed extensive experimental studies of binary mixed SAMs of surfactants on flat surfaces in the 1990s (7; 8; 10; 16–21). Some of the most important observations from these studies are

- The composition of the binary mixed SAM formed on a substrate often differs from their composition in solution (16). This happens because of the differences in affini-

ties of the surfactants for the solvent and substrate. The less soluble surfactant is preferentially adsorbed to the substrate relative to the more soluble surfactant. To compensate for this effect, if a SAM comprised of equal numbers of both surfactants is desired, experimentalists use a solution with a lower concentration of the high substrate-affinity surfactant. Through trial-and-error, one can determine the starting solution concentration and the dipping time required to obtain the desired composition of surfactants in the mixed SAM.

- If left in the solution for a sufficiently long time, only one surfactant will be present in the monolayer (17). As discussed earlier in the section, this effect is due to the fact that no two surfactants have the same solubility in the solvent. If the terminal tail-end group of the surfactant is the same, the longer molecule has a lower solubility in the solvent.
- If the mixed SAM is imaged out of equilibrium with the solvent, nanoscale phase-separated domains are usually obtained (17; 19–21). Using height differences in scanning tunneling microscopy images, one can obtain the domain map of the SAM (20). The nanoscale domains are either striped (20; 21) or consist of nanoscale islands/patches of one component in a pool of the other (8; 17; 19).
- In the case where nanoscale patches were formed, they were seen to merge and elongate over time (19; 20). The merging process was so slow that the final shape and size of the domains were difficult to predict. It is generally agreed that the process of domain growth is kinetically controlled (8).

Patchy and striped domains have both been observed in experimental images of binary mixed monolayers (22; 23; 54). Despite the large number of experimental studies, there are many open questions such as why patches or stripes are imaged in certain conditions and not in others, which of the two is the equilibrium pattern, and is it possible to accelerate the phase separation process to access the equilibrium state, etc. We will try to address all of these questions in this dissertation.

Polymer brushes grafted onto surfaces are similar to surfactant monolayers. Our survey of grafted polymer brush literature (55–60) indicates numerous examples of long, flexible polymers that can form loops and knots and show not only lateral but also perpendicular phase separation. We are interested in much smaller flexible molecules, but not those flexible enough to form loops, bend to the surface, or stretch enough to form a density gradient perpendicular to the surface.

On nanoparticles

Even though relatively few available studies discuss phase separation in monolayers on nanoparticle surfaces, the importance of such studies in terms of engineering applications is demonstrated by recent experiments from the Kotov group at the University of Michigan and the Stellacci group at MIT (11; 14). In the work from the Kotov group, a change in the stabilizer used for producing CdTe nanowires (to be subsequently coated with SiO₂), from thioglycolic acid (TGA) to mercaptosuccinic acid (MSA), drastically changes the appearance of the final SiO₂-coated CdTe nanowire from uniformly-coated to bristled (14). It was shown that when TGA is used, the silane coupling agent mercaptopropyl trimethoxysilane (MPS) uniformly displaces the TGA molecules covering the CdTe nanowire and there is no phase separation of MPS and TGA on the nanowire surface. Hence SiO₂ gets uniformly coated over the nanowire surface. However, when MSA is used and MPS displaces its molecules, the phase separation of MPS and MSA leads to the formation of patches of MPS on the surface of the nanowire. These patches act as a template for the growth of SiO₂ bristles on the surface leading to a centipede-like appearance.

Another example is the striped nanoparticle from the Stellacci group (11) produced when octanethiol (OT) and mercaptopropionic acid (MPA) adsorb and diffuse on the surface of a highly curved gold nanoparticle. It was proposed that curvature of the nanoparticle, which was comparable to the size of the surfactant molecules, is the main factor responsible for formation of these microphase-separated domains. This was based on the fact that such an arrangement of surfactant molecules was not observed when similar experiments were carried out on larger nanospheres (i.e. nanospheres with radius of curvature large compared to size of the surfactant molecules), and on flat gold surfaces. Another aspect of this study (28) was that the striped microphase separation resulted in two singularities (at the poles) that are highly reactive. The group exploited this reactivity to attach functional groups to the nanoparticles at the poles. The attached groups act as attractive patches placed diametrically opposite to each other on the nanoparticle surface, similar to the set-up in earlier computer simulation studies (31; 32). These patchy nanoparticles can be easily assembled into chains, triangles and rings.

These studies demonstrate that the possibilities of using phase separated mixed SAMs to synthesize precisely patterned nanobuilding blocks are compelling and not yet fully tapped. Computer simulations focused at understanding phase separation in SAMs on nanoparticles can provide useful guidelines for obtaining desired nanoscale patterns for the design of patchy particles and are the focus of this thesis.

2.3.2 Simulation studies of mixed SAMs

Surprisingly few simulation studies are available for phase separation in mixed SAMs on flat surfaces, and none exist for phase separation on nanoparticles. All of the studies for flat surfaces used lattice-based Monte Carlo methods (61–64). The focus of these studies was mostly to understand whether or not phase separation would occur in mixed alkanethiol monolayers on gold/silver surfaces and not so much on shapes and sizes of the separated domains. Unlike the disagreements in the experimental community, all simulation studies agree that phase separation would occur. Simulations for specific systems have predicted macrophase-separated (61), striped (64) and patchy (63) domains. Shevade et al systematically studied the role of length difference in phase separation. Key observations from this study are

- For fixed SAM composition, chain length difference is an important factor in determining whether phase separation occurs or not (61). If the tail end groups of the thiols are the same, phase separation is seen only when length difference is greater than three carbon atoms.
- For variable SAM composition, where adsorbed surfactants are in contact with the solution and are allowed to adsorb and desorb, given sufficient time, only the long surfactants would be present in the SAM.

Since very few simulations have been performed to study phase separation in monolayers and due to the presence of many outstanding questions in this area, we expect to contribute to the understanding of monolayer phase separation with a systematic study investigating the effect of substrate curvature, length/bulkiness difference between the surfactants, immiscibility, etc. using an off-lattice particle-based method detailed in this thesis.

Chapter 3

Simulation model and method

In this chapter we describe the development of simulation models and methods used in this dissertation work to simulate phase separation in surfactant monolayers. We describe dissipative particle dynamics (DPD), an off-lattice, particle-based method that has become a popular choice for soft matter simulations in recent years. We also discuss constrained dynamics, which is used to constrain the surfactants to the surface in our study. It allows the surfactant head groups to move on the surface but limits them from coming off the surface. Equations used for constrained dynamics on spherical, cylindrical and flat surfaces are provided. A survey of the types of systems that have been simulated using DPD is also provided.

3.1 Dissipative particle dynamics method

Dissipative particle dynamics (DPD) (65–73) is a mesoscale simulation technique in which groups of atoms are modeled by a single particle (coarse-grained (74; 75)) termed as a DPD bead and the interatomic forces are replaced by net forces acting on this bead. In DPD, just as in other particle-based methods (76; 77) like molecular dynamics (MD) and Brownian dynamics (BD), particle displacements are calculated over short, equal intervals of time called time steps. In each time step, the net force on a particle due to neighboring particles is calculated and then Newton's equations of motion are solved to determine the displacement and the final position of the particle at the end of the time step (76; 77). It has been shown that DPD is valid for simulating hydrodynamic systems (65) and reproduces the canonical (NVT) ensemble (66). A brief discussion on the essential elements of the DPD model and method is provided here.

In DPD, the total force, \mathbf{F}_i , on any particle i , is comprised of a conservative force, a dissipative force and a random force and is given by Equation 3.1. Force \mathbf{F}_i is calculated as the sum of the conservative, dissipative and random forces between particle i and all its

neighboring particles j .

$$\mathbf{F}_i = \sum_{j \neq i} [\mathbf{f}^C(\mathbf{r}_{ij}) + \mathbf{f}^D(\mathbf{r}_{ij}, \mathbf{v}_{ij}) + \mathbf{f}^R(\mathbf{r}_{ij})] \quad (3.1)$$

These three forces are discussed in detail below along with the advantages they impart to the DPD method.

3.1.1 Soft and repulsive pair potential

The conservative force, $\mathbf{f}^C(\mathbf{r}_{ij})$, given by Equation 3.2, is the pair potential acting between particles i and j . Here, $\mathbf{r}_{ij} = \mathbf{r}_j - \mathbf{r}_i$ (\mathbf{r}_i and \mathbf{r}_j being position vectors of particles i and j respectively), $\hat{\mathbf{r}}_{ij}$ is the unit vector in the direction of \mathbf{r}_{ij} and r_c is the cutoff distance of the potential. The conservative force depends only on the relative positions of the two particles and not on their velocities. A plot of the magnitude of the conservative force versus distance r_{ij} between particles i and j is shown in Figure 3.1.

$$\mathbf{f}^C(\mathbf{r}_{ij}) = \begin{cases} a_{ij}(1 - r_{ij})\hat{\mathbf{r}}_{ij} & r_{ij} < r_c \\ 0 & r_{ij} \geq r_c \end{cases} \quad (3.2)$$

In Equation 3.2, a_{ij} is a measure of interactions between the particles i and j , and is referred to as the interaction parameter. a_{ij} is always positive. For a binary mixture containing molecules of two different types, say A and B, the interaction parameters a_{AA} , a_{BB} and a_{AB} for interactions between two particles of type A, two particles of type B and a particle of type A and other of type B, respectively, are in general different.

As seen from Equation 3.2, the conservative force is finite even when $\mathbf{r}_j = 0$, i.e. even if two DPD beads completely overlap with each other, the repulsion between them is not infinite. Such potentials where overlap between particles is allowed, are termed soft potentials. The nature of this conservative force therefore makes DPD a soft-potential simulation method in which the DPD beads act more like fluid elements capable of diffusing through each other. Such a soft-potential conservative force renders DPD an ideal method to study phase separation in high density systems where the governing phenomenon is diffusion. Another advantage of the DPD conservative force is that it is purely repulsive. Integrating Equation 3.2 with respect to r_{ij} yields the potential energy which is always positive irrespective of r_{ij} and the types of particles interacting. Positive potential energy implies that all particles in DPD, whether of the same type or different types, are repulsive. Phase separation occurs in DPD because a particle of one type repels a particle of another type more than it repels a particle of its own type. Due to its functional form, there are no

attractive energy wells in the DPD conservative force. The interaction parameter has two parts, one that is independent of the types of interacting particles, a , and another, Δa , that does depend on the types. For example, the interaction parameter for a particle of type A interacting with a particle of type B is given as $a_{AB} = a + \Delta a_{AB}$. A large Δa_{AB} implies a large repulsion between particles of type A and B. To model incompatibility between two species A and B, we choose $\Delta a_{AA} = \Delta a_{BB} = 0$ while $\Delta a_{AB} > 0$. Therefore, repulsion between dissimilar particles is greater than that between similar particles. The parameter Δa_{AB} is a direct indication of the degree of incompatibility between the two surfactants and is an important parameter in our simulations. It is reported, in short, as Δa in this thesis.

A combined advantage of both these factors, i.e. softness and repulsiveness of the conservative force, is that there is a significant improvement in size of the time step that can be used. In commonly-used particle-based methods like MD and BD, the conservative force is of the Lennard-Jones type (76; 77). This potential has an attractive energy well at the equilibrium particle separation and if the separation is reduced further, the conservative force sharply approaches infinity. When using such potentials, a small time step has to be chosen so that the particle displacements in a given time step are small and the interparticle distances are never small enough to produce large conservative forces. If the chosen time step is not small enough, the simulation will become unstable as the particles will shoot out of the box under the influence of large forces. In DPD, since the conservative force is always finite, large time steps can be chosen.

3.1.2 Built-in Langevin Thermostat

The dissipative and random forces together act as a built-in Langevin thermostat in DPD simulations. The dissipative force, $\mathbf{f}^D(\mathbf{r}_{ij}, \mathbf{v}_{ij})$, given by Equation 3.3, represents the frictional force on a particle i due to another particle j . It depends on the positions and relative velocities of the particles i and j . Here, $\mathbf{v}_{ij} = \mathbf{v}_j - \mathbf{v}_i$ (\mathbf{v}_i and \mathbf{v}_j being position vectors of particles i and j respectively).

$$\mathbf{f}^D(\mathbf{r}_{ij}, \mathbf{v}_{ij}) = -\gamma \omega^D(r_{ij})(\mathbf{v}_{ij} \cdot \mathbf{r}_{ij}) \hat{\mathbf{r}}_{ij} \quad (3.3)$$

The parameter γ in Equation 3.3, is a coefficient controlling the strength of the frictional force between the particles. The term $\omega^D(r_{ij})$ is a weight function describing variation of the friction coefficient with distance. $\omega^D(r_{ij})$ also links the dissipative force to the random force as described later.

The random force, $\mathbf{f}^R(\mathbf{r}_{ij})$, in DPD is given by Equation 3.4. As the name suggests, the

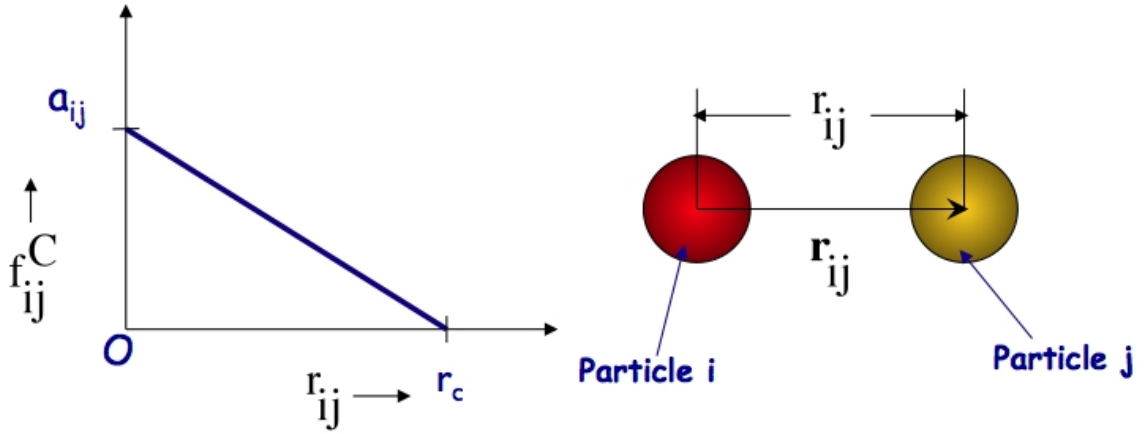


Figure 3.1 Left: A plot of the conservative force as a function of distance r_{ij} between particles i and j . Right: Definition of r_{ij} .

random force represents the random forces applied to particles in DPD to help conserve momentum and temperature. The random force is applied to simulate the effect of the random collisions of a particle with the surrounding solvent molecules. Here, σ_N is the magnitude of the pairwise random force between the DPD particles; ε_{ij} is a random variable with uniform distribution and unit variance and $\varepsilon_{ij} = \varepsilon_{ji}$. Similar to $\omega^D(r_{ij})$, $\omega^R(r_{ij})$ is a weight function.

$$\mathbf{f}^R(\mathbf{r}_{ij}) = \sigma_N \omega^R(r_{ij}) \varepsilon_{ji} \hat{\mathbf{r}}_{ij} \quad (3.4)$$

The dissipative and the random forces are tightly coupled and depend strongly on the temperature. Their magnitudes can therefore be manipulated to control the temperature of the system. It has been shown (65; 66) that the dissipative and random forces together, conserve thermodynamics and momentum when $\omega^D(r_{ij})$ and $\omega^R(r_{ij})$ are related by Equation 3.5 and γ and σ_N are related to the temperature, T by $\sigma^2 = 2k_B T \gamma$.

$$\omega^D(r_{ij}) = [\omega^R(r_{ij})]^2 \quad (3.5)$$

In terms of the use of dissipative and random forces to control temperature, DPD is similar to the well-established BD method, except that in DPD these forces are applied pairwise to the particles in the system. Therefore, dissipative and random forces act in an equal and opposite manner on a pair of particles in DPD. As a result, unlike BD, DPD

conserves linear as well as angular momentums and can be used to simulate hydrodynamic phenomena (65).

3.1.3 Integration method

We use the modified velocity Verlet algorithm (68; 76) to solve the Newtons equations of motion in our simulations. The algorithm is described by the following set of equations (Equation 3.6).

$$\begin{aligned}
 \mathbf{r}_i(t + \Delta t) &= \mathbf{r}_i(t) + \Delta t \mathbf{v}_i(t) + \frac{1}{2} \Delta t^2 \mathbf{f}_i(t), \\
 \tilde{\mathbf{v}}_i(t + \lambda \Delta t) &= \mathbf{v}_i(t) + \lambda \Delta t \mathbf{f}_i(t), \\
 \mathbf{f}_i(t + \Delta t) &= \mathbf{f}_i(\mathbf{r}_i(t + \Delta t), \tilde{\mathbf{v}}_i(t + \lambda \Delta t)), \\
 \mathbf{v}_i(t + \Delta t) &= \mathbf{v}_i(t) + \frac{1}{2} \Delta t (\mathbf{f}_i(t) + \mathbf{f}_i(t + \Delta t))
 \end{aligned}
 \tag{3.6}$$

Here, $\mathbf{r}_i(t)$, and $\mathbf{f}_i(t)$ are the position and force, respectively, for particle i at time t . Δt is the integration time step. $\tilde{\mathbf{v}}_i(t)$ and $\mathbf{v}_i(t)$ are the predicted and corrected velocities, respectively, at time t . γ is a constant that can be fine-tuned to enable larger time steps. For standard Verlet algorithm, $\gamma = 0.5$.

3.2 Simulation model

A two-dimensional cartoon describing the basic set-up of our simulations is shown in Fig. 3.2A. As shown in the figure, the surfactant chains are comprised of several beads and are grafted by one end to the spherical nanoparticle surface. The entire set-up is enclosed in a cubic (for spherical surfaces) or non-cubic (for cylindrical and flat surfaces) simulation box. For cylindrical surfaces, periodic boundary conditions are applied along the length of the cylinder while for flat surfaces they are applied in the plane of the surface. The two types of surfactants usually have a length difference or bulkiness difference between them. Length and bulkiness differences are measured in terms of the number of extra beads present in the bead-spring chain of the long/bulky surfactants as compared to those present on the short/less bulky ones. The two surfactants are denoted by different colors; in all the snapshots from DPD simulations shown in this thesis the longer/bulkier surfactants are shown in yellow while the shorter/less bulky surfactants are shown in red. The red and yellow beads are identical in all respects except that they are incompatible with each other.

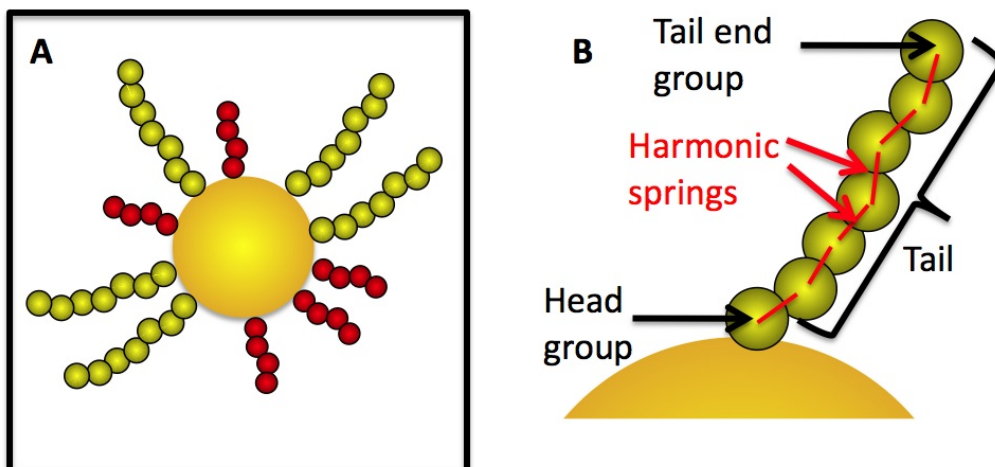


Figure 3.2 A. A two-dimensional cartoon of the simulation set-up. The orange circle in the center represents a gold nanoparticle. Red and yellow circles make up the short and the long surfactant chains respectively. The entire set-up is simulated in a cubic or non-cubic box. B. A single surfactant chain on a spherical nanoparticle.

All beads interact with the DPD forces described by Equations 3.1 to 3.5. Additional forces are applied to certain beads as described below.

3.2.1 Surfactants

In our study the surfactants are modeled as bead-spring chains as shown in Fig. 3.2B. The springs connecting consecutive beads in a chain are simple harmonic springs. For particles i and j connected by a spring, the force on particle i due to this single spring is given by Equation 3.7.

$$\mathbf{f}_i^{spring} = C\mathbf{r}_{ij} \quad (3.7)$$

One of the end beads of the surfactant chain is constrained to the nanoparticle surface using constrained dynamics (Section 3.2.2). This bead is called the head group of the surfactant. The rest of the chain is called the tail. The end of the surfactant tail that is farthest from the nanoparticle surface is referred to as the tail end group. The experimental systems that we are simulating, use short surfactants (less than 20 carbon atoms in length), with limited bending ability and unable to form loops. Use of bead-spring chains for surfactants in simulations, allows them to be flexible enough to bend and tilt but the short length prevents them from forming loops, similar to experiments.

The assumption that the two surfactants are incompatible with each other is derived from

the fact that they are soluble to different degrees in the solvent. The solvent itself, is treated implicitly in the DPD model. We therefore do not have any beads representing the solvent molecules in our simulations. Incompatibility between the two surfactants is enhanced if incompatible tail-end groups, e.g. $-\text{CH}_3$ and $-\text{OH}$ are present on them.

3.2.2 Substrate

In our minimal model the substrate is modeled as a virtual surface. The head groups of the surfactant molecules are constrained to move in the two dimensional surface of the substrate using constrained dynamics. The idea behind constrained dynamics is to first move the particle unrestricted according to the net forces on it due to the other particles. Next, depending on the constrain, back-calculate the force that should have been applied to the particle so that the constraint is exactly satisfied. Finally, use the estimated force to determine the position of the constrained particle. The step-by-step derivation of the equations for the spherical surface is provided in reference (76) in Chapter 15. The final equations that are used to determine the corrected force $\mathbf{F}_{constrained}(t)$ and the corrected position $\mathbf{r}(t)$ are given below. In these equations, $\mathbf{f}(t)$ and $\mathbf{r}_u(t + \Delta t)$ are the uncorrected or unconstrained force and position, respectively. $\mathbf{r}(t)$ is the position of the particle at time t , m is the mass of the particle and Δt is the integration time step. The section of the code to be implemented in the verlet integration scheme to incorporate constrained dynamics is provided in Appendix A.

Constrained dynamics on spherical surfaces

If R is the radius of the sphere to which the particle has to be constrained, the corrected force and position are given by Equations 3.8 and 3.9, respectively.

$$\mathbf{F}_{constrained}(t) = \mathbf{F}(t) - \frac{\lambda \mathbf{r}(t)}{(\Delta t)^2} \quad (3.8)$$

$$\mathbf{r}(t + \Delta t) = \mathbf{r}_u(t + \Delta t) - \frac{\lambda}{m} \mathbf{r}(t) \quad (3.9)$$

where λ is given by Equation 3.10.

$$\lambda = \frac{\mathbf{r}(t) \cdot \mathbf{r}_u(t + \Delta t) - \sqrt{[\mathbf{r}(t) \cdot \mathbf{r}_u(t + \Delta t)]^2 - R^2 [r_u^2(t + \Delta t) - R^2]}}{R^2/m} \quad (3.10)$$

Equations 3.8 and 3.9 have to be applied in all (x, y and z) directions. The derivation of

these equations is available in Chapter 15 of reference (76).

Constrained dynamics on cylindrical surfaces

The equations for constraining a particle on the surface of a cylinder of radius R , are the same as those for constraining it on a sphere of radius R . The only difference is that the equations are not applied in the direction along the length of the cylinder which is the direction in which the periodic boundary conditions are applied. The equations are only used to correct the forces and positions in the other two directions. The solution for λ remains unchanged as given by Equation 3.10.

Constrained dynamics on flat surfaces

For constraining a particle to a flat plane defined by, say, $z = R$, equations that determine the corrected force and position are still the same as those for the spherical and cylindrical surfaces (Equations 3.8, 3.9), but λ is now given by Equation 3.11,

$$\lambda = \frac{z_u(t + \Delta t) - R}{z(t)/m} \quad (3.11)$$

which is obtained by applying Equation 3.9 for the z component only and substituting $z(t + \Delta t) = R$. In Equation 3.11, $z(t)$ and $z_u(t + \Delta t)$ are the scalar z components of the old (at time t) position vector $\mathbf{r}(t)$ and the new (at time $t + \Delta t$), corrected position vector $\mathbf{r}_u(t + \Delta t)$, respectively.

3.2.3 Bulkiness

We have implemented two methods in order to model the bulkiness of the tail end groups of our polymers. In the first, illustrated in Fig. 3.3A, we increase the radius of the tail end bead. As seen from Equation 3.7, the equilibrium length for the harmonic springs connecting consecutive beads in a polymer is zero. For implementing bulkiness using the model shown in Fig. 3.3A, we need to increase this equilibrium length and also adjust the spring constants to prevent the smaller beads from going inside the larger bead. This is a tedious, trial and error process and we found that the system was difficult to stabilize using this model.

In the second method, illustrated in Fig. 3.3B, we attach additional beads to the tail end group to make it bulky. These additional beads are attached using simple harmonic springs (Equation 3.7). This method is also time consuming because in order to achieve the desired

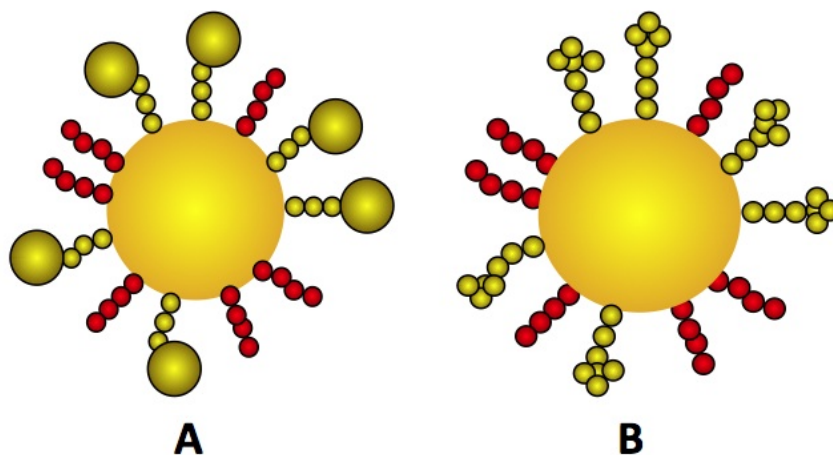


Figure 3.3 Two separate models implemented and tested to make one of the surfactants (yellow) bulkier than the other (red). A. The size of the tail end bead is increased to make it bulky. B. Additional beads are attached to the tail end bead to make it bulky.

overlap between beads, the spring constants for the springs between the tail end bead and the additional beads need to be fine-tuned. However, this method was found to be more robust than the first method and was stable for several, though not all, values of surfactant lengths and bulkinesses. All the simulation results for bulky surfactants reported in this thesis were obtained using this second method with additional beads.

3.3 Validation

We have validated our model, parameters and code by reproducing two known, expected results. These are discussed below.

3.3.1 Phase separation in simple incompatible mixtures on cylindrical surfaces

First, we tested our code by simulating a system of simple, incompatible single-bead surfactants (without the tails) on a cylindrical surface. Since incompatible mixtures completely phase separate into their two components into minimum interface configurations, we expect that as the circumference to length ratio of the cylinder is changed, there should be a change in the direction of the interface. Specifically, if R and L are the radius and length of the cylinder, respectively, the interface should form along the length of the cylinder when

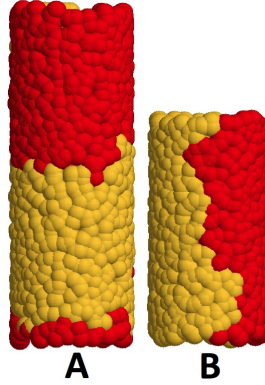


Figure 3.4 Interface direction switches from A. horizontal to B. vertical, when length of a radius = $3\sigma(2\pi R = 18.8)$ is changed from 22.0 to 15.0, where R is the radius of the cylinder

$2\pi R > 2L$ and along the circumference of the cylinder when $2\pi R < 2L$. Results from our simulations on cylinders with $2\pi R \simeq 18.8$ and lengths 22.0 and 15.0 confirm this behavior as shown in Fig. 3.4

3.3.2 Phase separation in block copolymers on spherical surfaces

Tang et al. (78) have performed theoretical studies of phase separation in diblock copolymers constrained to the surface of a sphere. They found that the block copolymers phase separate into striped patterns on the sphere as shown in Fig. 3.5. Fig. 3.5 shows evolution of the patterns in time.

The system studied by Tang et al, is the best system to verify and validate our code and parameters against. We can test, the constrained dynamics, as well as bead-spring polymer parameters by using our code to simulate phase separation in block copolymers on spherical surfaces. Fig. 3.6 shows the modified DPD model that we use. In the system of surfactants grafted on a sphere, we have two types of bead-spring chains that are separate from each other and only one bead in each chain is constrained to move on the sphere surface. In the system of block copolymers constrained to the sphere, both the two types of bead-spring chains are tied together and all beads are constrained to the spherical surface.

Fig. 3.7 shows the results of our test simulation for block copolymers. Using a surface density ρ of 4.0 and a repulsion parameter of Δa of 15, we were able to obtain stripes resembling the stripes obtained by Tang et al. (78) shown in 3.5. The simulation was very stable with respect to temperature control and took three hours to complete. Each segment of the block copolymer chain was comprised of three DPD beads and the radius of the sphere was five.

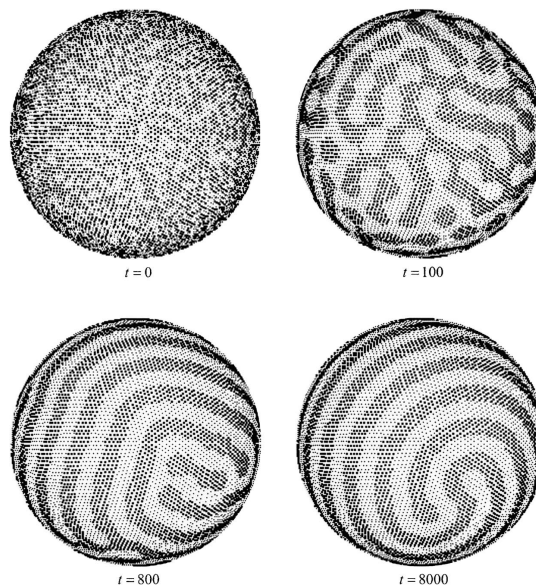


Figure 3.5 Phase separation of block copolymers in which two immiscible segments are bonded together. Different images show evolution of the pattern in time leading to the formation of a striped phase in the end (78).

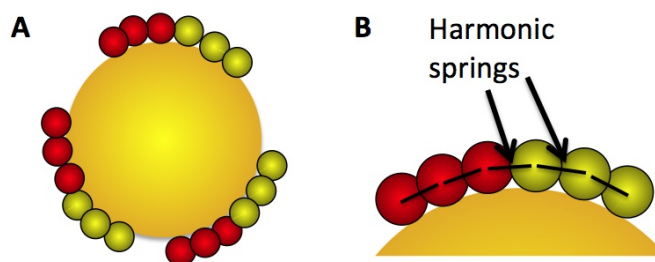


Figure 3.6 A. A two-dimensional cartoon of the set-up for simulating phase separation in block copolymers constrained to spherical surfaces. Red and yellow circles make up the immiscible segments of the block copolymer chains that are tied to each other. The simulation is carried out in a cubic box. B. A single block copolymer chain on a spherical surface. Each of the beads in the chain is tied to its neighbors by simple harmonic springs.

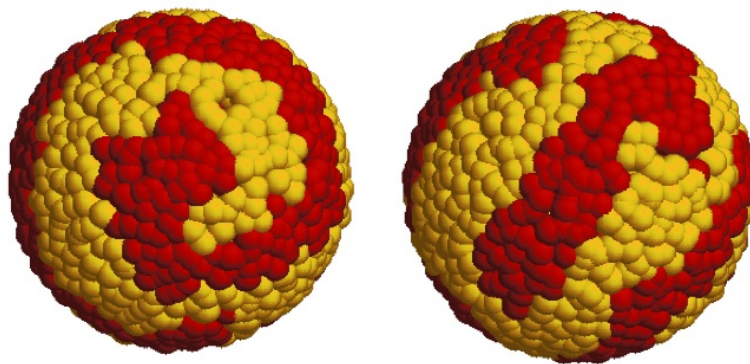


Figure 3.7 Two different views of the same simulated system showing striped patterns formed by phase separation in block copolymers constrained on a sphere.

3.4 Caveats

Despite the fact that DPD is a fast and efficient method for soft matter simulations, there are some issues that are important to bear in mind while using DPD.

3.4.1 Temperature control

Unlike other particle-based methods where an additional thermostat like the Nosé-Hoover or Berendsen thermostats is used to control the temperature, DPD has its own built-in thermostat (Section 3.1.2). This means that the degree and accuracy of temperature control depends on parameters that the user chooses. While steady increase or decrease, i.e. drifting, of the temperature is unacceptable, we find that the DPD thermostat has a tendency to stabilize the temperature at a slightly higher temperature than the set and the desired value. It is possible, though often time-consuming, to adjust the parameters to obtain the desired control. The parameters that help control the temperature are the noise amplitude, σ_N and the friction coefficient, γ . If the temperature is still difficult to control, the time step Δt has to be reduced. Since this is a trial and error procedure which has to be reapplied every time one simulates a new surfactant system, it is tedious and time consuming. However, once a set of parameters has been obtained, the DPD simulations are robust and much faster than simulations using other off-lattice, particle-based methods. We also notice that up to a 3% difference between the desired and the achieved temperature does not affect the final equilibrated pattern. In simulations of phase separating mixtures, this can be used as a practical tolerance for temperature in DPD. A variation in temperature in the first few hundred time steps is acceptable, as in many other systems. The temperature profile

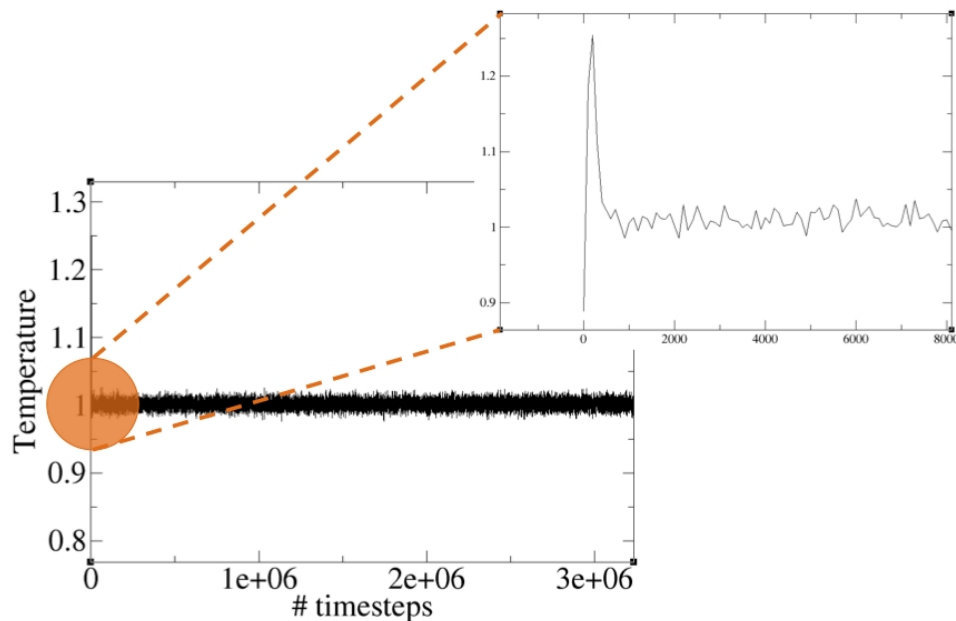


Figure 3.8 The temperature profile of a DPD simulation showing a situation in which excellent temperature control was obtained by fine-tuning several parameters. The figure also shows the zoomed-in region of the temperature profile at the beginning of the simulation.

from one of our simulations is shown in Fig. 3.8. The figure also shows the zoomed-in temperature profile during the first few time steps of the simulation, in which the temperature fluctuations are large.

3.4.2 Three-dimensional density

Since the cutoff distance for the soft pair potential is equal to the diameter of a single bead in DPD, the beads in DPD need to overlap in order to interact. While the number density in other particle based methods is a number between 0 and 1, the recommended (68) three-dimensional number density in DPD to enforce sufficient overlaps between particles is 3.0. The 3D surface density is relatively easier to control than the temperature, since it only requires tuning the surface coverage and polymer spring constants. Using a density much larger than 3.0 is acceptable but not recommended because it makes the simulations computationally expensive. It should also be noted that the 2D surface density required to simulate phase separation in SAMs on spheres is higher than that required on cylinders which is further higher than the 2D density on flat surfaces. This is because volume available to chains on a curved surface increases as we move away from the surface.

3.4.3 Parameter limitations

We are simulating bead-spring chains that are not in bulk but are attached by one end to a surface. Therefore, when the chains are very long, the overlap between consecutive beads on the chain is no longer the same. The beads closer to the surface are farther apart than beads away from the surface. The problem can be solved by using variable spring constants C in Equation 3.7 i.e. by using decreasing spring constants as we move away from the surface. This fix was not required for the short chains that we used in our simulations discussed in this thesis. There are also limitations on the values of bulkiness that we can simulate with the current model, as discussed in Section 3.2.3.

We now discuss the computational resource requirement for our simulations. We have used a serial code which typically takes 10 CPU hours on a 2.3GHz quad-core AMD Opteron processor to simulate 20000 particles for 1 million time steps of size 0.01 each. Even though this code is fast as compared to molecular dynamics codes, faster options are now available. An efficient and parallel DPD code is now available in the simulation software LAMMPS which can be modified to include constrained dynamics not currently provided with the package. Another option is to use graphic processing units (GPUs). Efforts are underway in the Glotzer group to incorporate DPD potential and thermostat into HOOMD-Blue, a fast, molecular dynamics software which runs on GPUs as well as CPUs. Finally, much simpler Monte Carlo models have also been developed recently to simulate these systems even faster (Section 8.2.1)

3.5 DPD in soft matter simulations

Here we provide a short review of the types of systems that have been successfully simulated and studied using DPD. Since its introduction in 1992 by Hoogerbrugge and Koelman (72), DPD has proved its versatility and usefulness by being the method of choice for simulating a wide range of systems and phenomena (69). Starting out as a method to simulate hydrodynamic phenomena (65; 71; 72; 79), DPD is now widely used to simulate phase separation and properties of polymeric systems such as surfactant systems (80–82), polymer solutions (83–85), homopolymer melts (68; 85; 86), block copolymer melts (70) and polymer brushes (87). It has also been used to study properties of colloidal systems (73; 88–90) including colloidal adsorption (91; 92).

In recent times, DPD has been used to study a variety of complex and interesting systems (67). For example, it has been used to simulate aggregation of gold atoms to form nanoparticles in the presence of ethers and organic solvents (93). It has been used to study

flow and rheological properties of solvent flow near polymer-coated walls (94) and channels (95). Other interesting problems studied with DPD include interfacial phenomena at solid-liquid interfaces (96) and packing in nanoparticle-polymer composites (97). Over the years, a variety of hybrid methods based on DPD have also been developed, some of them incorporating only the soft pair potential or the thermostat, others improving the potentials and/or integration schemes (67; 97–100). With such a wide range of applications, improved algorithms and hybrid models available, DPD is currently a very attractive method for simulating mesoscale systems and phenomena that are difficult or time consuming to simulate with traditional particle-based methods.

Chapter 4

Striped spherical nanoparticles

In this chapter we first present an entropy-based argument to explain the unexpected stripe formation on spherical nanoparticles coated with mixed SAMs. We find that the stripes are stabilized in systems in which the surfactant molecules are incompatible with each other and have a sufficient length and/or bulkiness difference. This microphase separation is explained by the interplay between energetic driving forces that tend to minimize the interface between the incompatible components and entropic driving forces that tend to maximize the interface. Next, we explore the effects of substrate curvature, surfactant length/bulkiness difference and surface coverage on the phase separated patterns. Our simulations predict a size range for nanoparticles on which ordered stripes are expected to form. Finally, we provide corroborating results from atomistic molecular dynamics simulations and experiments performed on mixed SAMs. The results presented in this chapter have resulted in publications (101) and (33). Part of the text and figures presented in this chapter have been taken from these publications.

4.1 Introduction

As discussed briefly in Section 1.1, unusual stripe-like domains were observed in experiments imaging surfactant-coated spherical nanoparticles. The first question we address in this chapter is whether stripes can indeed form in these systems and why. It is important to understand the driving forces behind phase separation in these systems because the striped nanoparticles have important applications due to their unusual molecular recognition properties (11) and their ability to penetrate cell membranes (30). These striped nanoparticles are also known to assemble into higher order structures like chains, triangles and rings (28) due to their unique surface morphology. Based on these observations, the second question that we want to address in this chapter is whether computer simulations can provide guidelines for tailoring surface patterns to design nanobuilding blocks.

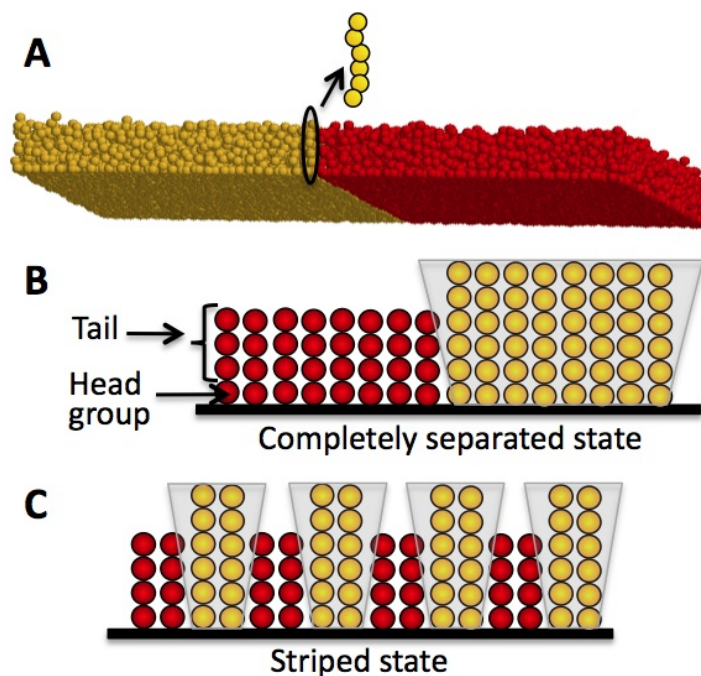


Figure 4.1 A. Completely separated configuration for a system of strongly immiscible surfactants with six beads each. B. and C. Free volume (shaded grey areas), available to long (yellow, six-bead) surfactant chains when arranged with short (red, four-bead) chains in B. completely separated and C. microphase separated striped states. The bead in the chain that is constrained to the surface is the head group and the rest of the chain is the tail of the surfactant. (142)

4.2 Energy and entropy in mixed SAMs

A mixture of two incompatible species is expected to undergo complete phase separation into its two components as shown for a flat surface in Fig. 4.1A and B. By macrophase separating in this way, the interface between the two components is minimized and the energetic gains are maximized. At low temperatures and when the degree of incompatibility is large, entropic contribution is negligible and energetic considerations dominate the phase separation process. Hence, for mixtures of highly incompatible species, complete phase separation minimizes the overall free energy of the system and is always preferred.

In mixed SAMs prepared by the one-step method in which the substrate is dipped in a solution of the two surfactants it is difficult to adsorb two highly incompatible surfactants. This is because the two highly incompatible surfactants, for example one hydrophobic and the other hydrophilic cannot both be soluble in the same solvent, e.g. water, thus making it difficult to create such a solution. Experimentalists therefore use moderately incompatible surfactants to obtain phase separating SAMs. We use moderately incompatible bead-spring chains, that don't always completely phase separate, in our simulations as well.

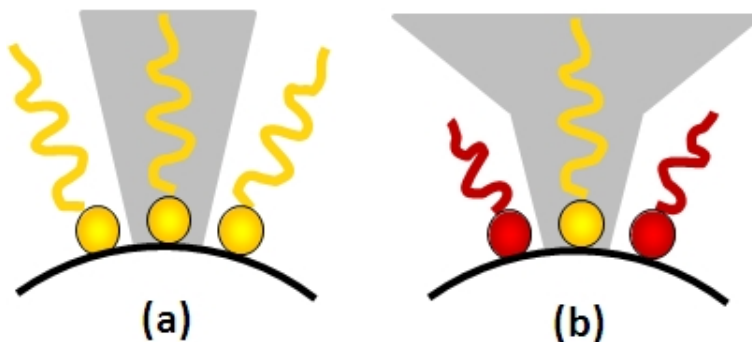


Figure 4.2 Free volume (grey region) available to a long (yellow) surfactant chain surrounded by A. two chains of the same length as itself. B. Two shorter (red) chains. The shaded area is larger when the neighbors are shorter.

We expect that these moderately incompatible surfactants would still show complete separation in the absence of any symmetry breaking parameters. Well-known symmetry-breaking parameters include anisotropic surface stress (102), external fields (103) and presence of chemical reactions (104–106). In mixed SAMs of incompatible species, we propose that a difference in length or bulkiness between the two species can break the symmetry and lead to pattern formation. If one of the surfactants is sufficiently longer or bulkier than the other, the longer chains gain considerable free volume and entropic freedom by placing themselves next to shorter/less bulky chains. This is demonstrated in Fig. 4.1B and C. The free volume associated with demixed or macrophase separated configurations is much smaller than that for microphase separated configurations. We hypothesize that with microphase separation, the entropic gain in terms of the conformational entropy of the long chains might outweigh the energetic cost of forming interfaces. Our hypothesis can be directly extended to curved surfaces as demonstrated in Fig. 4.2.

On spherical or curved surfaces, the entropic gain depends not only on the length/bulkiness difference but also on the curvature of the surface. As demonstrated in Fig. 4.3, a surfactant chain on a spherical surface has a larger available free volume when the radius of curvature of the substrate is small. We propose the interplay between energy and entropy as a possible reason for the formation of striped patterns on spherical nanoparticles in experiments. Traditionally in the context of binary mixtures, entropy versus energy arguments are based on the configurational entropy of the two species. In mixed SAMs, we argue that it is predominantly the conformational entropy, of the long polymer chains, which gives rise to competing interactions and leads to microphase separation. The competing energetic and entropic forces effectively act as short-range attractive and long-range repulsive interactions, respectively. Some other similar, and better-known, competing interactions that mediate

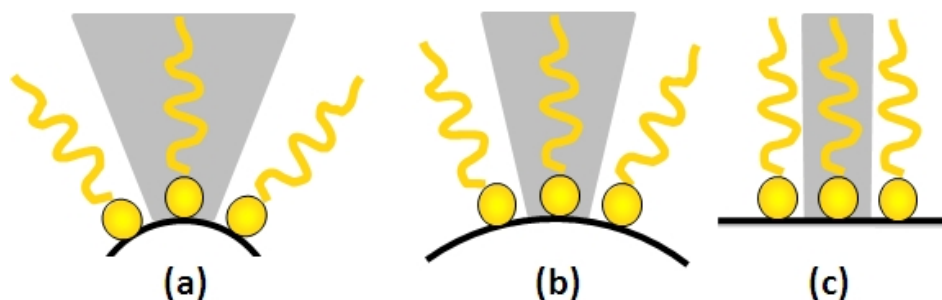


Figure 4.3 Free volume (grey region) available to a surfactant chain on surfaces of different curvatures. A. small nanoparticle, B. large nanoparticle, C. flat surface. (143)

immiscibility and produce stripes or patches are magnetic attraction in ferromagnetic films (107), electrostatic attraction in mixtures of charged species (108; 109), auto-catalytic reactions in reaction-diffusion systems (104–106) and chemical bonding constraints in block copolymer systems (110).

4.3 Simulations of SAMs on nanospheres

In this section we present our results from DPD simulations of mixed SAMs on nanospheres. We investigate the effect of length difference, bulkiness difference, surface coverage and degree of curvature.

4.3.1 Effect of increasing chain length difference

As discussed in Section 4.2, we expect equal-length, incompatible surfactants to completely separate from each other spatially. We observe this phenomenon in simulations, an example of which is shown in Fig. 4.4A. On increasing the length difference by one or two beads, we still see complete phase separation (Fig. 4.4B). On increasing the length difference further to three or more beads, we start observing striped patterns as shown in Fig. 4.4C, D and E. Note that only the positions of the head groups are shown in Fig. 4.4 and in all other simulation snapshots in this thesis. Tails have been removed for clarity and better visualization of the patterns. We do not see microphase separation for small length differences because the gain in conformational entropy of long chains placed next to short chains is significant only when sufficiently many beads from the long chains are free to explore the volume available over the short chains. Therefore, only for large length differences between surfactants, is the entropy gain large enough to compete with the energetic penalty of a larger interface

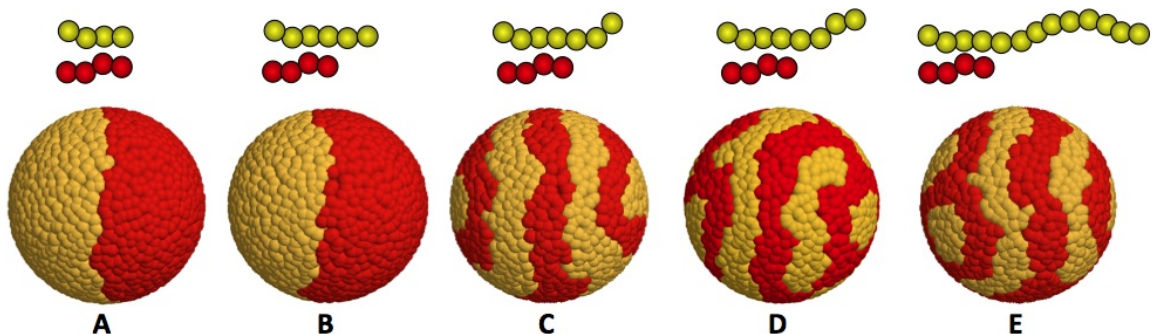


Figure 4.4 Effect of length difference on phase separated patterns formed in mixtures of incompatible long (yellow) and short (red) surfactant chains on the surface of a sphere. The radius of the sphere is 5σ where diameter of one bead is σ . The red and yellow chains on top of each simulation snapshot indicate the number of beads in the surfactants used for that simulation. The systems simulated from left to right are denoted by m_n where m and n are the number of beads in the short and long surfactants respectively. A. 4_4, B. 4_6, C. 4_7, D. 4_8, E. 4_13. Some of the images have been taken from reference (101).

between immiscible domains. For small differences in length, the gain in entropy is not sufficient to outweigh this energetic penalty of mixing. Although the observation that striped patterns occur only for length differences larger than a critical value is independent of the absolute lengths of the surfactants, the value of this critical length difference does depend on the absolute lengths of the surfactants as well as the curvature of the substrate.

4.4 Effect of increasing bulkiness difference

As discussed in Chapter 3, our models for bulky surfactants are tedious if we want to simulate all values of bulkinesses and lengths because of the need to fine-tune several different spring constants. Nevertheless, we are able to employ this model to simulate the systems needed to verify our hypothesis regarding bulkiness difference and stripe formation. We find that similar to the critical length difference, there is a critical difference in bulkiness that must be present in order to achieve microphase separation. Surfactant mixtures with small bulkiness differences show complete separation. As shown in Fig. 4.5A, B and C, this critical bulkiness difference (in terms of the number of extra beads on the bulky surfactant) determined from our simulations for 4-bead long short surfactants, is three. This is the same as the critical length difference required in simulations of 4-bead long short surfactants for microphase separation 4.4.

We also simulate systems in which one of the surfactants is long and the second is bulky. These differ from the other simulations we perform wherein only one surfactant is either

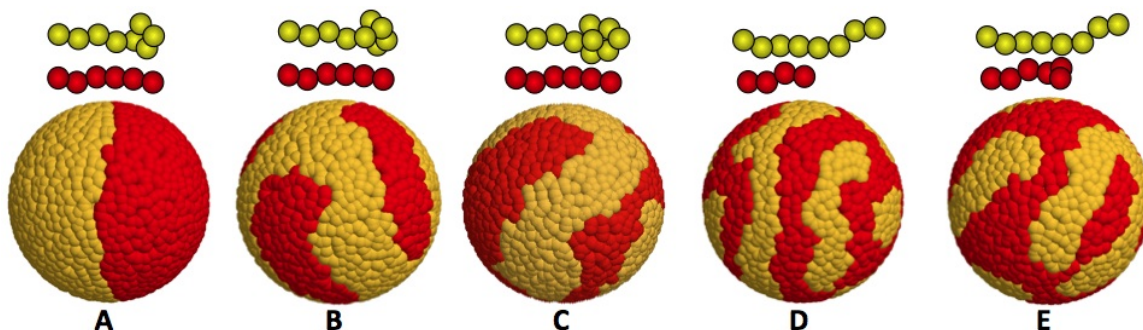


Figure 4.5 Effect of bulkiness difference on phase separated patterns formed in mixtures of incompatible surfactant chains on the surface of a sphere. The radius of the sphere is 5σ where diameter of one bead is σ . The red and yellow chains on top of each simulation snapshot indicate the number of beads in the surfactants used for that simulation. Some of the images have been taken from reference (101).

long or bulky relative to the second. In the simulations where one surfactant is long/bulky relative to the second, the long/bulky one prefers to microphase separate while the other (short/less bulky) prefers to macrophase separate. The system with one long and one bulky surfactant is interesting because both surfactants benefit from microphase separation. In Fig. 4.5D we show the case where only length difference is present between the surfactants. Since this length difference is equal to the critical length difference, the system microphase separates into stripes, as expected. On making the shorter surfactant bulky, we continue to obtain striped patterns. This shows that when one surfactant is long and the other bulky both prefer to microphase separate, causing the formation of stripes.

Comparing the system of Fig. 4.5A with that shown in Fig. 4.5E we note that the number of beads in the two surfactants in both systems are the same. Despite having the same number of beads, one (Fig. 4.5A) demonstrates complete phase separation while the other (Fig. 4.5E) forms stripes. This further emphasizes the role of entropy in stripe formation. Based on these simulations investigating bulkiness, we expect to observe microphase separation in systems for which the same surfactant is longer as well as bulkier than the other.

4.5 Effect of increasing surface coverage

In experiments it is also possible to control the surface coverage or number density of surfactant molecules on the substrate. One common way to achieve a small but uniform surface coverage is to use bulkier surfactants like adamantanethiols and carboranethiols (111–113). We have studied the effect of surface number density through DPD simulations.

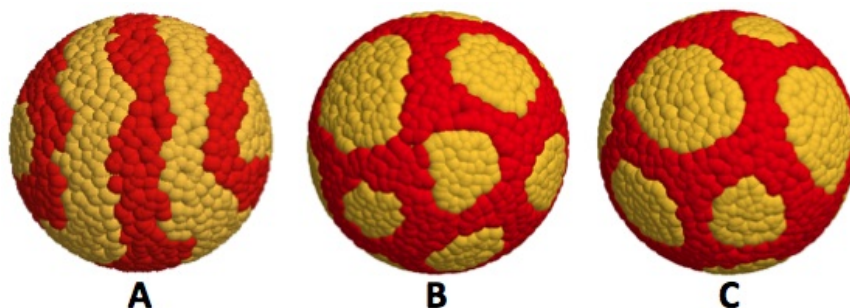


Figure 4.6 Effect of surface coverage on phase separated patterns formed in mixtures of incompatible long (yellow) and short (red) surfactant chains on the surface of a sphere. The radius of the sphere is 5σ where diameter of one bead is σ . Surface densities in number of beads per σ^2 are A. 4.0, B. 5.0, C. 6.0.

While lower surface densities like 4.0 beads/ σ^2 easily produce stripes (Fig. 4.6A), systems with higher surface coverage such as 5.0 and 6.0 beads/ σ^2 (Fig. 4.6B and C, respectively), become kinetically arrested in a patchy phase. We discuss this kinetically arrested phase in detail in Chapter 5 in the context of flat surfaces.

4.6 Effect of substrate curvature

We also investigate the effect of substrate curvature using DPD. As shown in Fig. 4.6A, we find that macrophase separation occurs on nanoparticles smaller than a critical size. Stripe-like domains are seen on nanoparticles larger than the critical size all the way up to the infinitely curved (flat) surfaces (Fig. 4.7B to E). The two important observations from these simulations are discussed below.

Prediction of Janus particles

On convex surfaces, the volume of a spherical shell at a given distance from the surface increases as we move away from the surface. For small nanoparticles that have a high degree of curvature, this increase in volume is significantly greater than that for a large nanoparticle. Hence any given surfactant chain on a small nanoparticle, like the one shown in Fig. 4.7A, will have a very large free volume (also see Fig. 4.3A) available to it for movement. A long chain therefore has sufficient entropic freedom on a small nanoparticle even without short surfactants for neighbors. Since the system already has maximum possible entropy, the energetic cost again becomes the deciding factor and macrophase separation occurs. This is

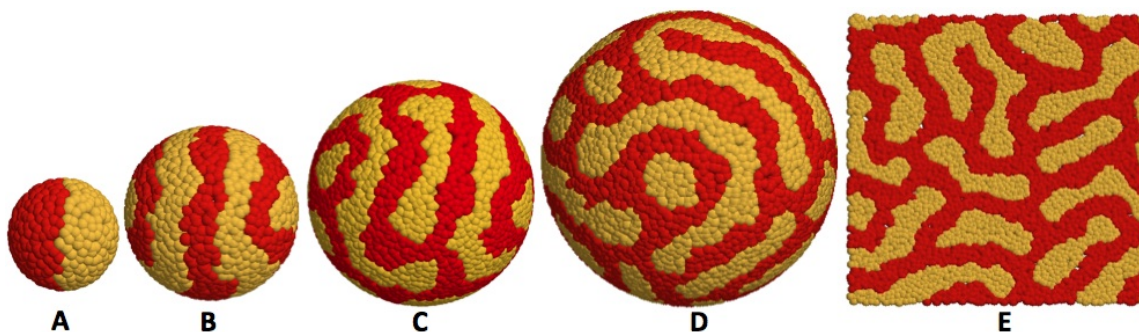


Figure 4.7 Effect of nanoparticle size on phase separated patterns formed in mixtures of incompatible long (yellow) and short (red) surfactant chains on a surface. The short and long surfactants are four and seven beads in length respectively. The radii of curvature for the surfaces shown are A. 3σ , B. 5σ , C. 8σ , D. 10σ and E. infinite. σ is the diameter of a single bead. The snapshots are not shown to scale. Some of the images have been taken from reference (101).

the first prediction of Janus nanoparticles formed using phase separating SAMs.

Prediction of a size range for formation of ordered stripes

Among the particles larger than the critical size, we see that the striped patterns form and are more aligned on smaller particles (Fig. 4.7B and C) than on larger ones (Fig. 4.7D). Defects, in the form of patches and disordered stripes, start appearing as the nanoparticles become large (Fig. 4.7D). This indicates an approximate size range in which ordered stripes might form. The lower and upper bounds for this size range are the Janus particles and patch-rich large particles, respectively.

These predictions were tested by experiments in the Stellacci group using an elegant method. They noticed that as a consequence of the ordered stripes on the nanoparticle, two poles get clearly defined. These poles were found to be highly reactive and can be functionalized using linkers such as mercaptoundecanoic acid as illustrated in Fig. 4.8 (28; 33). Once functionalized, the nanoparticles are easy to polymerize into chains that can be imaged using transmission electron microscopy (TEM). The images of such chains are shown in 4.9 taken from reference (28).

The formation of chains therefore indicates the presence of ordered stripes on nanoparticle surfaces. The absence of chains, on the other hand, indicates that either the particles were not striped or the stripes were disordered so that no clear poles were present. An analysis of experiments using nanoparticles of various sizes, performed by Carney et al. (33) revealed that chains are seen only in a certain size range of nanoparticle diameters. As shown in Fig. 4.10B the experimental range for nanoparticle diameters in which stripes form is 2nm to



Figure 4.8 Functionalization and polymerization of striped nanoparticles into chains (33).

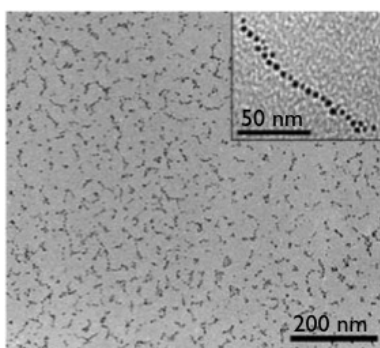


Figure 4.9 Transmission electron microscopy (TEM) images of gold nanoparticles linked through mercaptoundecanoic acid linkers into chains (28).

8nm. These experiments provide an indirect confirmation of our simulational predictions.

4.7 Comparison with atomistic simulations and experiments

Dr. Pradip Ghorai from the Glotzer group has performed atomistic molecular dynamics (MD) simulations of several equimolar mixtures of surfactants adsorbed on the surface of a nanoparticle 7.0 nm in diameter. These simulations were carried out using DL_POLY simulation software (114) with a fully flexible united atom model (115–117). Non-bonded interactions between atoms or groups of atoms on the same type of surfactants were modeled via a 6-12 Lennard-Jones (LJ) potential with a cutoff of 0.1 nm. The LJ potential parameters for the surfactants used in this study are available in references (115) and (117). Non-bonded interactions between unlike atoms or groups of atoms are modeled via the

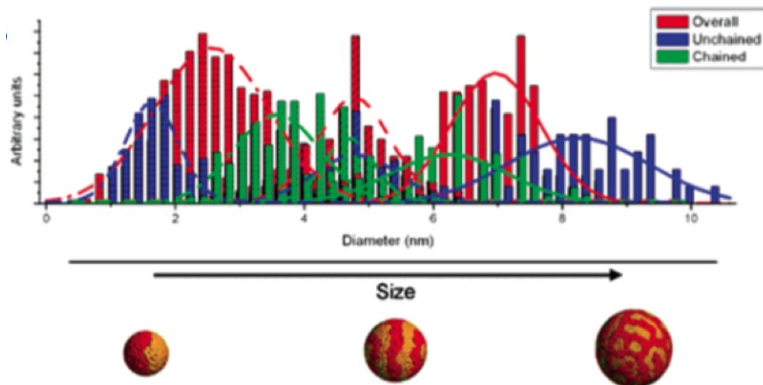


Figure 4.10 Size distributions before and after chaining for three different sets of nanoparticles. Chains form only for nanoparticles in a certain size range. Bars represent actual data; lines are Gaussian fits. Simulation images at the bottom show the patterns expected in the different size regimes. (33)

Buckingham potential without the attractive component ($U(r) = 500e^{-r/0.4}$), where r is the distance between unlike atoms/groups) and a cutoff given by the collision diameter σ_s . The simulations were carried out in the NVT ensemble using a Nosé-Hoover thermostat (77) at a temperature of 360 K. The NP surface was modeled as a sphere and the SHAKE algorithm (118) was employed to confine the surfactant head groups on the surface at a density of $0.07 \text{ chains}/\text{\AA}^2$. The surfactants were initialized in a mixed state at high temperature and the system was subsequently cooled to room temperature and allowed to evolve until no further change in structure was observed.

The simulations correspond to experimental systems selected from those studied by Jackson et al. (11). For the experiments, the synthesis of mixed ligand NPs and study of the morphology of the SAMs that comprise their ligand shell were performed according to procedures described in references (11) and (27). All the chemicals were purchased from Sigma-Aldrich and used as received. Flame annealed Au(111) on mica substrates were obtained from Molecular Imaging. SAMs were formed by immersing gold on mica substrates into a 1 mM ethanol solution (equimolar in $\text{SH}-(\text{CH}_2)_3-\text{CH}_3$ and $\text{SH}-(\text{CH}_2)_5-\text{CH}_3$), for nine days at 50°C . Substrates were removed from solution, rinsed with toluene, absolute ethanol and acetonitrile, and then air-dried. Scanning tunneling microscopy (STM) images were recorded in air using a Digital Instruments Multimode Nanoscope IIIa using an E scanner with mechanically cut platinum-iridium tips. The tip bias was between 900 to 1400 mV with set currents of 350 to 700 pA, and with tip speeds between 0.3 and $1 \mu\text{m/s}$. The integral gain used to obtain images was in the range of 0.3 to 0.65 with the proportional from 0.3 to 1.4.

Figs. 4.11(a) and (b) show the simulation results and experimental images, respectively,

of phase separated domains formed by a mixture of HS-(CH₂)₃-CH₃ (C4) and HS-(CH₂)₅-CH₃ (C6). Likewise, Fig. 4.11(c) and (d) show the simulation results and experimental images, respectively, of phase separated domains formed by a mixture of HS-(CH₂)₁₀-COOH (C11) and HS-(CH₂)₁₁-CH₃ (C12). Simulations and experiments demonstrate that stripe-like patterns form in both cases. These stripes persist, are not simply frozen patterns of intermediate or late-stage spinodal decomposition (119), and are independent of the cooling rate. In Fig. 4.11(a) and (b), the surfactants differ only in length, and in 4.11(c) and (d) they differ only in the tail-end group. For mixtures of short surfactants, e.g. HS-(CH₂)₂-COOH and HS-(CH₂)₂-CH₃, atomistic simulations show bulk phase separation despite the difference in bulkiness of the tail-end group (Fig. 4.11(e)). This demonstrates that for small enough molecular lengths, adsorbed surfactant mixtures behave as simple incompatible binary mixtures, in which contribution from the tail lengths is negligible. These short surfactants are equivalent to single-bead surfactants in DPD which, in the absence of conformational entropy considerations, will completely phase separate. Therefore, in both atomistic and DPD simulations, short surfactant mixtures undergo complete phase separation while for longer molecular lengths, microphase separation occurs. Stripe widths measured from several other experimental and corresponding simulational results are in good quantitative agreement (Fig. 4.11(f)).

Images from atomistic simulations and experiments showing phase separated domains in a mixture of HS-(CH₂)₃-CH₃ (C4) and HS-(CH₂)₅-CH₃ (C6) on flat surfaces also show good quantitative agreement (Fig. 4.12). These images are qualitatively the same as the images obtained from DPD simulations on flat surfaces shown in Fig. 4.7E. Therefore both, atomistic and experimental results, support our hypothesis that a difference in bulkiness and length can lead to formation of striped domains in SAMs on surfaces.

4.8 Geometric scaling relation for stripe width

Because stripe spacing depends on relative tail lengths and the radius of curvature of the substrate, it is physically intuitive to expect a geometric scaling relation for stripe spacing as a function of these parameters. We find that although it is straightforward to establish general trends (e.g. stripe thickness decreases with increase in surfactant length difference), it is not trivial to predict the stripe width for an arbitrary system. Our simulations appear to be in a cross-over regime between weak and strong segregation, where a purely geometric scaling relation is not possible. Nevertheless, it is useful to construct simulation-based phase diagrams describing regions in which stripes will form, and also plots estimating

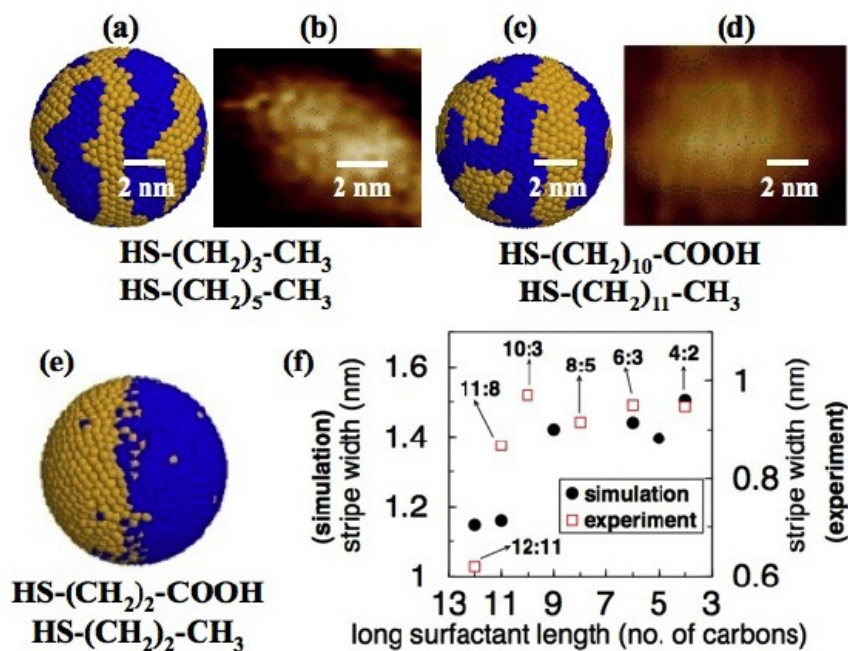


Figure 4.11 (a) and (b) C4:C6 SAMs from atomistic simulations and experiment, respectively. The tail-end groups are identical, but the lengths differ. (c) and (d) Dodecanethiol/ Mercaptoundecanoic acid (C11:C12) SAMs from atomistic simulations and experiment, respectively. Here the tail-end groups differ somewhat in size and the tail lengths are nearly identical. (e) Atomistic simulation of mixture of equal-length (C3:C3) surfactants, with different tail-end groups. For atomistic snapshots, blue (dark) and yellow (light) beads are head groups of surfactants that are short (or contain -COOH) and long (or contain -CH₃), respectively. In all cases, the head groups (-SH) are identical. (f) Variation of stripe width with the length of long surfactant in number of carbon atoms. The same trend is seen when stripe width is plotted against short surfactant length. The atomistic simulation data points are for equal-length surfactants. (101)

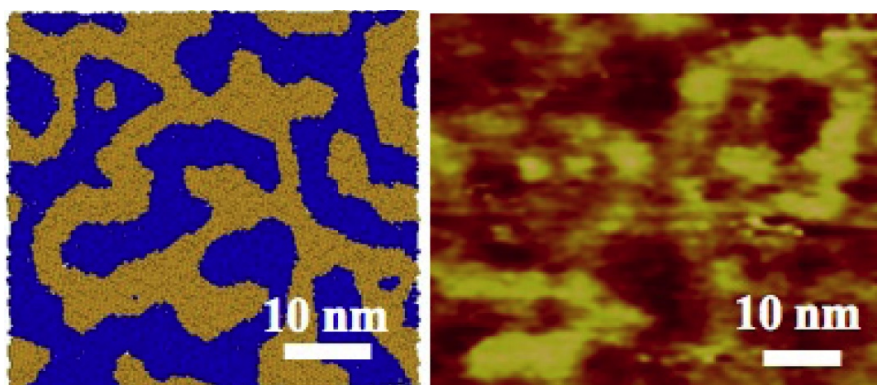


Figure 4.12 Images from atomistic simulations (left) and experiments (right) showing phase separated stripe-like patterns in SAMs on flat surfaces (101).

stripe width as a function of absolute surfactant lengths, length differences and substrate curvature. We have developed an Ising-type model that can be used to estimate and compare the conformational entropies and free energies of different arrangements of surfactants on a surface (120). This model is described in detail in Section 8.2.1. Since lattice Monte Carlo simulations using this model are much faster computationally than DPD, we are currently using it to generate phase diagrams and stripe-width plots.

4.9 Summary

Using simulations, we verified the formation of unusual and unexplained, nanoscale striped patterns in surfactant-coated gold nanoparticles. Based on our results discussed in this chapter, we were also able to provide an explanation for the formation of striped patterns based on an entropic argument. Traditionally, a discussion of energetic and entropic contributions in phase separation refers to configurational entropy of the two components. Our entropic explanation is however, is based on the conformation entropy of polymer chains, which is a new idea in the context of phase separating SAMs. Our minimal model, based only on incompatibility and length/bulkiness difference between grafted surfactant chains, predicts that a minimum length/bulkiness difference is required for formation of stripes. Below this critical difference in length or bulkiness, the surfactants would macrophase separate, as expected for simple incompatible mixtures.

In terms of design rules for obtaining desired patterns on nanoparticle surfaces, we have made several important predictions. These are summarized below.

Janus particles

We predict that Janus particles can form due to phase separation in SAMs on nanoparticle surfaces. Apart from the obvious case of SAMs comprised of highly immiscible surfactants, we predict that Janus particles can form in three cases: when nanoparticles are very small so that microphase separation is not required for long chains to gain conformational entropy; when length/bulkiness difference between the surfactants is small and conformational entropy gain is not large enough to overcome energetic penalty for microphase separation; and when the absolute length of the surfactants is small so that they behave as simple immiscible mixtures.

Stripes

We predict that stripes will form when a sufficient length or bulkiness difference is present between the surfactants to make microphase separation entropically favored. If ordered stripes are desired, nanoparticles in a certain size range should be used. Experimentally, this size range was found to be 2nm to 8nm diameter nanoparticles. In this range of nanoparticle diameters, the microphase separated stripes have a high tendency to align parallel to each other clearly defining two poles which can act as attractive, repulsive or reactive patches on nanoparticle surfaces. On large nanoparticles (> 10 nm in diameter), patches form along with stripes resulting in disordered stripes. However, if allowed sufficiently long time to evolve these defects should disappear and ordered stripes should form. Such large equilibration times are difficult to achieve in experiments as well as simulations.

Patches

Patches will form in SAMs on nanospherical surfaces when the surface coverage i.e. number of surfactants per unit surface area, is high. They will also form as defects when the nanoparticles are large. In both cases, patches form because the system requires large equilibration times to form the equilibrium striped phase.

Our simulations therefore provide useful guidelines for tailoring surface patterns to design desired patchy particles or nanobuilding blocks to be used in self-assembling higher order structures from the bottom-up.

Chapter 5

Striped versus patchy pattern formation in phase-separating mixed SAMs on flat surfaces

In this chapter we report the results from our DPD simulations for phase separation in mixed SAMs on flat surfaces. We investigate a long-standing controversy regarding nanoscale striped vs. patchy phase separation in mixed self-assembled monolayers on flat substrates. We provide simulation evidence to show that for symmetric mixtures of immiscible surfactants of different lengths, stripes are always the favored equilibrium phase while patches are a kinetically arrested, non-equilibrium phase. We further analyze how the phase-separated patterns depend on the composition of the two surfactants, measured in terms of the fraction $\phi = (\text{number of long surfactants})/(\text{total number of surfactants})$. In this thesis, we refer to kinetically-arrested, disordered islands of one species in a matrix of the other species as patches while equilibrium, ordered islands are called two-dimensional (2D) micelles. We show that depending on the surfactant lengths either aligned stripes or ordered, two-dimensional micelles can form in asymmetric mixtures. We show here that phase separating mixed SAMs can potentially be used to create nanoscale periodic patterns less than 5nm wide on flat surfaces as on nanoparticle surfaces. In terms of ordering of patterns, both aligned stripes and hexagonally-ordered two-dimensional (2D) micelles, can be obtained by changing the relative composition of the co-adsorbed surfactants. Preliminary experimental results confirm our simulation predictions and show that less than 5nm 2D micelles can be obtained using phase separating SAMs on flat surfaces. These micelles are more monodisperse in size and circular in shape than the irregularly shaped patches of various sizes reported in prior experimental studies. Finally, we discuss a novel interfacial instability that spontaneously occurs in simulations of initially de-mixed symmetric mixtures and ultimately leads to the striped pattern. The results presented in this chapter are presented in the reference (121).

5.1 Introduction

Phase-separating mixed SAMs, in which more than one type of surfactants are co-adsorbed on the substrate, have important applications in the areas of catalysis, nanoelectronics and sensing (11–15). Further, mixed SAMs are important because they form patterns that are similar to those formed in cell membranes and proteins (122) and also because the shapes and dimensions of phase-separated patterns strongly affect the wetting behavior and other properties of the substrate (12; 29). While for these applications, the most important attribute of the surfactant-coated surface is the domain size, for several other applications ordering of domains on the surface is an additional requirement. These include fabrication of high-density and high-speed storage media, nanoporous filters, nanoscale transistors and capacitors, ceramic membranes, photonic crystals and electrophoresis media (123–130). Block copolymer thin films are currently the preferred material for creating nanoscale patterned templates for such applications (131–133). The feature size of patterns in block copolymer thin films ranges between 5nm and 50nm (131). It was recently shown that phase separation in mixed SAMs creates ordered stripes less than 5nm wide, when present on nanoparticle surfaces (11). Studies investigating the size and periodicity of domains in SAMs on flat surfaces have not demonstrated such feature sizes and ordering (8; 16–21). The smallest feature sizes observed in mixed SAMs on flat surfaces are ~ 5 nm, similar to block copolymer feature sizes. The domain shapes that have been reported vary from irregular patches with highly non-uniform size distributions to disordered stripes (8; 16–21). In this chapter, we investigate the possibility of using phase-separating SAMs to pattern substrates on a nanometer scale.

5.2 Contradicting experimental observations

As described briefly in Section 2.3.1, different nanoscale striped and patchy patterns have been observed in SAMs on flat surfaces. STM images of some of these patterns are shown in 5.1. Figs. 5.1A and B show stripe-like patterns from (21) and (20), respectively. Figs. 5.1C and D show elongated patches and merging patchy patterns from reference (19). As illustrated by these images, all experimental studies agree that nanoscale phase separated patterns form in mixed SAMs on flat surfaces. However, there is a disagreement on the shape of the domains. In a survey of available experimental literature, we found that stripe-like domains have been observed in SAMs on flat surfaces in some but not all experiments (20; 21; 101). Several other experiments (8; 17; 19) report presence of only patchy domains. It was also concluded that the patterns are not equilibrium patterns since images

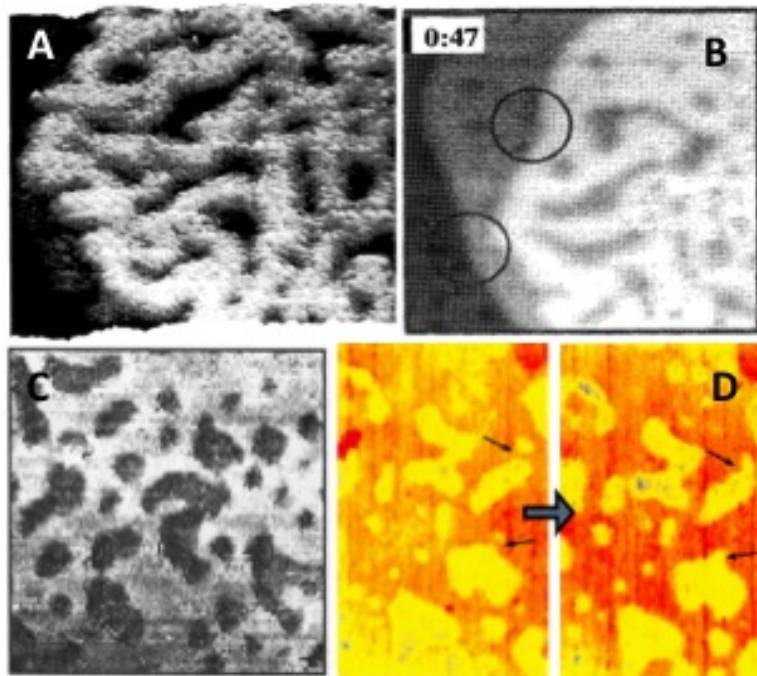


Figure 5.1 Experimental, STM images of striped and patchy phase separated patterns imaged in mixed SAMs on flat surfaces taken from references (19-21).

at progressing times show that small patches merge into big patches to form even bigger domains. Since the phase separation in SAMs is a slow, kinetically-controlled process (17), equilibrium configurations are often difficult to access in experiments. In this chapter, we revisit mixed SAMs on flat surface and address the question of whether patches or stripes are the equilibrium pattern in symmetric mixtures on flat surfaces.

Based on our discussion in Section 4.2, we expect that the entropic argument is valid on flat as well as nanoparticle surfaces and therefore, microphase separated domains should be observed in experiments on flat surfaces. The entropic argument we presented in Section 4.2, explains the formation of microphase separated domains but does not predict whether the domains will be stripe-like or patchy. We therefore use our newly developed simulation model and code to investigate the controversy of striped vs. patchy phase separation in mixed monolayers.

5.3 Simulations of symmetric mixtures

We use the term "symmetric mixtures" to refer to mixtures in which both surfactants are in equal numbers. We define an asymmetry fraction $\phi = (\text{number of long surfactants})/(\text{total$

number of surfactants) to measure degree of "asymmetry". For symmetric mixtures, $\phi = 0.5$. In this section we describe our simulation results for symmetric mixtures. Results for asymmetric mixtures are described in Section 5.4.

5.3.1 Effect of length difference, surface coverage and degree of immiscibility

Figure 5.2A shows the temporal progression of phase separation in immiscible surfactants of equal lengths. As expected, they undergo complete thermodynamic phase separation via spinodal decomposition (134; 135). On increasing the length difference Δl (Fig. 5.2B and C), we see that the mixtures no longer completely phase separate, but instead microphase-separate into a striped phase. We see that the evolution of phase separation in equal-length (Fig. 5.2A) and unequal-length (Fig. 5.2B and 5.2C) surfactant mixtures appears similar during the initial stages, in that, small patches of the long species are formed early-on in both cases. Beyond this point, for equal-length mixtures, the islands continue merging until complete phase separation occurs. In contrast, for surfactants with sufficient difference in length, the merging of patches is accompanied by elongation of the domains and continues until a stable striped phase is obtained. All our simulations of surfactant mixtures with a length mismatch of five or more beads evolve to a stable striped phase. This conclusion is based on multiple runs for each surfactant system and a variety of initial configurations. In all these simulations patches may form as an intermediate phase but the equilibrium pattern is always striped. Even on varying surface coverage ρ (Fig. 5.2D) and Δa (Fig. 5.2E) over a fairly wide range, we always observe a predominantly striped phase. All the striped phases appear to evolve towards a perfect lamellar (aligned stripe) configuration, which exceeds the time scale of our simulations when ρ or Δa is high. (We note that defect-free parallel lamellae are formed in 12 million time steps for $\rho = 3.0$ while for $\rho = 4.0$, it would take more than 30 million time steps to form them, equivalent to 400 CPU hours on a 2.3GHz AMD Opteron processor). Similarly, for $\Delta a = 5$, perfect parallel lamellae are formed in as few as 2 million time steps while lamellae formed for $\Delta a = 10$ and 20 are not defect-free even at 14 million and 32 million time steps, respectively. Based on simulations spanning over a wide range of Δa from 5 to 80 (results not shown), we find that narrower domains are formed for small Δa (weakly immiscible surfactants or weak segregation) as compared to domains formed for larger Δa (strongly immiscible surfactants or strong segregation).

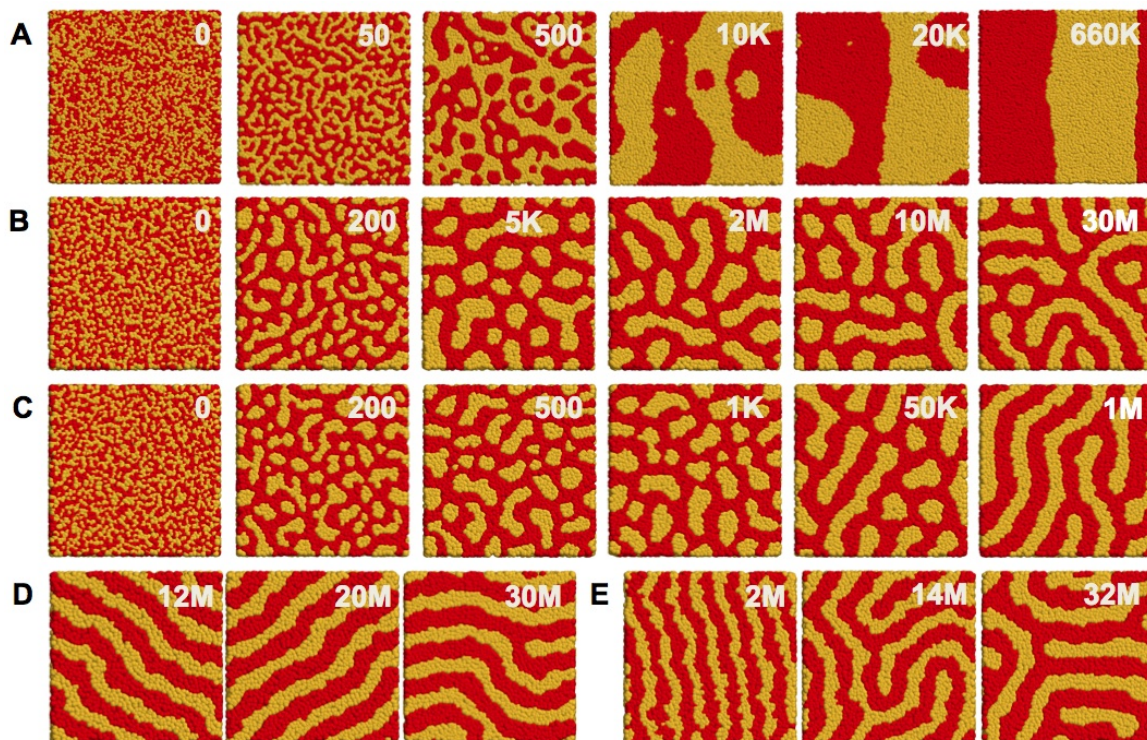


Figure 5.2 A. to C. Simulation snapshots of phase separation in symmetric ($\phi = 0.5$) mixtures at surface density of $\rho = 4.0$ of immiscible ($\Delta a = 15$) surfactants of various lengths of short and long surfactants, respectively. A. 4 and 4 (equal-length mixture), B. 4 and 9, C. 4 and 14. Snapshots from left to right show progression of phase separation in time. The number in the top right corner indicates the time step at which the snapshot was taken, where K refers to thousands and M refers to millions of time steps, D. Simulation snapshots of equilibrium patterns formed for unequal length surfactants (4, 13 beads long) with ρ of 3, 3.5 and 4, respectively, from left to right. E. Simulation snapshots of patterns formed for unequal length surfactants (4, 13 beads long) with Δa of 5, 10 and 20, respectively, from left to right. Red (dark) and yellow (light) beads represent short and long surfactant head groups, respectively. Surfactant tails have been removed for clarity. (121)

5.3.2 Effect of different starting configurations

Based on the results shown in Fig. 5.2, a possible explanation for the frequent imaging of patchy structures in experimental setups is that after patches are formed, the process of merging and elongation is so slow that the equilibrium, striped phase is never reached. To test this hypothesis, we simulate phase separation in a system that is likely to form patches and is also likely to become kinetically arrested once they form. Comparing results shown in Fig. 5.2, we find that surfactants with smaller Δl (Fig. 5.2B) form more patchy domains than those with larger Δl (Fig. 5.2C). From Figures 5.2D and 5.2E, we find that systems with a large Δa or a large ρ require more time to form the perfect lamellar configuration because both factors hinder diffusion of the head groups. We therefore simulated a system

with a small length difference of $\Delta l = 3$, strong segregation $\Delta a = 15$ and high density $\rho = 4.0$. This combination of parameters has a strong likelihood of causing the system to become kinetically arrested. We find that, unlike the mixtures with large length differences (Figs. 5.2B and 5.2C) that evolve into the same final striped pattern irrespective of the starting configuration, simulations of this system lead to different patterns when started from different initial configurations. The time evolution snapshots of the phase separation process in this system starting from two extreme configurations - uniformly mixed and completely separated, are shown in Figures 5.3A and 5.3B, respectively. Other initial configurations and their corresponding final patterns are shown in Figures 5.3C to 5.3J. The initial configuration closest to the initial state in an experiment is the uniformly mixed configuration (Fig. 5.3B). This is one of the configurations that evolves into patches, which is also the pattern seen in several experiments (8; 17; 19). Further, we observe that patches in Figure 5.2B continuously merge to form fewer and larger patches as the simulation progresses, which is also consistent with observations in experiments (8; 17; 19). On the other hand, stripes (Fig. 5.3A) never break up to form patches and consistently evolve towards parallel lamellae. Thus although our simulations demonstrate that stripes are the equilibrium pattern, kinetically trapped, slowly merging patches may arise in experiments and simulations under certain conditions.

To further establish that patches are kinetically arrested intermediate structures, we introduce local perturbations by merging neighboring patches into larger patches, to test whether the system returns to a state of smaller patches or evolves away from it. Computationally this is done by choosing a large patch and moving all the surfactants from 2-3 neighboring patches into this larger patch. This is possible in DPD since the beads are soft and are allowed to overlap each other. After moving the small patches into the larger patch, holes are left in the places where the small patches were present and the large patch becomes denser in the number of surfactants. The simulation is started from this non-uniformly dense configuration. The density becomes uniform again in a few hundred time steps. On continuing the simulation we find that instead of breaking up into smaller patches, these large patches elongate into stripe-like domains (Fig. 5.3K). This further demonstrates that patches are only an intermediate, kinetically arrested pattern.

Next, we compare the pairwise potential energies, U , and the interface lengths, L , in terms of percentage of long surfactants at the interface, to understand why stripes are preferred over patches in symmetric mixtures of immiscible surfactants with sufficiently mismatched lengths. Both configurational and conformational entropies in these systems are large when long surfactants are next to short ones (101). Therefore, the percentage of long surfactants at the interface between the long and short surfactants can be used as an

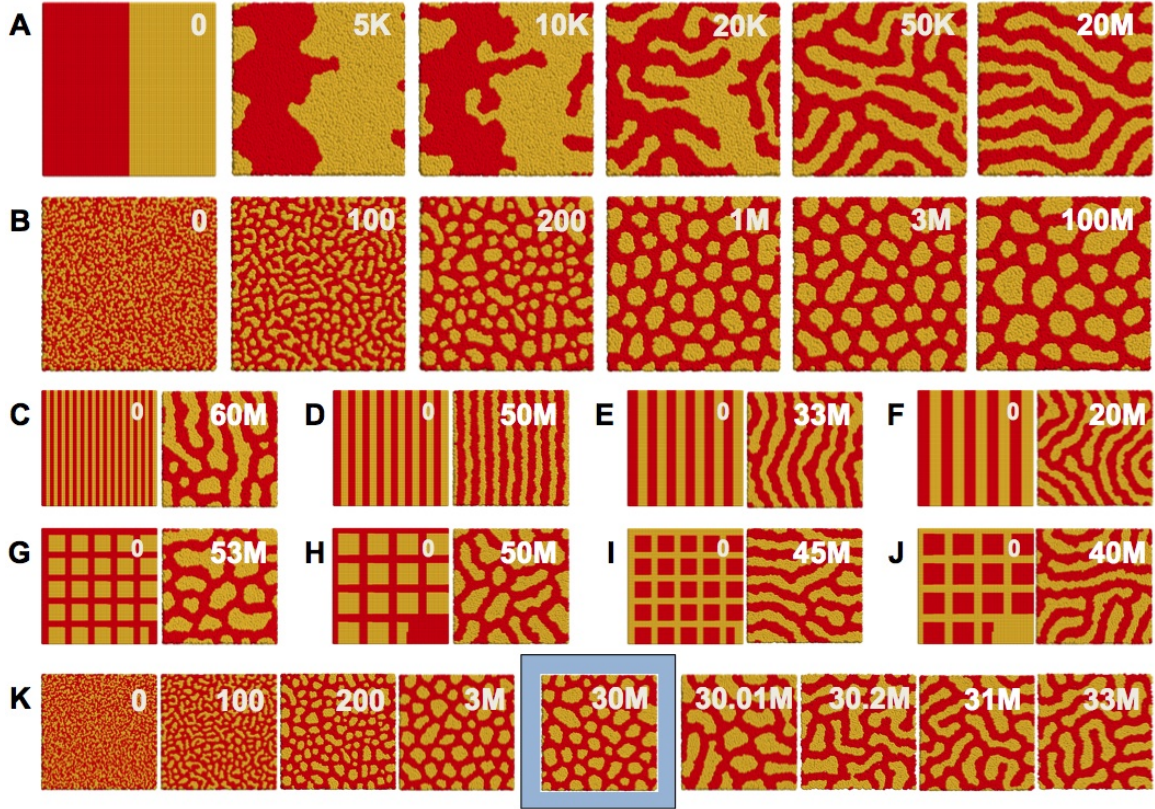


Figure 5.3 Simulation images of phase separation in symmetric mixtures ($\phi = 0.5$) of 4-bead (red) and 7-bead (yellow) surfactants starting from different initial patterns. A. and B.: Evolution starting from completely separated and uniformly mixed configurations, respectively. The number in the top right corner is the time step at which the snapshot was taken, where K refers to thousands and M to millions of time steps. C. to J.: Initial (left) and final (right) patterns. K. Phase separation in the system shown in B, continued after locally perturbing the system after 30 million time steps. The blue square indicates the perturbed configuration. Snapshots to the right of the blue square show evolution of the perturbed state. (121)

estimate of entropy of these systems. Patterns with smaller U are energetically favored, while patterns with larger L are entropically favored. Bar graphs of U and L for the final patterns shown in Figure 5.3A to 5.3J are plotted in Figure 5.4. We find that the values of U for different patterns are nearly the same (standard deviation = 0.006). L values for different patterns are fairly different especially that of parallel lamellae (Fig. 5.3D). Parallel lamellae have significantly higher L (50% higher than the average L). This is an indication that the potential energies of all patterns are roughly the same but the entropy of parallel lamellae is significantly greater than that of any other pattern. Based on these observations, we infer that the tendency towards stripes is strongly entropy-driven and the equilibrium pattern for symmetric mixtures of immiscible surfactants of sufficient length mismatch is

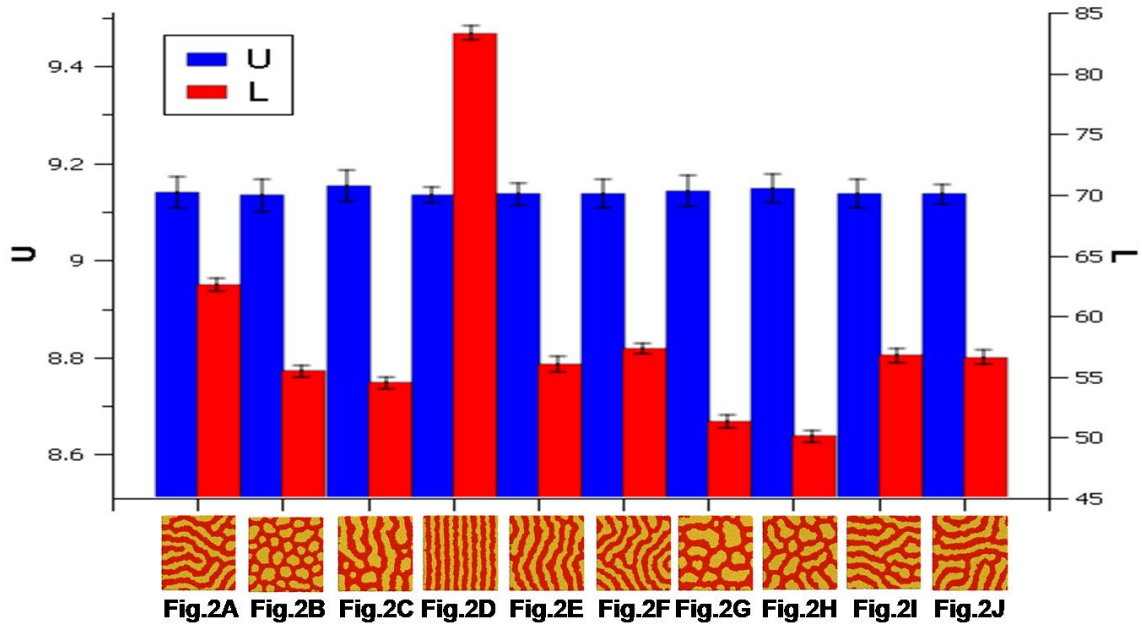


Figure 5.4 U (blue) and L (red) for different final patterns shown in Figs. 5.3A to J. (121)

parallel lamellae.

5.4 Simulations of asymmetric mixtures

In this section we report our results for asymmetric mixtures with asymmetry fraction ϕ varying between 0.20 and 0.80. We also show the results for $\phi = 0.5$ (symmetric mixtures) for comparison.

5.4.1 Varying relative composition and degree of immiscibility

After determining the effect of length difference, immiscibility, density and initial configuration on phase-separated patterns in mixed SAMs, we now study the patterns formed by mixtures of varying compositions ($0.17 \leq \phi \leq 0.83$). Figure 5.5 shows the simulated patterns formed by mixtures of varying compositions and immiscibilities but with identical surfactant lengths and densities.

For weakly immiscible mixtures (Fig. 5.5A), irregular domains are formed and both patchy and elongated domains are observed. As we increase the immiscibility, the interfaces become more regular and the domains elongate and become larger and fewer (Figs. 5.5B to

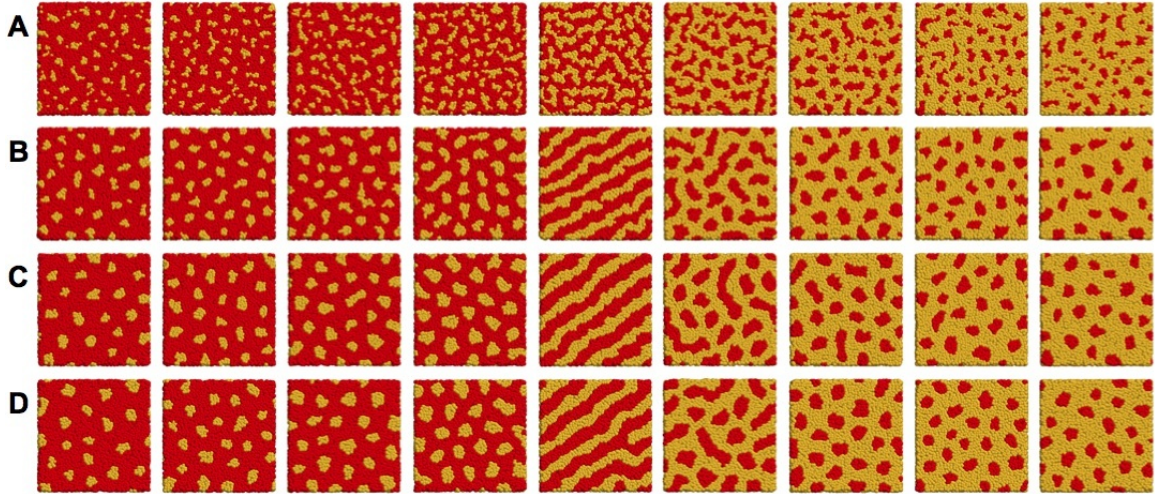


Figure 5.5 Simulation snapshots of microphase separation in asymmetric mixtures of 4 bead (red) and 13 bead (yellow) surfactants for increasing fraction of long surfactants $\phi = 0.17, 0.20, 0.25, 0.33, 0.50, 0.67, 0.75, 0.80, 0.83$ (from left to right). A. $\Delta a = 5$; B. $\Delta a = 10$; C. $\Delta a = 15$; D. $\Delta a = 20$. (121)

5.5D). For all asymmetric mixtures with a majority of short surfactants ($\phi < 0.5$), we find that 2D micelles are the equilibrium phase. Note that we refer to these domains as "micelles" in the spirit of 3D micelles in surfactant and block copolymer systems. As discussed later in this section, these 2D micelles are an ordered (Section 5.4.3), equilibrium phase (Section 5.4.2) as opposed to the patches discussed in Section 5.3. There is a sharp transition to the expected striped phase for symmetric mixtures ($\phi = 0.5$). Striped domains are present up to $\phi = 0.67$ beyond symmetric mixtures, and disappear as the ratio is increased further.

5.4.2 Two-dimensional micelles as the equilibrium phase

It is evident from the results shown in Fig. 5.5 that the patterns are not completely symmetric about $\phi = 0.5$, as they would be for binary mixtures with no symmetry-breaking parameter(s), e.g. mixtures of unlike point charges (109), or diblock copolymer melts (78). This is because the short surfactants always prefer to completely phase separate while long surfactants prefer to create interfaces, depending on entropic and energetic considerations.

We calculate the interface lengths for all the patterns shown in Fig. 5.5, similar to the analysis done in Section 5.3.2 and shown in Fig. 5.4. A plot of L for patterns from Figure 5.5D shows that there is a continuous decrease in the percentage of long surfactants at the interface as ϕ increases (Fig. 5.6). The values of L for mixtures with $0.17 \leq \phi \leq 0.50$ are comparable with the L value of perfect lamellae (Fig. 5.3D). Therefore, 2D micelles are

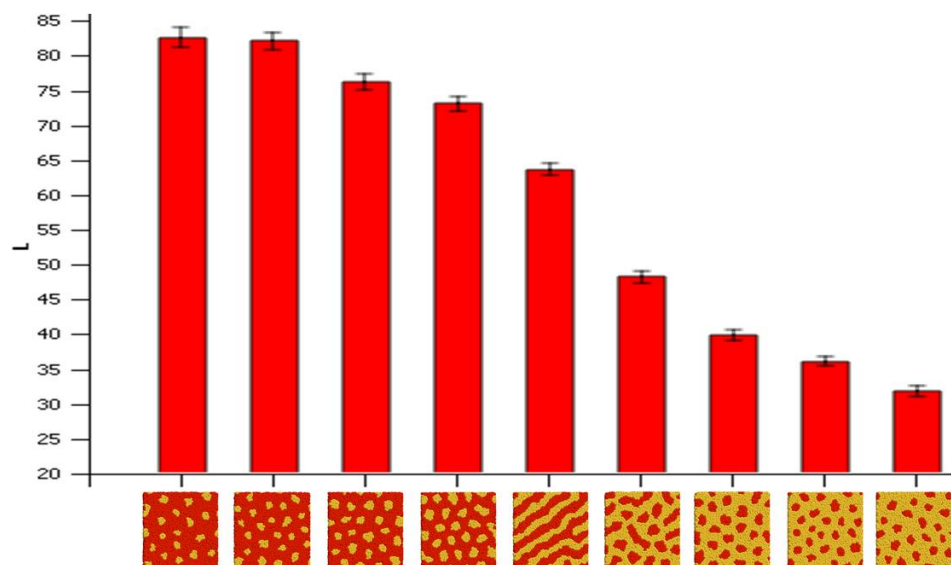


Figure 5.6 L for patterns from Fig. 5.3D and an arbitrary striped pattern at $\phi = 0.83$ (enclosed in blue square). (121)

expected to be entropically stabilized. The L values for the other patterns ($\phi > 0.5$) are small but comparison with the L for an arbitrary striped configuration with $\phi = 0.83$ (Fig. 5.3) shows that stripes, if formed, would have an even lower percentage of long surfactants at the interface and hence are entropically less favored than micelles for this composition. The L for these ratios ($\phi > 0.5$) can only be increased by phase separating into smaller domains and is maximized when the two species are uniformly mixed. However, those patterns will have very high values of U and are therefore not formed. This analysis explains why symmetric mixtures prefer to form stripes while sufficiently asymmetric mixtures form micelles. In experiments it is difficult to control the composition of the surfactants on the flat surface. This is probably why close-to-symmetric mixtures and perfect stripes are difficult to obtain in experiments. This is likely another reason for frequent imaging of the patchy or micellar phase in experiments.

5.4.3 Micelle ordering

An analysis of the radial distribution functions and micelle coordination numbers of the micellar patterns of Figure 5.5D shows that the local order of the micelles is hexagonal (Fig. 5.7), similar to mixtures of unlike point charges and diblock copolymer melts. The coordination number for the micelles (number of micelles nearest to any given micelle) is equal to 6.0 (within 4% error), predicting hexagonal packing (Fig. 5.7). The coordination


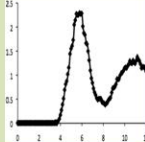

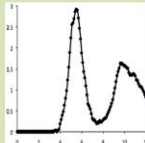

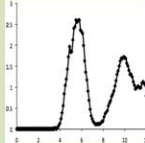

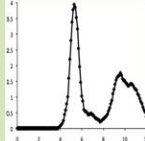
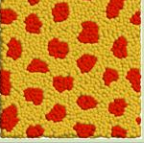
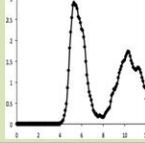

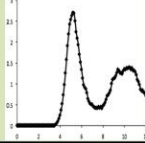
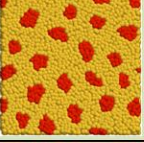
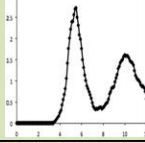
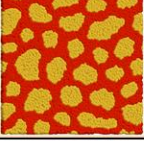
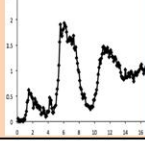
ϕ	Image	RDF plot $g(r)$ vs. r	Coordination number	Average domain size
0.17			6.22	15.16 ± 3.31
0.20			6.08	16.30 ± 3.96
0.25			6.03	20.57 ± 5.20
0.33			5.83	27.43 ± 7.50
0.75			6.00	22.60 ± 5.31
0.80			6.05	15.62 ± 3.53
0.83			5.93	13.71 ± 3.22
0.50			5.46	87.50 ± 34.04

Figure 5.7 The figure shows, in tabular form, plots of the radial distribution functions (RDF), $g(r)$ of centers of mass of micelles shown in Fig. 5.5D and patches shown in Fig. 5.3B. The nearest neighbor micelle/patch coordination numbers were calculated by integrating over the first peak in $g(r)$ plots. The table also lists the average domain (patch/patch) size and the standard deviation in the domain size. The large standard deviation of the patch size distribution relative to standard deviations of the micelles indicates that the patches are non-equilibrium while micelles are equilibrium patterns. Note that the terms patch and micelle have been selected to mean kinetically-arrested, non-equilibrium islands versus equilibrium islands, respectively. Since the number of patches/system is small, we were only able to study order up to second nearest neighbors. Simulating larger systems is computationally expensive and was not undertaken. (121)

number corresponding to hexagonal order and a highly uniform size distribution of the micelles (as determined from standard deviations of micelle sizes; Fig. 5.7) together suggest that the micellar phase is the equilibrium phase. Similar analysis for the patches formed in Fig. 5.3B yields a coordination number of 5.46 and a large standard deviation of 34.04 in the average patch size of 87.50 (Fig. 5.7), further confirming that the patches formed for symmetric systems are non-equilibrium and kinetically-arrested.

5.4.4 Varying relative composition and length difference

We have also performed simulations for asymmetric mixtures of different surfactant length differences. Figure 5.8 shows the results of these simulations for $0 \leq \Delta l \leq 9$. We find that for $\Delta l < 3$ (Fig. 5.8A to C), complete phase separation is seen for all values of ϕ . Also, all asymmetric mixtures with $\Delta l \geq 3$ and $\phi < 0.5$ (i.e. majority short surfactants) form micelles (Fig. 5.8D to H). For highly asymmetric mixtures with majority long surfactants, stripes are formed in a very narrow range of $3 \leq \Delta l \leq 5$. In this range, the length difference is sufficient for microphase separation ($\Delta l > 3$) but not large enough to favor the high-entropy micellar phase as per the discussion of Section 5.4.2 and the analysis shown in Fig. 5.6. For $\Delta l > 3$, the behavior is as shown in Fig. 5.5.

5.4.5 Comparison of DPD results with experiments

Experiments have also been performed on asymmetric SAMs on flat surfaces in the Stellacci group. For these experimental studies, the substrates used were commercially available, thermally evaporated Au(111) films on freshly cleaved mica (Molecular Imaging). To obtain a homogenous monolayer in which the lying down phase (136) was absent (as confirmed by extensive imaging), the as-received substrates were cleaned by immersing them in Piranha solution for five minutes, followed by cleaning with deionized water and drying through a nitrogen flow. SAMs comprised of varying combinations and compositions of octanethiol, mercaptopropionic acid, butanethiol, nonanethiol, pentanethiol and 3-mercapto-1-propane sulfonic acid were investigated. All SAMs were prepared by immersion in ethanol for five days followed by a thorough rinse with ethanol and acetonitrile and were imaged using a Digital Instrument Multimode Nanoscope IIIa scanning tunneling microscope (STM). Additional experimental details are available in reference (137).

Figure 5.9 shows the STM images obtained for symmetric and asymmetric SAMs on flat surfaces. Striped domains that are less than 5nm wide, imaged for a symmetric mixture of hexanethiol and dodecanethiol, are shown in Fig. 5.9A and B. Comparison with prior

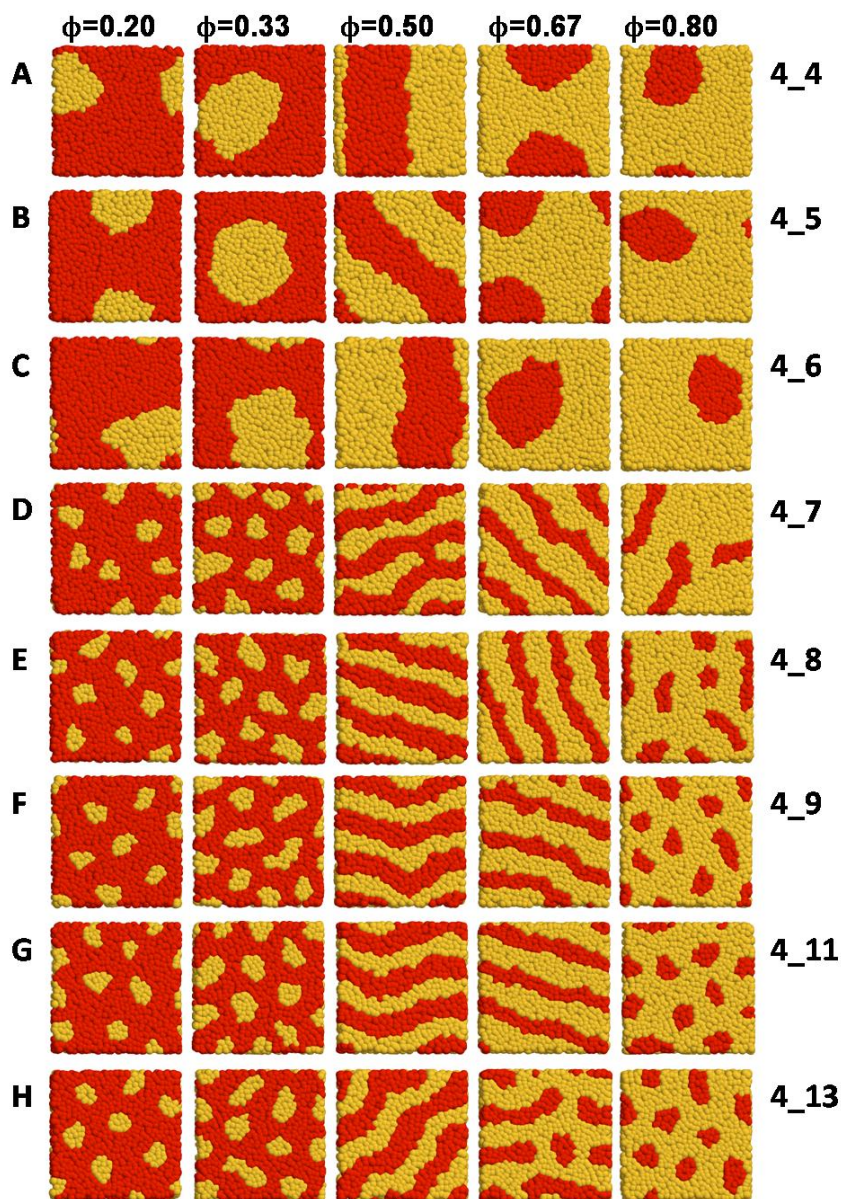


Figure 5.8 A. to H.: Equilibrium patterns formed by asymmetric and symmetric mixtures of surfactants with increasing length differences. A. to C.: $\Delta l < 3$. Complete phase separation is seen for all values of ϕ ; D. to H.: $\Delta l \geq 3$. All asymmetric mixtures with $\phi < 0.5$ form patches. Stripes are formed by all symmetric and asymmetric mixtures when $0.5 \leq \phi \leq 0.67$. For highly asymmetric mixtures with a majority of long surfactants ($\phi > 0.67$), stripes are formed for a very small range of $2 < \Delta l < 5$ while patches are formed for all larger values of Δl . As shown in Fig. 5.6, ordered, 2D micelles are entropically preferred over stripes for highly asymmetric mixtures with a majority of long surfactants. When Δl is large (> 4 beads), the gain in conformational entropy for long surfactants by forming patches is large. However when Δl is just sufficient for microphase separation ($2 < \Delta l < 5$), the conformational entropy gain for the long surfactants by forming micelles is small and stripes are energetically and entropically favored. (121)

experimental studies of patchy domains (8; 17; 19) in flat SAMs demonstrates that the images shown in Figure 5.9 are considerably more monodisperse and regular in shape. All images shown in Figure 5.9, are comprised of domains smaller than 7 nm and some, smaller than 5 nm. The ordering of domains, as predicted by simulations, is however, is not seen in these experiments. One of the reasons is the presence of etch pits in the substrate, seen as the dark regions in the STM images. The etch pits disrupt the surface continuity and reduce the possibility of ordering. Other possible reasons include long equilibration times, presence of anisotropic stress in the substrate prior to adsorption and presence of defects in the form of single molecules or smaller clusters that, if given sufficient time, would merge into the larger domains. More images, including some showing patches of short surfactant in a matrix of longer ones will appear in a forthcoming publication (121). Analysis of all these images confirms the presence of order and relative monodispersity in size and shape of the domains as compared to all previously published studies (8; 17; 19).

5.4.6 Comparison with other phase-separating mixtures confined to flat surfaces

As discussed earlier, block copolymer thin films are commonly used to pattern substrates. Block copolymers are made up of two immiscible polymeric segments chemically bonded to each other. The immiscibility between the two segments provides the short-range attraction while the chemical bond provides the long-range repulsion. Patterns vary depending on whether the block copolymers are symmetric, i.e. the two immiscible segments are of the same length, or asymmetric i.e. the segments are of different lengths. Symmetric block copolymers are known to form lamellae (131–133; 138) while asymmetric block copolymers form hexagonally-ordered dots (132; 133; 139) when confined to flat surfaces. A similar behavior is seen in mixtures of incompatible, unlike point charges confined to flat surfaces (109; 140; 141). In this system, the immiscibility between the two species provides the short-range attraction while the electrostatic repulsion between similar charges is the long-range repulsion. The charge ratio between the two species can be varied to obtain symmetric (charge ratio = 1) and asymmetric (charge ratio \neq 1) mixtures. In asymmetric mixtures, the number of point charges of each type and the charge on each species are different while the electroneutrality of the system is maintained. Similar to block copolymer thin films, mixtures of charged particles also form lamellae or ordered dots depending on whether the mixture is symmetric or asymmetric, respectively (109; 140; 141).

Patterns formed in our system of phase-separating SAMs on flat surfaces are therefore very similar to the patterns formed in block copolymer and unlike point charge systems

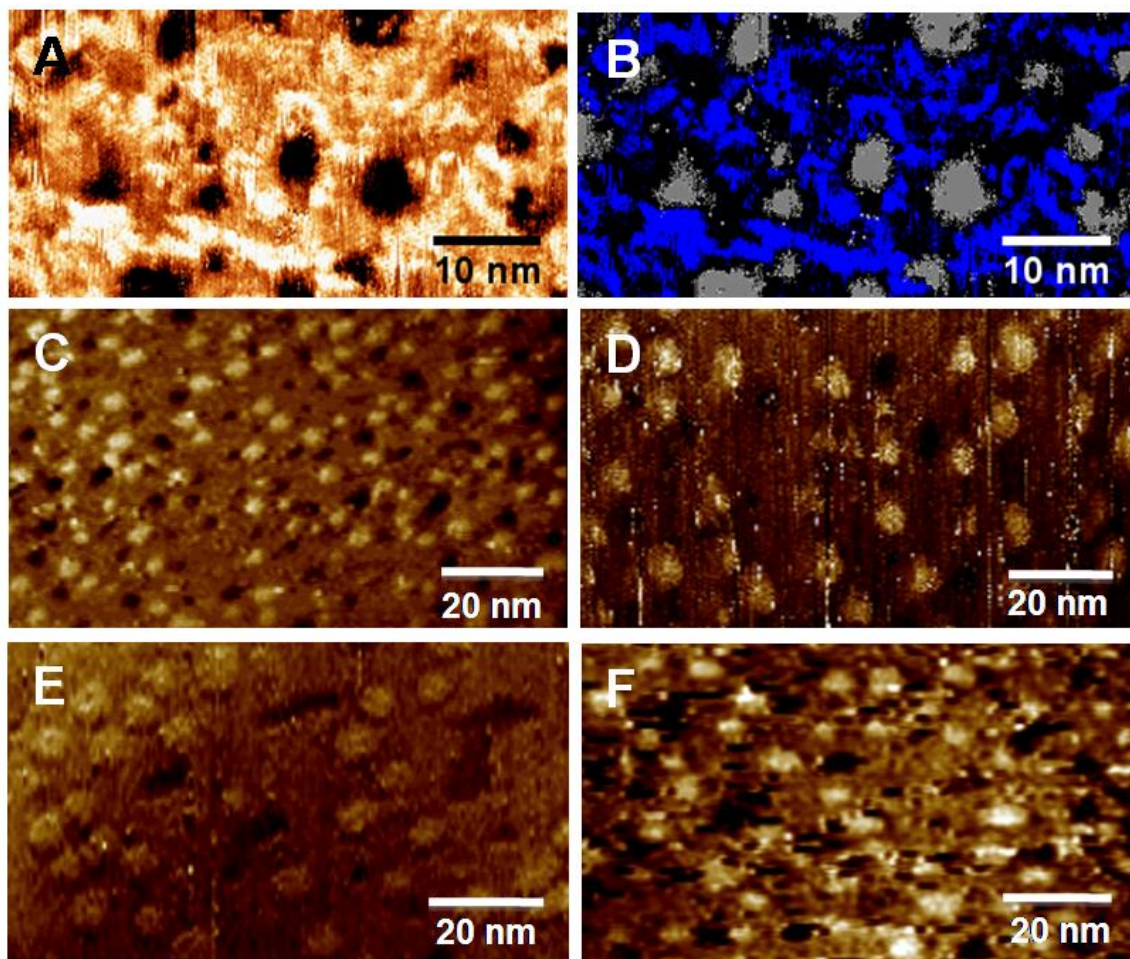


Figure 5.9 STM images showing nanoscale domains in SAMs on flat surfaces. Surfactant combinations and approximate relative compositions obtained by image analysis are: A. and B. Hexanethiol and dodecanethiol, $\phi = 0.50$, B is the contrast image of the original STM image shown in A, C. Octanethiol and mercaptopropionic acid, $\phi = 0.26$, average domain size = 3.4 ± 0.4 nm, D. Butanethiol and nonanethiol, $\phi = 0.15$, average domain size = 6.1 ± 1.4 nm, E. Butanethiol and pentanethiol, $\phi = 0.22$, average domain size = 6.5 ± 1.5 nm, F. Octanethiol and 3-mercaptopropionic acid, $\phi = 0.24$, average domain size = 4.0 ± 0.9 nm. In the STM image, bright spots, dark/black spots and the background represent locations of long surfactants, etch pits and short surfactants, respectively. In the contrast image shown in B, blue, black and grey regions represent locations of the long surfactants, short surfactants and etch pits, respectively. (121)

confined to flat surfaces. We also observe formation of lamellar or micellar domains depending on whether the system is symmetric or asymmetric. The domains formed for asymmetric SAMs are also hexagonally ordered and circular in shape like patterns formed in the corresponding asymmetric mixtures of block copolymers (132; 133; 139) and unlike charges (140; 141). There is however, one difference in the patterns formed in our system versus the patterns formed in these other microphase-separating systems. In our system, the patterns are not the same about the asymmetry fraction ϕ , i.e. the patterns formed for $\phi < 0.5$ are not the same as the patterns formed for $\phi > 0.5$. This is because the long surfactants prefer to microphase separate while the short surfactants prefer to macrophase separate. In both the block copolymer and unlike charge system, this is not the case since both blocks of the block copolymer or both types of point charges are indistinguishable except for the mutual incompatibility.

Mixed SAMs and mixtures of unlike point charges are also different from the block copolymer system in that if the incompatibility between the immiscible segments/species is high, complete phase separation will occur in mixed SAMs as also in mixtures of unlike charges (109). Such macrophase separation is not possible in block copolymers, even when the two blocks are highly immiscible, since the two blocks are bonded together and hence are inseparable from each other.

5.5 Summary

We study phase separation in mixed SAMs on flat surfaces using a minimal model that employs only the immiscibility and length difference between the co-adsorbed surfactants. We demonstrate that in SAMs comprising of symmetric mixtures of immiscible surfactants (equal numbers of both surfactants), on flat surfaces, stripes are the equilibrium phase. Even though the surfactants are immiscible, they do not completely phase separate due to entropic factors as discussed in Section 4.2. Due to the absence of substrate curvature, the same mixture of surfactants has an effectively higher density on a flat surface as compared to a spherical surface. This slows down the phase separation process and makes the equilibrium striped phase difficult to access in experiments as well as simulations. Due to an overall lower density on spherical surfaces, the striped phase readily forms on spherical surfaces and is often imaged in experiments (discussed in detail in the previous chapter on spherical surfaces). On flat surfaces, an intermediate, kinetically-arrested patchy phase is imaged instead.

In our simulations, we obtained the equilibrium striped phase by reducing the surface

coverage and the degree of immiscibility between surfactants, both of which speed up the phase separation process. We also designed systems that had a high potential to get kinetically-trapped in the patchy phase and demonstrated that such systems indeed form a slowly-evolving patchy phase. We confirmed by several methods that the patchy phase is kinetically-arrested while stripes are the equilibrium phase.

Similar to block copolymers and mixtures of incompatible point charges, SAMs comprised of asymmetric mixtures of surfactants phase separate into ordered, equilibrium, 2D micelles. This has been confirmed by our DPD simulations as well as experiments performed on several different sets of surfactants. We have ascertained that these 2D micelles formed for asymmetric mixtures are equilibrium structures while patches formed for symmetric mixtures are kinetically-trapped patterns.

Our studies and analyses in this chapter provide key insights into the phase separation process in mixed SAMs. We show that patches will be imaged in experiments only when: the number density of surfactants on the surface is large; when the length difference or immiscibility between the surfactants is high; and/or when asymmetric mixtures are adsorbed. There is another important factor, which we have not investigated, that controls the phase separated patterns. The total as well as relative number of surfactants adsorbed from a solution onto a surface depends strongly on the length of time that the substrate is left in the solution. In our simulations, the composition of the SAM remains fixed. Experimental studies show that if the substrate is left in solution for long enough times, only one surfactant - the one with a relatively lower solubility in the solvent, will be adsorbed. Simulations of adsorption and simultaneous phase separation can be performed in a grand or semi-grand canonical ensemble but have not been performed in this thesis work. Such studies can provide an even better understanding of phase separation in mixed SAMs.

Chapter 6

Surfactant-coated nanowires and nanorods

In this chapter we discuss self-assembly in SAMs on cylindrical surfaces that describe nanotubes and nanowires. The patterns formed by phase separation in long and short immiscible surfactant mixtures on cylindrical surfaces are similar in many respects to those seen on spherical (Chapter 4) and flat (Chapter 5) surfaces. The key difference is that the unidirectional nature of the cylindrical curvature helps in preferably aligning the stripes along the circumference of the cylinder rather than the length. Therefore, stripes on cylinders are more ordered than those on spherical or flat surfaces. We also describe how imparting a curvature to the flat surface can help relax kinetically arrested patterns, discussed in Chapter 5, into equilibrium patterns. This is a novel method to modify patterns on a surface, post-adsorption. We have performed simulations that verify the use of this technique to modify patches formed on flat surfaces into stripes, and recent experiments confirm our predictions. The results provided in this chapter have resulted in the publication (142) and a manuscript being prepared for submission (143). Part of the text and figures presented in this chapter have been taken from these manuscripts.

6.1 Dependence on cylinder dimensions

6.1.1 Effect of cylinder radius

Similar to the results on spherical surfaces, we find that there is a critical cylinder radius below which complete phase separation occurs (Fig. 6.1A). The reason is also the same: on narrow cylinders, the long surfactant chains have sufficient free volume for movement and do not need to have shorter neighboring chains to gain conformational entropy. However, unlike spherical surfaces, an upper bound on formation of ordered stripes is not present.

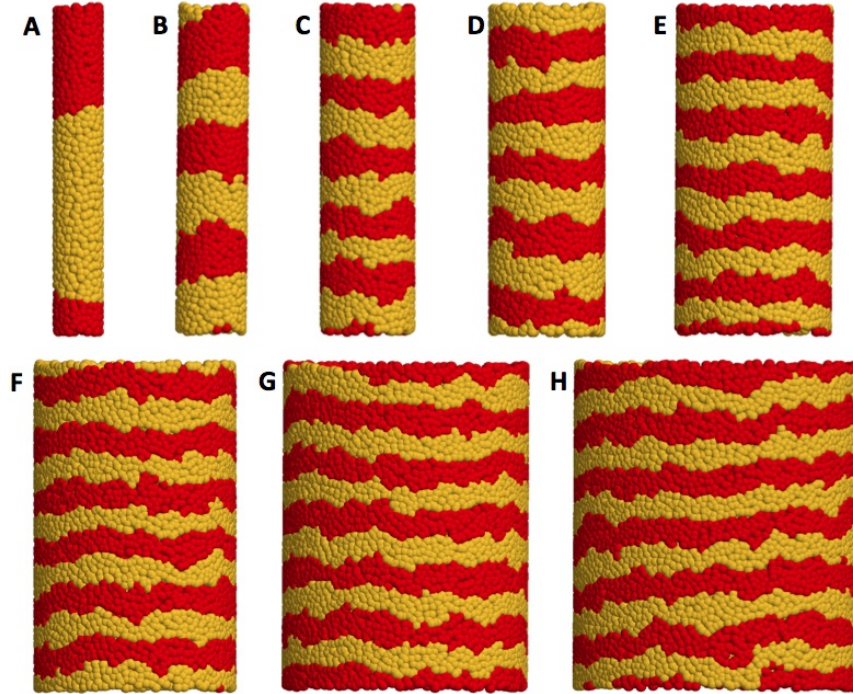


Figure 6.1 Effect of cylinder radius on phase-separated pattern formed in mixtures of long (7-bead, yellow) and short (4-bead, red) surfactants grafted on a cylinder surface. The radii of the cylinders are A. 2σ , B. 3σ , C. 4σ , D. 5σ , E. 7σ , F. 9σ , G. 11σ , H. 13σ . (143)

Very ordered stripes are formed even on wide cylinders. This is because the unidirectional curvature of the cylinder helps align the stripes. The direction in which stripes are aligned is perpendicular to the axis of the cylinder. The preferred direction of stripe alignment is discussed in more detail in Section 6.1.3.

6.1.2 Effect of cylinder length

As described in Chapter 3, the periodic boundary conditions for our simulations on cylindrical surfaces are applied along the length of the cylinder. This raises concerns that the boundary conditions might promote ordering of the stripes. For sufficiently long cylinders however, such finite-size effects are expected to disappear. Fig. 6.2 shows the results of our simulations on cylinders with a wide range of lengths. Since cylinders of all lengths form stripes, and the stripe width is uniform across the lengths, we conclude that our system does not suffer from finite size effects.

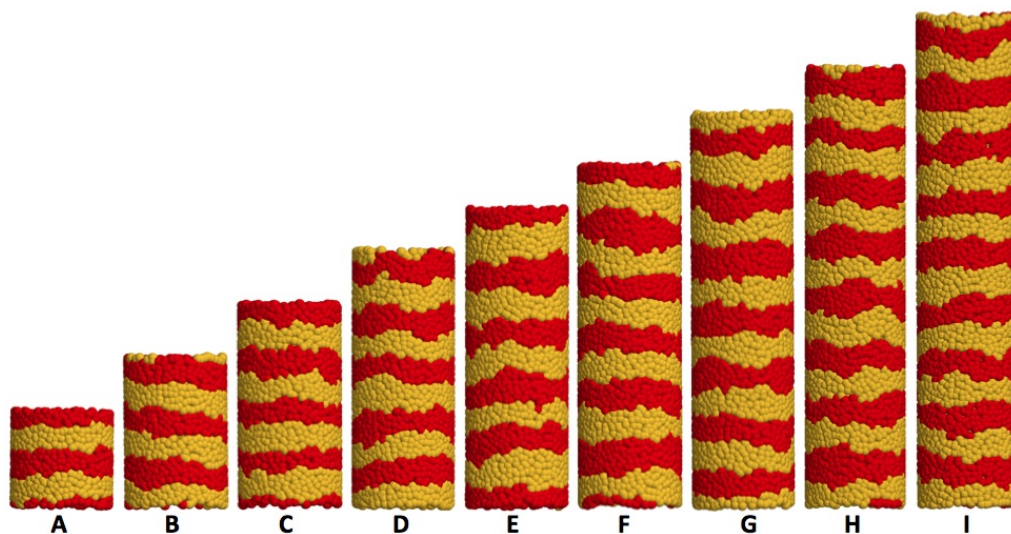


Figure 6.2 Effect of cylinder length on phase-separated pattern formed in mixtures of long (7-bead, yellow) and short (4-bead, red) surfactants grafted on the cylinder surface. The lengths of the cylinders are A. 10σ , B. 15σ , C. 20σ , D. 25σ , E. 30σ , F. 35σ , G. 40σ , H. 45σ , I. 50σ . Radius of the cylinder is 5σ in all cases. (143)

6.1.3 Effect of aspect ratio

The aspect ratio of a nanocylinder (cylinder diameter/cylinder length) is an important parameter that needs to be considered when dealing with most incompatible mixtures. For example, for single-bead (tail-less) surfactants or equal-length surfactants, conformational entropy does not play a role in phase separation. The driving force for these mixtures is simply to minimize the interface. Therefore, for an immiscible mixture of single-bead species, the interface may switch directions from being horizontal to vertical just by changing the cylinder length as shown in Fig. 6.3, and/or the changing cylinder radius.

In length-mismatched systems, however, such switching of interface or change in direction of stripes is not observed. In the results shown in Fig. 6.2, the aspect ratio of the cylinder changes from 1.0 (in Fig. 6.2A) to 5.0 (in Fig. 6.2I) and the circumference to length ratio changes from 3.14 to 0.63. Despite such a large change in circumference-to-length ratio, the direction of the stripes is always horizontal. In all of the simulation results discussed in this chapter, whenever stripes form, they are always along the circumference and never along the length of the cylinder. The reason for such preference for formation of horizontal stripes over vertical stripes is also entropic in nature and is illustrated in Fig. 6.4.

If vertical stripes form (Fig. 6.4A), the long surfactants can bend only along the circumference of the cylinder and feel a crowding effect along the length of the cylinder. However, when horizontal stripes form (Fig. 6.4B), the long surfactants have free volume around

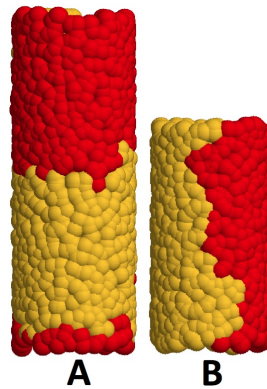


Figure 6.3 Interface direction switches from A. horizontal to B. vertical, when length of a radius $= 3\sigma$ ($2\pi \cdot \text{radius} = 18.8$) is changed from 22.0 to 15.0, for simple, incompatible binary mixtures guided by incompatibility alone rather than competing interactions.

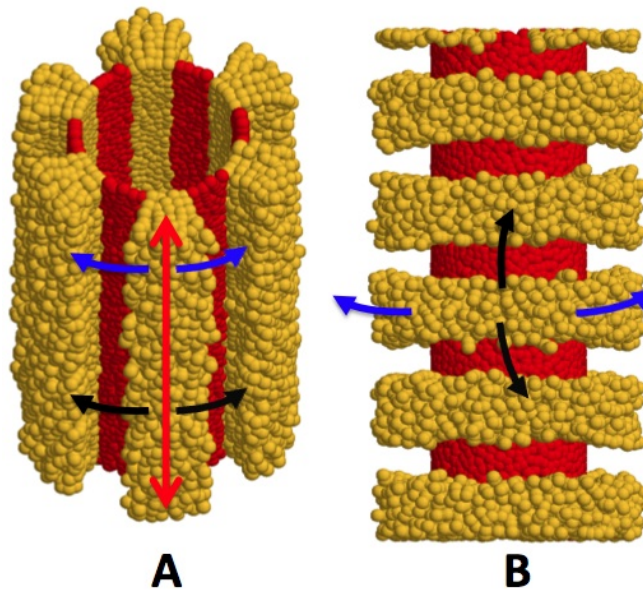


Figure 6.4 Entropic considerations in A. vertical versus B. horizontal stripes. Red and yellow beads represent short and long surfactants respectively. The tails of the short surfactants have been removed for clarity. In the central stripe comprised of long surfactants, blue and black arrows represent the direction(s) in which the long surfactants can bend to take advantage of the cylinder curvature and neighboring short chains, respectively. The red arrow in A. represents the direction in which the long surfactants are crowded. (143)

the circumference (due to the cylinder curvature) and they have additional free volume available along the length because of neighboring short surfactants. Therefore, for two configurations with the same interface width, the horizontal stripes are always preferred over vertical stripes.

6.2 Dependence on the properties of the surfactant mixture

6.2.1 Effect of increasing immiscibility

In our simulations, we can make the two surfactants more (less) immiscible by increasing (decreasing) the repulsion parameter Δa . As expected for small values of Δa (i.e. barely immiscible surfactants) the phase separated domains are fast-changing, small domains of irregular shapes and sizes (Fig. 6.5A). On slightly increasing the immiscibility, stripe like domains start appearing (Fig. 6.5B). Even though the surfactants are only slightly immiscible at this point, preference for horizontal stripes is already evident. On further increasing the immiscibility clear, ordered horizontal stripes form (Fig. 6.5C to E). These stripes are perfect rings of nearly uniform width. The stripe width is a strong function of the immiscibility. As expected, the stripe width increases as the immiscibility is increased until the point at which the two surfactants become so immiscible (Fig. 6.5F) that energetic penalty for microphase separation outweighs any possible conformational entropy gain, and complete phase separation occurs. We see that at this point, defects start to appear in the system because high degree of immiscibility hinders diffusion of the molecules on the surface and slows down the phase separation process. For example, it would take a very long time for the few red molecules in the middle of the yellow domain in Fig. 6.5F to cross the wide section of yellow molecules and reach the closest red domain.

6.2.2 Effect of increasing length difference

The critical length difference Δl that the surfactants should have to microphase separate into stripes is the same on a cylinder as on the sphere and the flat surface, and it is equal to three beads (Fig. 6.6). Complete phase separation occurs for $\Delta a < 3$ (Fig. 6.6A and B). Then there is a transition to forming stripes at $\Delta l = 3$ (Fig. 6.6C) beyond which stripes always form.

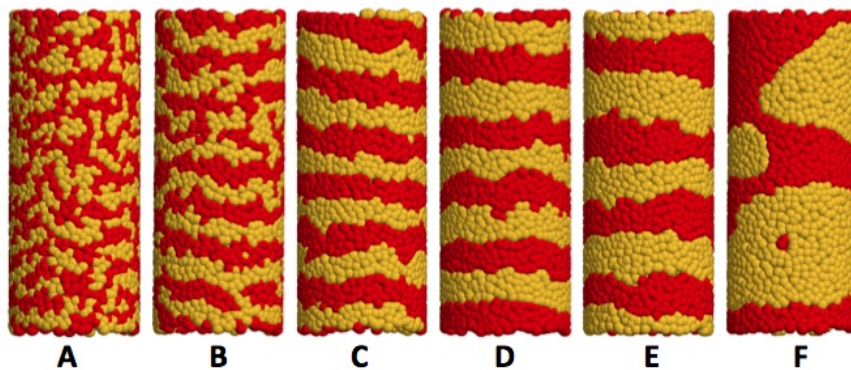


Figure 6.5 Effect of surfactant immiscibility on phase-separated pattern formed in mixtures of long (7-bead, yellow) and short (4-bead, red) surfactants grafted on a cylindrical surface. The values of the repulsion parameter, Δa (larger Δa implies higher immiscibility) are: A. 3, B. 5, C. 10, D. 15, E. 20, F. 25. (143)

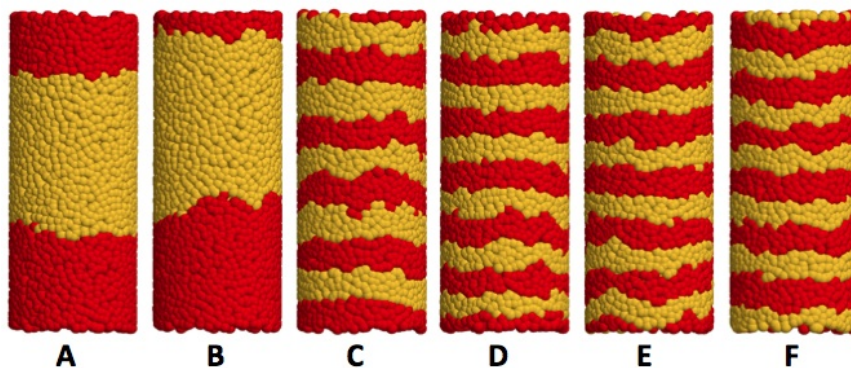


Figure 6.6 Effect of surfactant length difference on phase-separated pattern formed in mixtures of long (7-bead, yellow) and short (4-bead, red) surfactants grafted on a cylindrical surface. The systems simulated from left to right are denoted by m_n where m and n are the number of beads in the short and long surfactants respectively. A. 4_4, B. 4_6, C. 4_7, D. 4_9, E. 4_11, F. 4_13. (143)

6.2.3 Effect of increasing surface coverage

Similar to the effect of increasing surface coverage i.e. the number of surfactants per unit area of the surface, on a spherical surface, kinetically-arrested patchy patterns form on cylinders as well. Fig. 6.7A shows the patchy pattern formed on cylinders for a large surface density of 5.0. The unrolled pattern is shown in Fig. 6.7B. High surface density is a likely reason for the formation of patches in the experiments by Wang et al. (14) discussed in Section 1.1. The non-uniform size distribution of the patches confirms that they are kinetically-arrested, similar to the analysis for flat surfaces (Section 5.4.3).

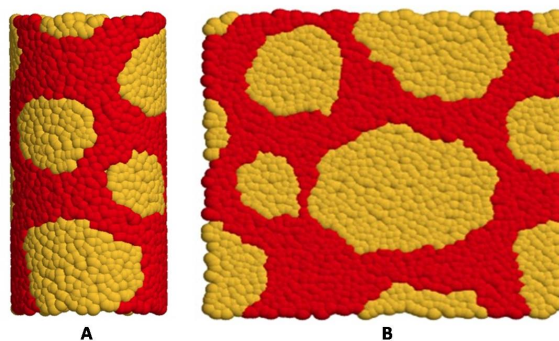


Figure 6.7 A. Patchy pattern formed on a cylinder of radius 5σ and surface coverage of 5.0 particles per σ^2 . B. Unrolled view of the result shown in A.

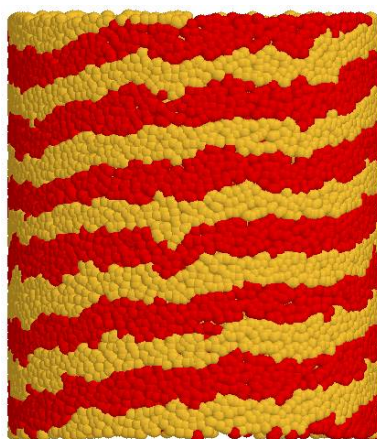


Figure 6.8 Helical pattern formed by phase separation in SAMs.

6.2.4 Helices

Helices with a small pitch are sometimes formed in our simulations. There are no specific conditions under which helices form in our systems. Out of several simulations starting from slightly different initial conditions or using different random number seeds, one run might yield a helix. We believe that helices are kinetically trapped structures that are not able to relax into the equilibrium horizontal stripes since their free energy is close to that of horizontal stripes. Once helices form, it is very difficult for them to relax into stripes because that will require breaking and rearrangement of stripes, both of which are expected to have high kinetic barriers. By an extension of the discussion in Section 6.1.3 and the illustration in Fig. 6.3, horizontal stripes will have a higher conformational entropy than helices and therefore will be preferred over helices. Fig. 6.8 shows images of a helix formed in our simulation which is formed for the same surfactants and conditions as the horizontal stripes shown in Fig. 6.1H, starting from different initial configurations.

6.3 Exploiting substrate stress to modify nanoscale surface patterns

6.3.1 Introduction

There is evidence to show that substrate stress can affect adsorption of molecules on surfaces (102; 144; 145). Recent theoretical studies have further shown that phase-separated patterns formed on unstressed substrates differ from those formed on substrates that are stressed prior to adsorption (146–148). In this section we demonstrate that stress applied post-adsorption affects the diffusion of adsorbed molecules on the surface and can thus be used to modify surface patterns formed by phase separation in SAMs. We also show how stress can be used to relax non-equilibrium, kinetically arrested patterns formed on flat substrates towards equilibrium. Specifically, using computer simulations we predict that a kinetically arrested pattern of phase-separated patches formed in a mixed SAM of surfactants on a flat substrate can be progressed to form the equilibrium, striped pattern by stressing the substrate through induction of curvature. The motivation for this work comes from observations that a mixed SAM of surfactants of unequal length and/or bulkiness readily organizes into stripes on highly curved substrates like small nanoparticles (Chapter 4, references (11; 28; 149)), while patchy domains are often formed on substrates with a low degree of curvature or no curvature (flat substrates) (8; 17; 19), even when stripes are the equilibrium phase in both cases, as discussed in Chapter 5. Highly curved substrates therefore appear to aid in the progression of the metastable patchy phase into the equilibrium striped phase but no systematic studies have been conducted to test this. Using a simple method, we show that curvature indeed speeds up the separation process substantially. The results of this section were published in reference (142).

6.3.2 Curvature induction in simulations

The simulation is first performed on a flat surface until we obtain a pattern that is stable over a long period of time. Next, we roll the flat surface into a cylinder and continue the simulation on the cylindrical surface to understand the role of substrate curvature and stress. The head groups of the surfactants are now constrained to move on the cylinder, instead of a flat surface, and the tails spread out radially from the cylinder surface. To roll the flat substrate into a cylinder, we map the positions of the head groups of the surfactants onto a cylinder of radius $R = L_x/(2\pi)$ and length $L = L_y$, where L_x and L_y are the dimensions of the flat substrate in the x and y directions, respectively (Fig. 6.9). The total area occupied by

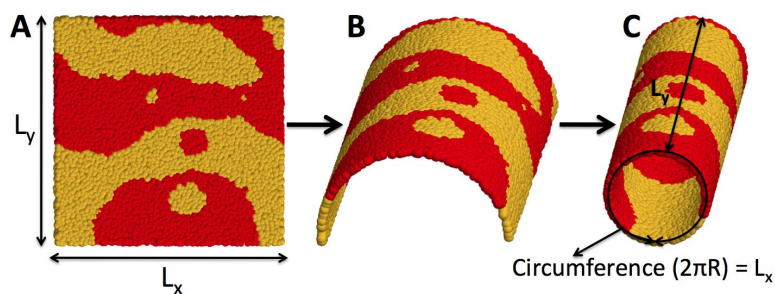


Figure 6.9 Transfer of an arbitrary pattern from a flat surface onto a cylinder. A. Starting pattern on flat surface. B. Intermediate curved surface. C. Final pattern on cylindrical surface. (142)

the head groups therefore remains unchanged.

The time evolution of the pattern on the flat surface starting from a uniformly mixed state is shown in Fig. 6.10. The resulting patchy pattern is found to be stable over long timescales (tens of millions of DPD time steps of 0.01 unit each). On induction of cylindrical curvature, this patchy pattern, which had previously arrested, now evolves quickly, with patches merging and elongating to form stripes. Patches that are stable and stay nearly unchanged on flat substrates for millions of time steps start merging to form elongated domains in as few as 50,000 time steps when transferred to the cylindrical surface, and all patches merge into stripe-like domains within 5 million time steps. Calculations of the diffusion constant of molecules in the kinetically-arrested patchy pattern on the flat surface and in the equilibrium, striped pattern on the cylinder show that they indeed diffuse faster on the cylinder than on the flat surface. Diffusion constants of the head groups on the flat and cylindrical surfaces are $0.0432 \pm 1.9E-5$ and $0.0535 \pm 1.9E-5$ bead diameter² time⁻¹, respectively. Figure 6.10 shows the complete process of curvature induction; starting from formation of the arrested patchy pattern, transfer to a cylindrical surface, and subsequent evolution of the pattern on the cylindrical surface. The snapshots taken post curvature induction are taken by un-rolling the cylinder back into a flat surface only for visualization while the simulation progresses on the cylinder. The fast pattern change that we observe serves not only to establish the role of curvature in formation of striped patterns on small nanoparticles, but also to demonstrate how surface patterns can be modified post-adsorption. In terms of applications, it should be possible to use this method experimentally to modify surface patterns post-adsorption as well as to speed up the change from kinetically arrested to equilibrium patterns. The unidirectional curvature of the cylinder aids in the formation of defect-free parallel stripes.

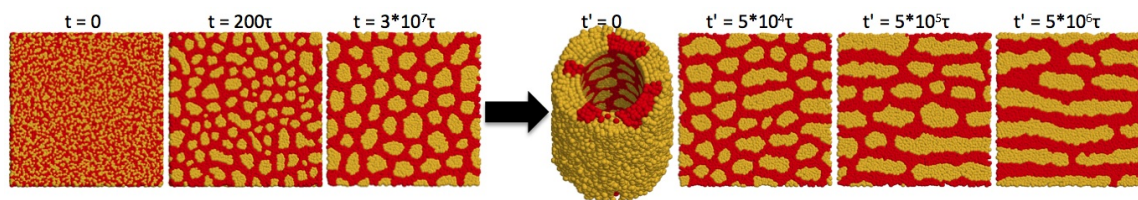


Figure 6.10 Simulational procedure for curving a flat, surfactant-coated substrate. Snapshots, from left to right: phase separation of long (yellow) and short (red) surfactants on a flat substrate leading to the formation of the patchy pattern which is stable over many time steps (tails removed for clarity); a patch-covered cylinder obtained by rolling the patch-covered flat substrate; the remaining four snapshots show evolution of the patchy pattern on the surface of the cylinder - the cylinder has been un-rolled for better visualization of the changing pattern - the simulation is conducted on a cylindrical surface (tails removed for clarity). t and t' indicate time for the simulations on flat and cylindrical substrates respectively. τ is the time step used in both simulations (0.01 unit each). (142)

6.3.3 Curvature induction in experiments

To test the procedure experimentally, our colleagues in the Stellacci group at MIT prepared SAMs of octanethiol ($\text{CH}_3\text{-(CH}_2\text{)}_7\text{-SH}$) mixed with mercaptopropionic acid ($\text{COOH-(CH}_2\text{)}_2\text{-SH}$) and of octanethiol ($\text{CH}_3\text{-(CH}_2\text{)}_7\text{-SH}$) mixed with methyl benzenethiol ($\text{CH}_3\text{-(C}_6\text{H}_4\text{-SH)}$). The substrates obtained were imaged using STM. These mixtures of surfactants form patches on flat substrates (Fig. 6.11A); specifically it was found that the longer surfactant forms patches in a matrix of the shorter surfactant, as in the simulations. The patchy phase stayed unchanged even after a long equilibration time of two weeks when it was imaged to obtain the pre-stressed image. To induce curvature and stress, the surfactant-coated substrate was wrapped around a cylindrical vial (radius 1.5 cm), and then incubated. This process induced a slight curvature and generated a mild stress in the substrate. The substrate was then flattened out and reimaged to compare with the pre-stressed image and to record the change in pattern. Figure 6.11A shows the STM images of the octanethiol and mercaptopropionic acid coated substrate taken before and after induction of curvature. The post-stressed image showed presence of string-like sequences of patches that were starting to merge. These sequences were absent in the pre-stressed image, which only showed separate and unaligned patches. Images of patches aligning and merging were obtained using the other surfactant combination (octanethiol and methyl benzenethiol) as well (Fig. 6.11B).

The string-like domains seen in Fig. 6.11 resemble intermediate stages from our DPD simulations (Fig. 6.10), observed before the patches merge to form a stripes-only phase. The experimental and simulational results are, therefore, in good agreement.

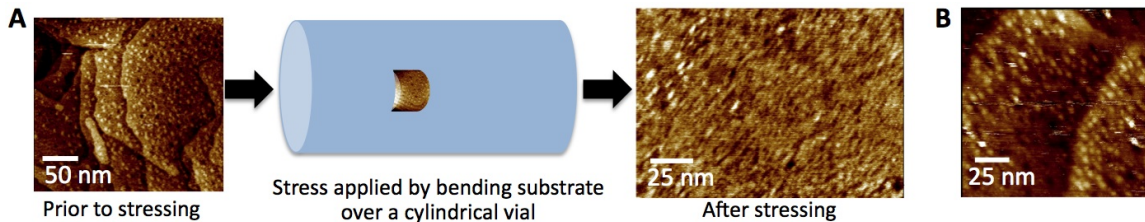


Figure 6.11 Experimental images, from left to right: A. STM image of a patchy pattern on flat substrate formed by octanethiol and mercaptopropionic acid surfactants; cartoon showing application of stress; and alignment and merging of patches after stressing. Dark and light regions indicate short and long surfactants respectively. B. STM image of aligning and merging patches obtained after stressing another surfactant system: octanethiol and methyl benzenethiol. (142)

6.3.4 Discussion

It is interesting to note that in our simulation study, patches always merge in the direction of the curvature, i.e. along the circumference, and never along the length of the cylinder. Our results closely resemble the patterns obtained by He and Huang (148) for phase separation on a flat substrate that is stretched pre-adsorption. Their theoretical results show that the domains formed on stressed substrates are larger, fewer and more elongated compared to those formed on unstressed substrates. They compare equilibrium patterns formed on un-stressed and pre-stressed substrates while our starting patchy pattern prior to stressing is non-equilibrium. Although it is not possible to stretch the substrate in our method, we can and have tested (Sections 6.1 and 6.2) whether the patterns formed on pre-stressed and post-stressed substrates are essentially the same. Our simulations starting with randomly distributed surfactants on the cylinder itself show that in these simulations also, stripes always form along the circumference of the cylinder rather than along the length. We therefore conclude that patterns formed by applying stress prior to and post adsorption are similar and that the specific direction of the stripes is an outcome of the unidirectional nature of the substrate curvature.

Another important fact is that although both substrate-stretching and curvature-induction are methods to induce stress in the substrate, and patterns formed by both appear to be similar (148), the mechanisms for pattern formation are likely different. This is because the free volume available to a surfactant chain in a stretched substrate is different from that on a curved surface. Our method does not allow us to compare the two methods.

In related studies on flat and curved substrates, researchers have shown analytically that in mixtures of immiscible cationic-anionic co-assembled amphiphiles stripes are the equilibrium pattern on cylinders while patches are the equilibrium pattern on flat substrates (146). This is not the case in our SAMs of immiscible, length-mismatched surfactants. In

our system stripes are the equilibrium pattern on both cylinders and flat surfaces.

6.4 Unique alignment of stripes in experiments

There are very few experimental studies focusing on phase separated SAMs on nanocylinders. Our collaborators in the Stellacci group have performed several experiments testing the validity of our predictions (Section 6.1.3; Fig. 6.4) that for length mismatched immiscible surfactants, horizontal stripes are preferred over vertical ones. For the experimental studies, gold nanorods capped with surfactant hexadecyltrimethylammonium bromide were synthesized following standard methods. A 2:1 (molar ratio) mixture of mercaptopropionic acid and octanethiol was then introduced onto the nanorods through a place exchange reaction. The nanostructures were then extensively washed to remove the excess residue. STM images were obtained using a Veeco Multimode IIIa Scanning Probe Microscope. The STM samples were prepared by dropping a concentrated solution onto Au (111) thermally evaporated on mica substrates (Molecular Imaging, AZ). Pt-Ir mechanically cut tips were used (Veeco, CA). The imaging approaches are described in detail in references (11; 27; 137; 150). The bias voltage was varied from 500 mV to 1000 mV and the current varied from 400pA to 700 pA. Imaging gains varied from 0.4 to 0.7 for the integral and proportional. The rods were imaged in various directions relative to the slow axis of scanning. Some of the STM images are shown in Fig. 6.12. In the case shown in Figure 6.12, a nanorod captured in a series of 21 images at different tip speeds, varying from $0.17 \mu\text{m} / \text{s}$ to $2.2 \mu\text{m} / \text{s}$, is shown. Similar to simulation predictions, experiments also show formation of horizontal stripes only. None of the experimental systems formed stripes along the length of the cylinder.

6.5 Comparison with other phase-separating mixtures confined to cylindrical surfaces

Among phase separating mixtures with competing interactions confined to cylindrical surfaces, the system of unlike point charges has been most extensively studied (146; 151–156). Phase separation in this system is governed by competing short-range attraction and long-range coulombic repulsion, similar to the effective interactions in our system of phase-separating SAMs. Comparison of phase-separated patterns formed by this system and our results for phase-separating SAMs, reveals several differences. For example, in the system of unlike point charges, stripes perpendicular or parallel to the cylinder axis, as well

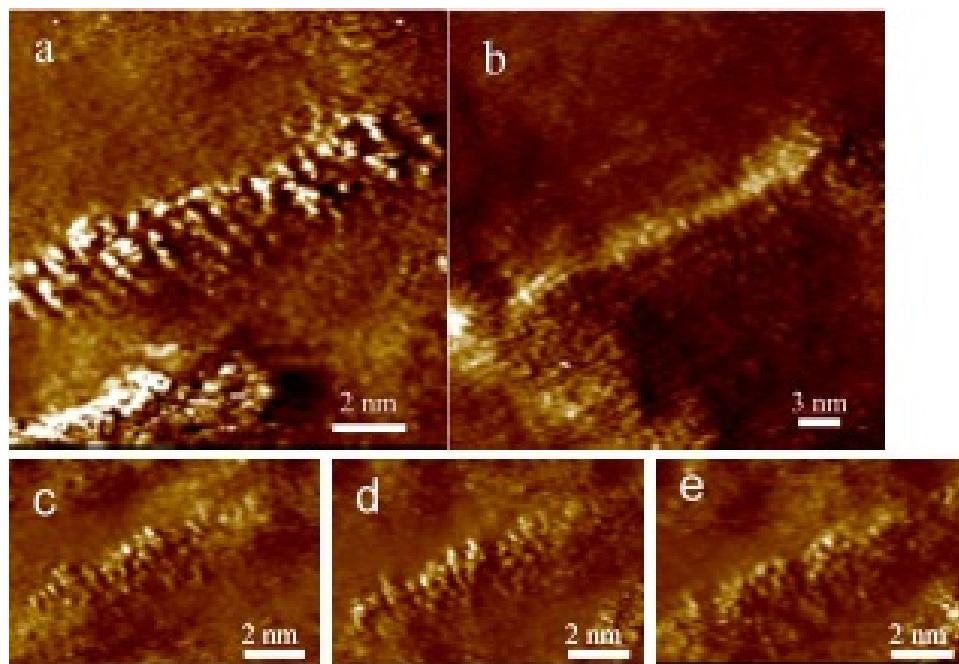


Figure 6.12 STM current images of phase separating octanethiol and mercaptopropionic acid SAMs on gold nanorods showing an average stripe width of 0.85 nm. The images have been obtained at different scanning speeds varying from 0.17 $\mu\text{m/s}$ to 2.2 $\mu\text{m/s}$. (143)

as zig-zag stripes may form while in our system only rings perpendicular to the axis form (152). Defect-mediated stripes are also seen in this system (152) while defects in our system appear only when the surfactants are highly immiscible or the surface coverage is very high, both of which slow down the phase separation process so that the equilibrium structures are difficult to access in the time scale of the simulation. Another important difference is that in the charged particle system, all kinds of patterns varying from helices to rings might form on very narrow cylinders (151) while in our system, only macrophase separation occurs on narrow cylinders. In general, the wide variety of patterns formed in the system of charged particles is not seen in phase separating SAMs on cylindrical surfaces (151; 152). As discussed in Section 6.2.4, helices with a short pitch might form in phase-separating forms but are likely kinetically-trapped structures unable to relax into stripes due to the small free energy difference between stripes and helices and hence, a small driving force for the transition from trapped helices to equilibrium stripes. This is yet another difference between phase-separating SAMs and mixtures of unlike point charges in which helices are often formed and are the equilibrium structures (151–154).

6.6 Summary

The important contributions from this chapter are the prediction of ordered stripes always oriented perpendicular to the cylindrical axis, and the description of a novel method that can be used for relaxing kinetically-arrested patchy patterns formed on flat surfaces into the equilibrium striped patterns. We explain how long surfactant chains gain more free volume and conformational entropy when SAMs phase separate into horizontal stripes (perpendicular to the axis of the cylinder), as compared to entropic gain by forming vertical stripes. Helices are sometimes formed in our system because their free energy is expected to be close to that of the horizontal stripes. However they are very likely kinetically trapped structures with a large kinetic barrier to forming horizontal stripes. In this chapter, we also describe how cylindrical curvature can be used to relax the kinetically-arrested patchy patterns formed in symmetric mixtures on flat surfaces, into the equilibrium striped patterns. This is a novel method for modifying surface patterns post-adsorption.

Our key results in this chapter have also been confirmed by recent experimental studies of phase separation in surfactant-coated nanorods. Experimental studies of phase separation (Fig. 6.12), as well as stress induction on kinetically arrested patches formed on flat surfaces (Fig. 6.11), support our predictions that horizontal striped patterns form on nanocylindrical surfaces and the curving a substrate is a useful technique to modify surface patterns post-adsorption.

Chapter 7

Interfacial properties of striped nanoparticles

In this chapter we describe our completed and on-going studies of interfacial properties of striped nanoparticles. We explain the unusual non-monotonic dependence of work of adhesion of striped nanoparticles on the composition of the hydrophilic surfactant on their surface. This non-monotonicity is unusual because it opposes the traditional thermodynamic view that properties of surfaces coated with more than one components are weighted averages of the properties of the individual components. We propose that two molecular-level phenomena - cavitation and confinement compete with each other to result in the non-monotonicity in work of adhesion. The results provided in this chapter have resulted in the publication (12) and a manuscript being prepared for submission (157). Part of the text and figures presented in this chapter have been taken from these manuscripts.

7.1 Introduction

It is traditionally believed that surfaces coated with more than one type of species can be treated as either uniformly coated with the different species or comprised of sufficient large domains of each so that the different components can be assumed to interact with the solvent independent of each other (158). As a first approximation, the properties of surfaces coated with two or more surfactants can be considered to be weighted averages of the properties of surfaces coated with one surfactant only (159). Since, the interactions between surfactants affects surface properties, this is not always true and non-linear, monotonic dependence of the properties on surface composition has also been reported (160). Recently, it has been shown that presence of confined spaces or nanoscale domains can affect the molecular-level organization and behavior of the nearby solvent molecules (161; 162), which can in turn affect the surface properties in complex ways. This is certainly the case for striped nanoparticles surrounded by solvent molecules. Domain sizes, measured as the average striped width,

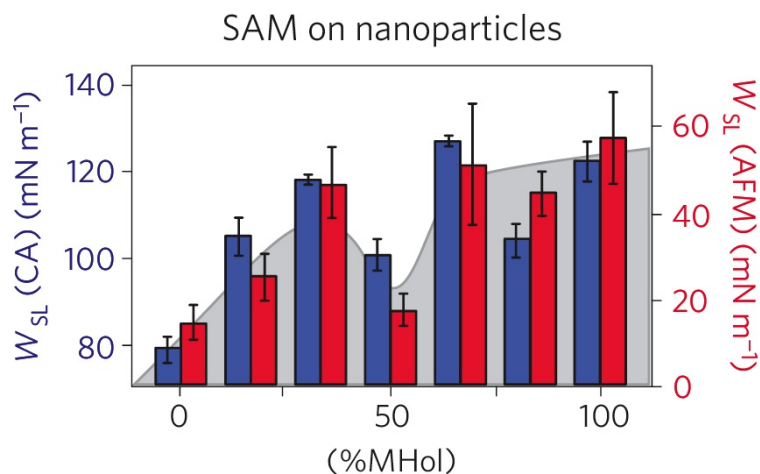


Figure 7.1 Non-monotonic behavior of work of adhesion of striped nanoparticles coated with octanethiol (OT) and mercaptohexanol (MHol) with water solvent, obtained using contact angle measurements (blue) and AFM (red). (12)

on these nanoparticles are often of the order of 5\AA and always less than 2 nm (11), small enough to affect the organization of surrounding solvent molecules. Recently, Centrone et al. (29) demonstrated that the solubility of striped nanoparticles depends not only on the relative composition of the two surfactants in the SAM coating these nanoparticles, but also on the stripe widths of each of the two components. Additionally, out of the two components, one might be solvophobic and the other solvophilic, further disrupting any possible, uniform distribution of solvent molecules around the surface. It is therefore interesting to study the interfacial properties of striped nanoparticles and to investigate how domain sizes on nanometer and Angstrom scales might affect them.

Recent experiments by Jeffrey Kuna and Kison Voitchovsky in the Stellacci group present a surprising finding that the work of adhesion, $W_S L$ of the striped nanoparticles in a variety of solvents varies not only non-linearly but also non-monotonically as a function of the surface composition. This is clearly an unusual and unprecedented behavior and suggests that interactions of solvent with nanopatterned substrates are much more complex than previously believed. The experimental plot is shown in Fig. 7.1 where the work of adhesion $W_S L$ of striped nanoparticles coated with octanethiol (OT) and mercaptohexanol (MHol), determined using contact angle measurements and AFM is shown to be a non-monotonic function of the composition of the hydrophilic component MHol. Specifically, the nanoparticles covered by 33% and 67% MHol were found to have an unexpectedly large work of adhesion relative to the 50% MHol coated nanoparticle. The ligand shells of these nanoparticles were comprised of stripes less than 2 nm in width.

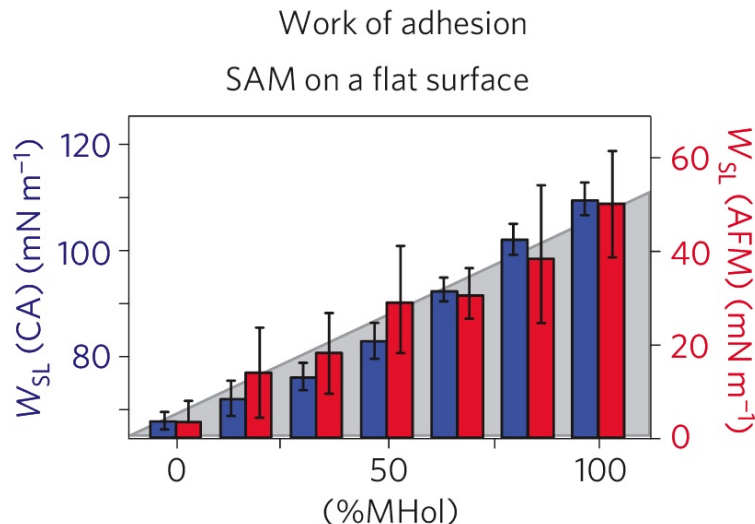


Figure 7.2 Linear and monotonic behavior of work of adhesion W_{SL} of flat surfaces coated with > 5 nm stripes of octanethiol (OT) and mercaptohexanol (MHol) with water solvent. The measured values of W_{SL} were obtained using contact angle measurements (blue) and AFM (red). (12)

In contrast, work of adhesion of flat surfaces coated with SAMs comprised of domains wider than 5 nm in size, was a non-monotonic and even linear function of the composition of the hydrophilic component, as shown in Fig. 7.2. The simulation results, analyses and reasoning presented in this chapter is aimed at providing a possible explanation for the non-monotonic behavior of W_{SL} on composition and at improving our understanding of the interfacial phenomena near substrates with nanoscale patterning.

7.2 Experiments

The surfactants used in the experiments are octanethiol (OT) and mercaptohexanol (MHol). On flat surfaces, > 5 nm domains of OT and MHol were obtained by immersing the flat gold surfaces in dilute ethanol solutions with varying ratios of OT and MH, for a week at room temperature. The work of adhesion of these surfaces was then determined using contact angle and atomic force microscopy (AFM) measurements. Details of the measurement procedure are available in (12). For measuring work of adhesion of the striped nanoparticles, striped nanoparticles were first prepared by known methods (11) and then nanoparticle films were prepared by layer-by-layer assembly of five layers of nanoparticles. Since the nanoparticles are covered with < 2 nm domains of OT and MHol, this procedure resulted in reasonably flat, extended surfaces with < 2 nm domains. A schematic showing surface preparation is provided in 7.3. Detailed statistical analyses were performed to characterize

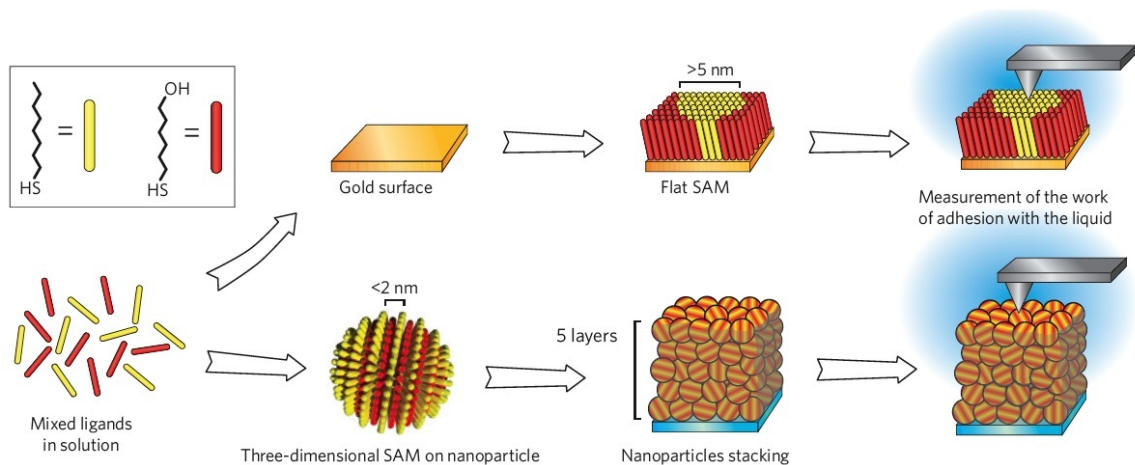


Figure 7.3 Procedure for substrate preparation. For domains $> 5\text{nm}$, flat gold surfaces are immersed in a solution of the two surfactants. For domains $< 2\text{nm}$, striped gold nanoparticles are first prepared and then deposited layer-by-layer to form an extended flat surface. OT and MHol are shown in yellow and red, respectively. (12)

the nanoparticle films as well as for the measurements of W_{SL} to quantify all possible errors.

As mentioned in Section 7.1, the largest deviation from the linear behavior of Fig. 7.2 was found for 33% and 67% MHol coated nanoparticles and both had much larger W_{SL} 's than the 50% MHol coated nanoparticle, leading to the non-monotonicity. The experimentally measured MHol (OT) stripe widths for 33%, 50% and 67% nanoparticles, in nanometers are 0.6 (1.2), 0.7 (0.7) and 1.2 (0.6), respectively. These widths are quite narrow which is why the surface morphologies of these nanoparticles are expected to have a strong effect on their W_{SL} .

Although the set of surfactants used (OT and MHol) was not changed, two solvents - water and glycerol were tried. Both solvents showed similar trends with respect to the non-monotonicity in W_{SL} . W_{SL} plots for glycerol are available in (12). Since most of the studies and analyses, including the simulation studies were performed using water, the remaining discussions in this chapter will focus on water only.

7.3 Simulations

All-atom molecular dynamics (MD) simulations were performed by Dr. Hao Jiang in the Glotzer group with explicit solvent (water) molecules. I performed part of the analysis and helped design the simulations and interpret the results. The details of the MD simulations are as follows. The simulations were carried out in the NVT ensemble at 300 K for a striped

nanoparticle of core diameter 40.6 Å. The nanoparticle was coated with MHol and OT. We simulated three different compositions of MHol and OT keeping the total number of surfactants (362) constant with a surface density of 14.3 Å²/molecule. We used a cubic simulation cell with periodic boundary conditions applied in all three dimensions. For each of the three compositions of MHol and OT, the length of the box sides were determined using separate equilibrium NPT (P = 0) simulations. Our simulations contained 12944 water molecules modeled with the SPC/E force field (118). The coated NP was placed at the center of the simulation box. The surfactants were modeled using the OPLS all-atom force field (116), with the thiol groups held fixed throughout the simulations. The Lorentz-Berthelot combination rule (77) was used to determine the parameters for the Lennard-Jones (LJ) interactions between unlike molecules. The electrostatic interactions were treated with Wolf’s method (163). A cut-off radius of 10 and 14 Å was used for the LJ and electrostatic interactions, respectively. We employed an integration time-step of 1 fs. Equilibration was performed for 50 ps. Post-equilibration production runs were carried out for 500 ps for all the cases investigated, and the data stored at intervals of 0.5 ps for subsequent analysis.

We simulated nanoparticles with six different surface patterns shown in Fig. 7.4. The Janus particles (Fig. 7.4A to C) were simulated as control cases for the striped nanoparticles (Fig. 7.4D to F). The experimental stripe widths for the different compositions was used in simulations as well, for the striped nanoparticles. The surface pattern, i.e. the positions of the head groups were kept fixed while the surfactant tails and the surrounding 12944 water molecules were allowed to move. The equilibrated number density profiles of water molecules around the striped nanoparticles are shown in 7.5.

7.4 Two competing, molecular-level phenomena lead to non-monotonicity in the work of adhesion, W_{SL}

We hypothesize that the non-monotonicity in W_{SL} arises from a competition between two molecular-level phenomena, both of which depend on the hydrophilic and hydrophobic stripe widths and effect number densities of water molecules above the hydrophobic and hydrophilic domains and therefore affect W_{SL} . These phenomena are described in detail below. The number density of water molecules immediately over the hydrophilic and hydrophobic domains are denoted by n_{MHol}^W and n_{OT}^W , respectively.

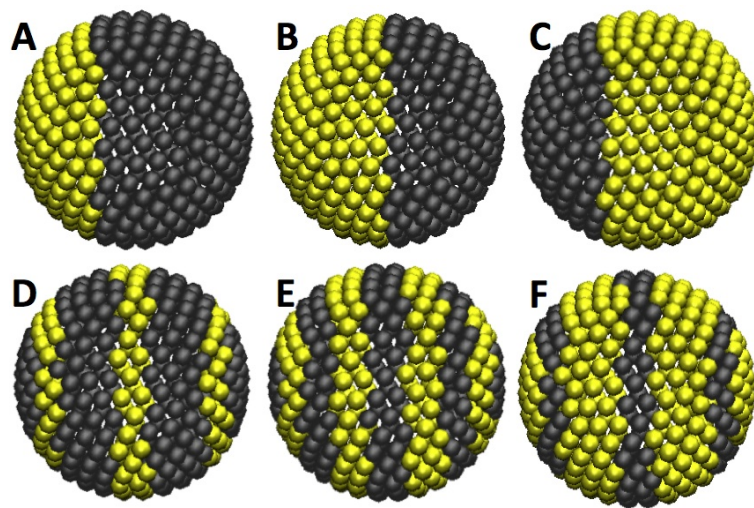


Figure 7.4 Surface patterns (head group positions) simulated with MD. The surfactant tails and surrounding water molecules have been removed. Grey and yellow beads are the headgroups of the hydrophobic (OT) and the hydrophilic (MHol) surfactants, respectively. A. to C. Janus particles with 33%, 50% and 67% MHol, respectively. D. to F. Striped nanoparticles with 33%, 50% and 67% MHol, respectively. Stripe widths of MHol (OT) for the striped nanoparticles are same as the experimental stripe widths: D. 0.6 (1.2) nm, E. 0.7 (0.7) nm, F. 1.2 (0.6) nm. (12)

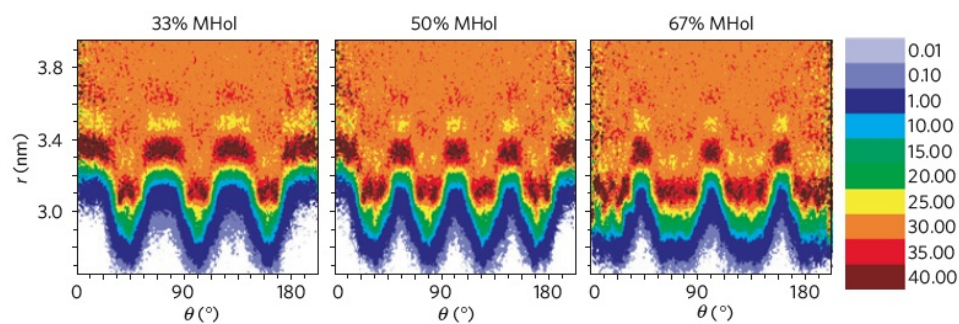


Figure 7.5 Water number density near the striped nanoparticle surface as a function of the radial coordinate along the direction perpendicular to the stripes. Peaks and troughs represent the regions over OT and MHol, respectively. The white regions represent the depletion layer over OT domains, including the tail-end groups of the OT molecules. (12)

7.4.1 Cavitation

The idea of cavitation comes from the theory of solvation of hydrophobic solutes (164). The theory states that for large hydrophobic solutes surrounded by water molecules, dewetting of the solute occurs and the hydrogen-bond network of the water molecules near the solute surface breaks up. However, if the solute is small enough, the surrounding hydrogen-bonded water network does not need to break but can instead strain itself slightly to accommodate the solute. This happens when the diameter of the solute is of the order of 1.0 nm. Since the widths of the hydrophobic domains in the striped nanoparticle is of the order of 1.0 nm, this idea of intact hydrogen-bonded water network or cage surrounding the hydrophobic domains can be extended to our system as well. In our case, surface-bound half cavities (SBHCs) or bridges form that are anchored at the neighboring hydrophilic domains. Fig. 7.6 illustrates this idea. The figure shows three bridges highlighted for very narrow hydrophobic and hydrophilic stripes. These bridges allow the surrounding water molecules to come closer to the hydrophobic surface than they would if there was dewetting, as in the case of purely hydrophobic nanoparticle. Cavitation leads to an increase in the number density of water molecules over the hydrophobic domains (n_{OT}^W) and to a corresponding decrease in the number density over the hydrophilic domains n_{MHol}^W . The degree of cavitation strongly depends on the stripe width and increases as the hydrophobic stripe width decreases. Since cavitation allows the water molecules to come closer to the surface, it enables enhanced van der Waals interactions between the waters and the nanoparticle and therefore increases W_{SL} . We now refer to the formation of SBHCs as bridging and efforts to further quantify the bridging effect are underway (157).

7.4.2 Confinement

While cavitation depends mainly on the width of the hydrophobic domains, confinement depends on the width of the hydrophilic domains. Since in our simulations and experiments, the hydrophilic molecules (MHol) are slightly shorter than the hydrophobic molecules (OT), a molecular pocket is created bounded on two sides by the hydrophobic domains with the hydrophilic domains as the base. This pocket is shown in 7.6. When the pocket is large, there is no restriction on water molecule to reside in the pocket. However, when the pocket becomes narrow, i.e. the hydrophilic stripes become narrow, there is a loss of entropic freedom for the water molecules going into the pocket. Confinement therefore reduces the number density of water molecules over the hydrophilic domains n_{MHol}^W and decreases W_{SL} . The degree of confinement is also a strong function of the stripe width and increases

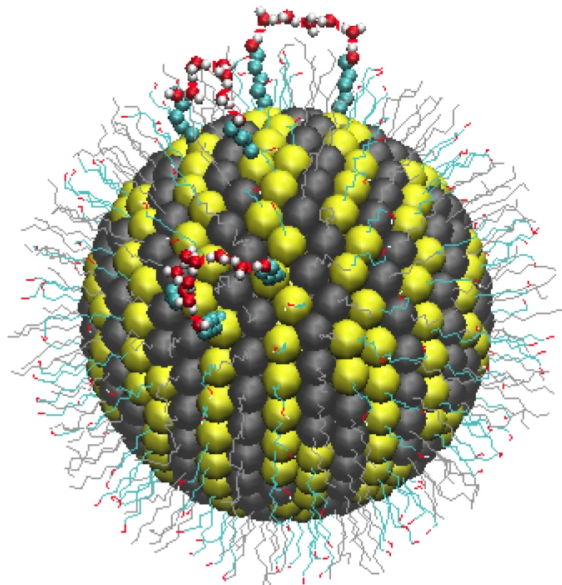


Figure 7.6 Striped nanoparticle coated with narrow hydrophobic (grey) and hydrophilic (yellow) stripes. Three bridge-like structures have been highlighted showing the participating hydrophilic chains that act as anchors and the water molecules that form the hydrogen-bonded network to complete the bridge. Rest of the water molecules have been removed for clarity. (12)

as the hydrophilic stripe width decreases. We note that recent results (157) may indicate that confinement is a much weaker phenomena than bridging and also that studying the dependence of density fluctuations and pair correlation functions of water molecules on the surface structure provides additional, important insights into the interfacial behavior of solvent molecules near nanostructured surfaces.

Since both phenomena, cavitation and confinement depend on the stripe widths and have opposing effects on W_{SL} , they might combine to have a net non-monotonic effect on W_{SL} as a function of the stripe widths. Through our simulations and the measurement of the number density of water molecules in the interfacial region (< 1.3 nm away from the nanoparticle surface), we are able to confirm the presence of both cavitation and confinement. Fig. 7.8 shows n_{MHol}^W and n_{OT}^W as a function of the composition of MHol obtained from simulations. From 33% to 50% MHol, when the hydrophilic stripe width stays almost unchanged while the hydrophobic stripe width decreases significantly, we expect that many more bridges will form on 50% MHol nanoparticle, leading to a decrease in n_{MHol}^W and an increase in n_{OT}^W . This is confirmed by 7.8. On moving from 50% to 67% MHol, the hydrophobic stripe width is nearly unchanged but the hydrophilic stripe width increases significantly. Therefore, from 50% to 67% MHol, confinement is significantly reduced and n_{MHol}^W should increase. This is what we see in 7.8. Since, the hydrophobic stripe width does not change much, n_{OT}^W

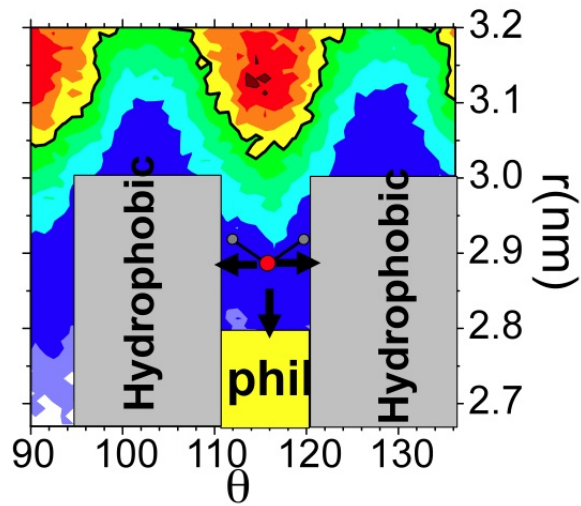


Figure 7.7 A water molecule shown confined in three directions in a molecular pocket formed over a hydrophilic domain (yellow) bordered by hydrophobic domains (grey). (12)

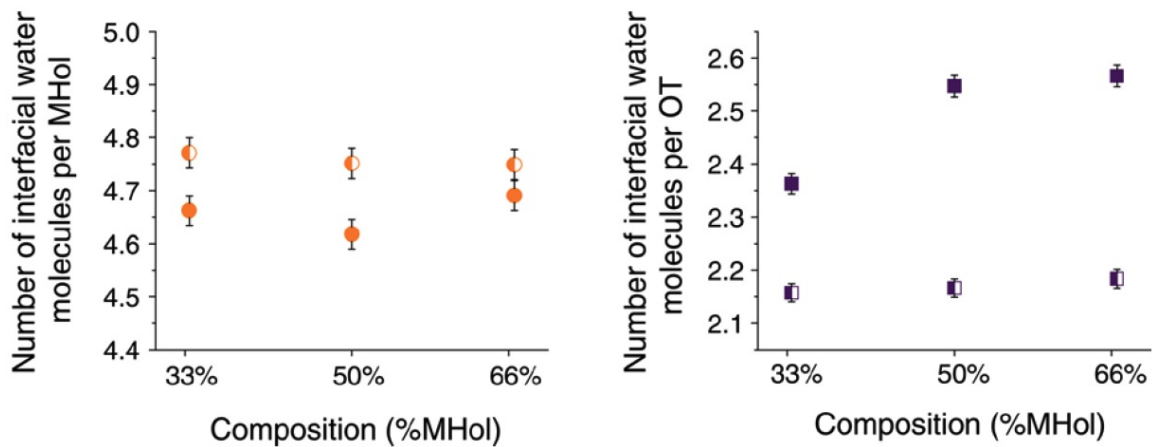


Figure 7.8 Local number densities n_{MHol}^W and n_{OT}^W of water molecules immediately above the hydrophilic (Left) and hydrophobic (Right) domains, respectively. The open and closed symbols indicate striped and Janus particles, respectively. (12)

stays almost constant from 50% to 67% MHol. The number densities over hydrophilic and hydrophobic domains for the control case of Janus particles of varying compositions, stay nearly constant further confirming that the local number densities n_{MHol}^W and n_{OT}^W depend strongly on the hydrophobic and hydrophilic stripe widths.

7.5 Summary

Through experimental and simulation results discussed in this chapter, we showed that cavitation (bridging) and confinement are both molecular-level phenomena present in surfaces coated with nanoscale hydrophobic and hydrophilic domains. Calculations of number densities immediately above the hydrophobic and hydrophilic domains demonstrate not only the presence of these effects but also the relative increase/decrease in their strength as a function of MHol concentration. Since total work of adhesion is certainly related to the number densities over hydrophobic and hydrophilic domains, we can conclude that these two phenomena that affect the number densities will also affect the work of adhesion. Further, since the phenomena have opposing influences on W_{SL} , it is likely that they combine to make the W_{SL} a non-monotonic function of the surface composition. We were therefore able to explain the unusual non-monotonic dependence of the work of adhesion of striped nanoparticles in water and other solvents, on surface composition and morphology.

Chapter 8

Conclusions and outlook

We conclude by summarizing the key contributions of this dissertation work on self-assembly of surfactants on nanostructured surfaces. There are several related projects that have been inspired by this study. Some of them have been published or have been submitted for publication, while manuscripts are being prepared for others for submission. We briefly discuss each of these projects and the progress made so far. We also discuss the outstanding question not addressed in this thesis. Finally, we provide directions for future research that can be carried out in continuation of this work.

8.1 Contributions

In this dissertation work, we used dissipative particle dynamics computer simulations to understand the patterning of self-assembled monolayers on nanostructured surfaces, specifically on spherical nanoparticles, nanowires and nanorods. We focused on understanding how factors like (i) nanoscale substrate curvature, (ii) surfactant length and/or bulkiness difference, (iii) degree of immiscibility, (iv) surface coverage, (v) starting configuration, and (vi) asymmetry affect phase-separated patterns on surfaces. Most of these parameters can be easily varied experimentally. For example, by using a longer hydrocarbon chain in a thiol, the length of the surfactant molecule adsorbed on a gold surface can be changed. Replacing a small tail end group, like $-\text{CH}_3$, by a larger group, like $-\text{COOH}$, can change the surfactant bulkiness. Immiscibility between surfactants can be tuned by changing the solvent or the tail end group. Surface coverage can be varied by using highly bulky surfactants like adamantanethiols (165; 166) and carboranethiols (167) that form scarce but uniform SAMs. Our work can therefore provide useful guidelines for designing experiments to obtain desired nanoscale patterns on flat and nanoparticle surfaces. The ability to tailor and design patterns on such a small scale has important implications in the broad areas of nanoscience and nanotechnology.

Our simulations on spherical nanoparticles explain the unexpected formation of striped patterns on surfaces of gold nanoparticles coated with a binary mixture of immiscible surfactants. In most immiscible systems, such stripe formation would be energetically disfavored due to the high energetic costs of interface formation. However, if there is sufficient length difference between the surfactants, the gain in conformational entropy of the long chains by microphase separation can outweigh the energetic costs of mixing so that the overall free energy of the system is decreased by forming nanoscale patterns. Striped nanoparticles can further be functionalized to behave as nanobuilding blocks for novel materials. The understanding of the formation of stripes provides experimentalists with useful insights into pattern control and might help to design different types of building blocks in the future.

An important feature of our study was the prediction of formation of Janus nanoparticles - particles that have different properties when viewed from diametrically opposite directions. Due to this unique surface morphology, Janus particles are interesting for potential applications in a broad range of fields including medicine, colloidal chemistry and hierarchical assembly. From our simulations we conclude that Janus particles define the lower bound of an effective size range of nanoparticle sizes in which ordered striped patterns can be obtained experimentally. When the spheres become very large, defects start appearing in the form of patches and misaligned stripes. Such a size range was also observed in experiments and is an important contribution in understanding how to design precisely patterned patchy particles.

Moving from spherical nanoparticles to flat substrates we expected that stripe-like patterns should form on flat surfaces as well. However, in practice, kinetically arrested patches are frequently obtained in simulations and experiments. These patches are slowly evolving patterns that, if given sufficient time, will merge and elongate into the equilibrium striped phase. Due to the slow dynamics, the equilibrium phase is difficult to access in simulations as well as experiments. Our work demonstrates that for symmetric mixtures i.e. mixtures with equal numbers of both surfactants, the patchy phase is indeed a kinetically arrested phase while stripes are equilibrium. The curvature of the spherical nanoparticle helps to speed-up the phase separation process which is why the patchy phase is not seen on spherical surfaces.

In asymmetric mixtures, i.e. mixtures with an unequal number of both surfactants, either ordered 2D micelles or stripes form depending on the length difference and the asymmetric fraction $\phi = (\text{number of long surfactants})/(\text{total number of surfactants})$. 2D micelles are an equilibrium phase as inferred from the fact that their coordination number is close to 6.0 which corresponds to hexagonal ordering and also that they have a uniform size distribution. This is why we refer to them as 2D micelles in the spirit of 3D micelles in surfactant and

block copolymer systems, while we refer to the kinetically arrested islands as patches. In summary, patches or micelles might form in experiments due to either of the following reasons: (i) Surface coverage is very high, surfactant length difference is small, or immiscibility between the surfactants is high. These factors will lead to the formation of patches. (ii) The adsorbed composition on the surface is far from symmetric. This will lead to the formation of micelles.

For flat surfaces we described an interface instability that spontaneously occurs in initially demixed configurations and ultimately leads to the striped phase. Efforts to characterize this instability are continuing.

We developed a novel, experimentally feasible way to relax the arrested patchy phase into striped patterns. The method involves imparting a slight curvature to the flat substrate. The curvature not only speeds up the process of patch merging and elongation, but also helps to align stripes. The procedure was validated experimentally and was found to be effective. This is the first example of using substrate stress or curvature to modify surface patterns post-adsorption.

The cylindrical surfaces were found to aid in the formation of perfect parallel rings around the circumference of the cylinder. We demonstrated that there is a clear preference for formation of horizontal stripes as opposed to vertical ones in length-mismatched surfactant systems on cylindrical surfaces. The reason for this preference is entropic in nature stemming from the fact that the long chains are able to utilize the available volume better when the stripes are horizontal than when they are vertical. Helices with a short might form since they are close in free energy to the equilibrium rings but are kinetically trapped, rather than equilibrium patterns.

We have explained the unusual non-monotonic dependence of work of adhesion of striped nanoparticles on the relative composition of the surfactants on their surface. Two molecular-level phenomena - cavitation (bridging) and confinement - combine in a complex way to result in the non-monotonicity of work of adhesion. Cavitation appears when the hydrophobic stripe width is narrow while confinement occurs for narrow hydrophilic stripe widths. Both affect work of adhesion and compete with each other. We propose ways to quantify both effects in order to obtain a better molecular-level understanding of the interfacial phenomena on the nanoparticle surfaces.

Besides being able to predict phase separation patterns and surface behavior, we have validated our predictions through collaborations with experimentalists. We hope that our work will help in tailoring surface patterns on flat as well as nanoparticle surfaces and help in the design of precisely patterned patchy particles to serve as building blocks for hierarchical assembly.

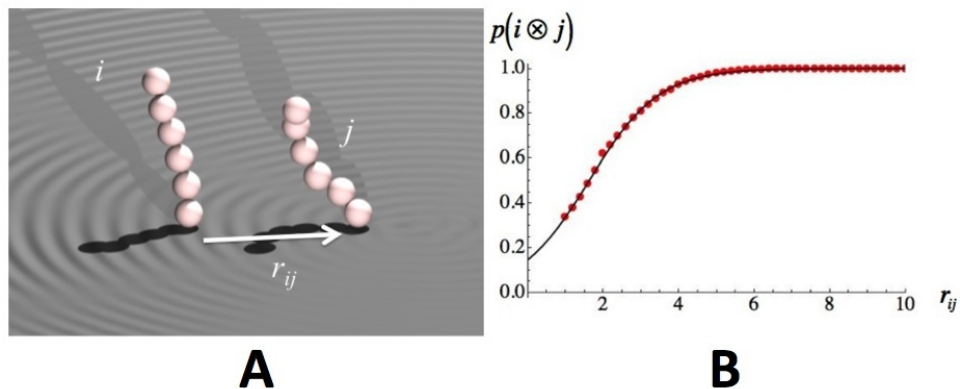


Figure 8.1 A. A snapshot showing one of the several possible conformations for surfactants i and j when the head groups of the surfactants are separated by a distance r_{ij} . B. Plot of the avoidance probability $p(i \otimes j)$. Red circles denote measured probabilities while the solid black line shows the fitted function given by Equation 8.1, where $m = 0.56442$ and $\phi = 0.97332$. (120)

8.2 Related projects

8.2.1 Ising-type model simulations as an alternative to DPD simulations

In order to reduce the time needed to obtain the phase separating patterns using DPD, an Ising-type model has recently been developed by Dr. Aaron Santos (120) in the Glotzer group, for flat surfaces and faceted nanoparticles. This model can be used in Monte Carlo simulations as an alternative to the DPD simulations. In this model, an approximate functional form for the entropy of a surfactant i at a distance r_{ij} from another surfactant j is calculated as follows: First, the head groups of the two surfactants are placed at r_{ij} distance from each other. Next, several independent conformations of the tails are generated. Fig.8.1A shows one such set of surfactant i and surfactant j conformations. The number of times that at least one of the beads in i and j overlaps, is counted. The probability of avoidance is calculated as $p(i \otimes j) = (\text{number of times no bead in surfactant } i \text{ overlaps a bead in surfactant } j) / (\text{total number of configurations generated})$. The typical number of configurations generated is 1000. This data is shown in Fig. 8.1B and was seen to fit well to the functional form given by Equation 8.1 where m and ϕ are parameters that change on changing the surfactant lengths.

$$p(i \otimes j) = 0.5 \tanh[mr_{ij} + \phi] \quad (8.1)$$

Once the avoidance probability is available, an approximate measure of the entropy of

surfactant i in the presence of surfactant j , S_{ij} is given by Equation 8.2.

$$S_{ij} = k_B \ln[p(i \otimes j)] \quad (8.2)$$

When several surfactants are present, we need to consider all surfactants in the vicinity of surfactant i to calculate its entropy. The cutoff distance to define vicinity is the distance r_{ij} in Fig. 8.1B beyond which $p(i \otimes j)$ is always unity. If $\{k\}$ is the set of all surfactants in the vicinity of surfactant i , the entropy of surfactant i , S_i is calculated using Equation 8.3 and the total entropy of the system can be obtained using Equation 8.4, where N is the total number of surfactants in the system.

$$S_i = k_B \ln\left[\prod_{j \in \{k\}} p(i \otimes j)\right] \quad (8.3)$$

$$S = \sum_{i=0}^{N-1} S_i \quad (8.4)$$

The energy E , of the system can be obtained by summing over the interaction energies of all surfactants with their first near neighbors. For a pair of surfactants i and j , the pair interaction energy $E_{ij} = -\varepsilon$ if i and j are of the same type and $E_{ij} = 0$ if they are of different types. All such E_{ij} 's can be summed without double counting to obtain the total energy E of the system. Using this approximation we now have the free energy of the system $F = E - TS$, where T is the temperature. By calculating , the surfactant tails have effectively been coarse-grained and both E and S and hence F , only depend on the 2D configuration of the head groups alone. Metropolis Monte Carlo can then be used to obtain free energy minimizing configurations.

We have used this model to obtain the phase-separated patterns in flat surface SAMs as a function of length difference and degree of immiscibility (Fig. 8.2). We find that the patterns are in good qualitative agreement with the DPD results (120). Efforts to develop a Ginzburg-Landau theory for length-mismatched surfactant SAMs are also underway.

8.2.2 Quantifying cavitation (bridging) across hydrophobic domains

We are currently working on a follow-up of the interfacial phenomena study (Chapter 7). We are trying to use more quantitative measures to estimate the degree of cavitation and confinement in striped nanoparticles. We have developed a code that identifies the hydrogen-bonded water bridges present between hydrophilic stripes on striped nanoparticles. This code is provided in Appendix B. The algorithm for bridge identification is as follows: we

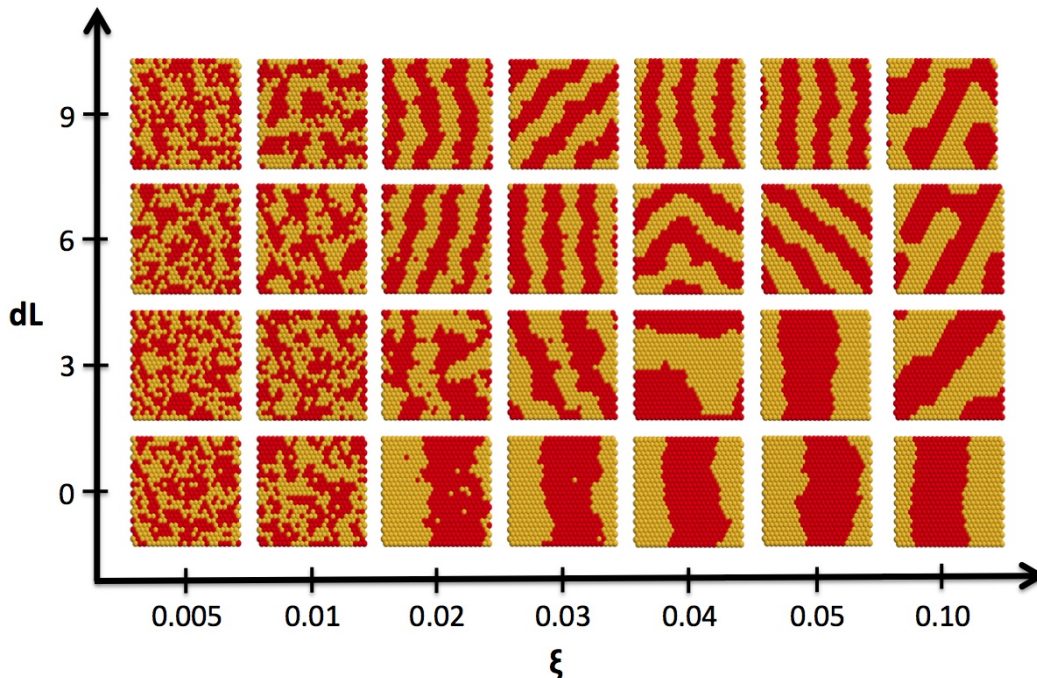


Figure 8.2 System configurations obtained as a function of tether length difference dL and strength of attraction ε . As observed in DPD and atomistic simulations, stripes are observed for sufficiently large dL provided ε is not too large. (120)

first create a list of hydrogen-bonded neighbors for each molecule. This list is created for both hydrophilic and water molecules. Next, we iterate over all hydrophilic molecules and trace all hydrogen-bonded networks that end in a neighboring stripe. All bridges, some of them branched, are stored. Various kinds of analyses can then be performed on the bridges, for example their height above the surface, defined as the coordinate of the highest water molecule in the bridge, can be calculated; histogram of bridge lengths can be prepared; average number of bridges per hydrophilic molecule can be determined, etc. Such analysis is a useful method to quantify the cavitation (bridging) effect and will be included in a forthcoming publication (157).

Other, related atomistic molecular dynamics simulation studies being undertaken include studies of ion-entrapment and catalytic properties of striped nanoparticles in the presence of explicit solvent.

8.2.3 Ternary mixtures

We have modified our code for binary mixtures to simulate ternary mixtures of surfactants on surfaces. Addition of just one more component to a SAM, expands the phase space

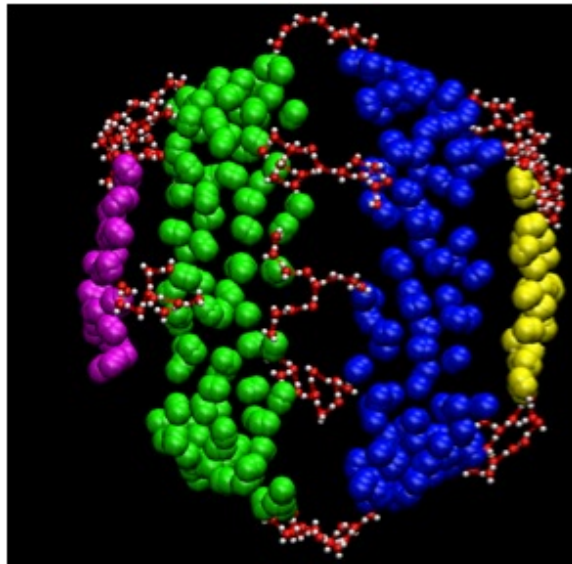


Figure 8.3 Output of the bridge identification code showing several hydrogen-bonded water bridges anchored at the hydrophilic (violet, green, blue and yellow) stripes and over the hydrophobic domains (removed for clarity). All other water molecules and surfactant chains have been removed for clarity. Different hydrophilic stripes are shown in different colors. Hydrogen bonds are shown by dashed lines.

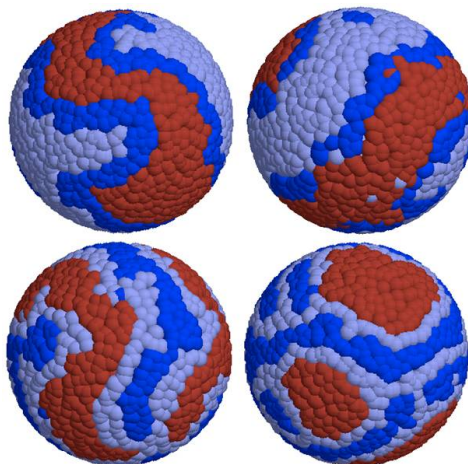


Figure 8.4 Preliminary results for patterns formed in ternary SAMs. Both striped and patchy patterns are seen. Dark blue, red and light blue beads indicate head groups of longest, intermediate length and shortest surfactants, respectively. The patterns are preliminary and possibly not equilibrated.

considerably and a much richer variety of patterns, some of which are impossible to obtain with binary mixtures can be obtained. Some of the preliminary results that we have obtained using this code are shown in Fig. 8.4.

Graduate student Ines C. Pons is currently using the code to study phase-separated

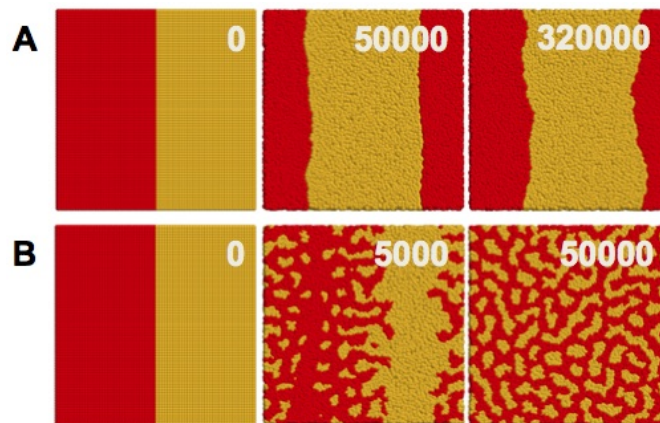


Figure 8.5 A. Snapshots of time evolution of highly immiscible ($\Delta a = 30$) surfactants showing complete separation. B. Snapshots of time evolution of slightly immiscible ($\Delta a = 5$) surfactants showing formation of jagged stripe-like and patchy domains. Yellow and red beads represent long (7 beads) and short (4 beads) surfactants respectively. The number in the top right corner is the time step at which the snapshot was taken, where K refers to thousands of time steps. (121)

patterns in ternary SAMs on spherical nanoparticles. Since the parameter space for ternary mixtures is much larger than that for binary SAMs, the focus of this study is on predicting design rules rather than entire phase diagrams. A less computationally expensive model like the Ising-type model discussed in Section 8.2.1 is better suited to obtain phase diagrams, if desired.

8.2.4 Characterization of interface instability

Our simulations show that when domains of immiscible surfactants of different lengths meet at an interface in a thermodynamically unstable configuration, the entropic forces spontaneously destabilize the interface (Fig. 5.3A). Random motion of the surfactant tails induces small perturbations in the interface that grow with time and lead to fingering (168) and ultimately form stripes of fairly uniform thickness. If the surfactants are highly immiscible, the instability is no longer seen and the surfactants stay completely separated (Fig. 8.5A), indicating the dominance of energetic forces over entropic ones. If the surfactants are only slightly immiscible, fingers form and subsequently break into droplets (Fig. 8.5B). Both these effects, fingering and breaking out of fingers into droplets are reminiscent of patterns formed by well-known hydrodynamic instabilities (168).

The interface instability seen in initially-demixed systems is an interesting finding in the context of phase separating SAMs and we are interested in characterizing it in terms of universality classes for instabilities. The first steps are to obtaining scaling relations and

critical exponents for the interface length and width as a function of time, and also as a function of system parameters like surfactant length and immiscibility. These can then be compared with the scaling relations and exponents for some well-known hydrodynamic instabilities like Hele-Shaw, Rayleigh-Taylor and Richtmyer-Meshkov (169–171).

8.3 Directions for future research

There are two outstanding questions that were not addressed in this dissertation. The first is based on the need to obtain phase diagrams and stripe-width plots for the several parameters in the system - absolute lengths of the surfactants, length difference, degree of immiscibility, radius of curvature of the substrate relative to the surfactant lengths and surface coverage. It is difficult to obtain phase diagrams since DPD although faster compared to other particle-based methods is not fast enough to be used to generate phase diagrams, unless now-available parallel and commercial DPD codes like LAMMPS-DPD are used. Using lattice-based models like the one described in Section 8.2.1 are therefore more suited to generating phase diagrams. With regard to stripe widths as a function of the various parameters also, lattice based models are better suited as compared to DPD. As shown in Fig. 8.6, the difference between stripe widths for two systems with different surfactant length differences might be very small. The errors in the DPD method due to particle overlap and surface density fluctuations is expected to be larger than this small difference in stripe widths for two given systems which makes it an unreliable method to determine stripe widths. Efforts to adapt the Ising-type model (Section 8.2.1) to perform Monte Carlo simulations of surfactants on spherical and cylindrical surface are underway. Subsequently, phase diagrams and dependence of stripe width on various system parameters will be obtained using the adapted models.

The second unanswered question is related to the effect of curvature on patterns formed in asymmetric SAMs. Preliminary results shown in Fig. 8.7 demonstrate that, unlike the behavior on flat surfaces (Section 5.4), asymmetric mixtures with majority long surfactants form predominantly stripe-like domains even when the asymmetry ratio, ϕ is close to unity. On flat surfaces, stripes were seen to form only in a narrow range of ϕ values. Such a large difference in phase separation seen in mixtures with majority long and majority short surfactants is unusual and has not been observed for in any other phase-separating mixture. A detailed study further investigating the reasons behind such behavior are therefore required.

There are several other studies can be performed in continuation of the work discussed in this dissertation. We have developed the tools and computer code needed to simulate

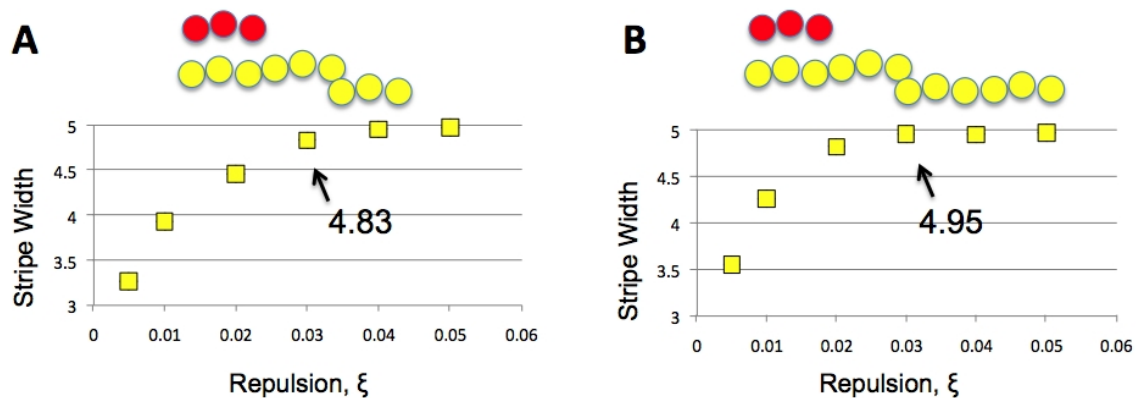


Figure 8.6 Plots of stripe widths as a function of the degree of immiscibility between the two surfactants for A. 4-bead and 9-bead surfactants and B. 4-bead and 12-bead surfactants. The short and long surfactants are shown in red and yellow respectively. The stripe widths for $\varepsilon = 0.3$ for the two systems are 4.83 and 4.95 respectively. The plots have been obtained using the Ising-type model described in Section 8.2.1. Such a small difference in stripe width is difficult to capture using DPD.

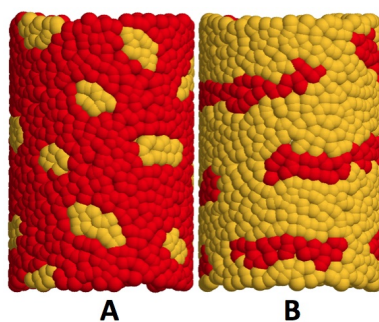


Figure 8.7 Phase separated patterns formed in mixtures of 4-bead (red) and 13-bead (yellow) surfactants on cylinders of radius 5σ . A. $\phi = 0.20$ and B. $\phi = 0.80$.

assembly of molecules on simple surfaces. The code can be modified to perform simulations on surfaces of variable curvature e.g. surfaces with convex as well as concave sections. Additionally, it would be instructive to consider more complicated surfaces like cones, tetrapods etc. to determine if the emerging patterns are different from those seen on spheres, cylinders and flat surfaces. The code can be used with minor changes to study phase separation in vesicles and also cylindrical and spherical pores. In the case of pores, the surfactant tails need to be constrained inside the sphere rather than outside as done for SAMs. Since restricting the tails to a smaller volume inside the sphere increases the overall density, the effective surface density required to simulate these systems with DPD is smaller than the density needed for SAMs. Therefore, pore simulations will run much faster than SAM simulations. Another interesting study could be performing grand canonical

ensemble simulations to study adsorption of surfactants from the solution onto the surface and simultaneous phase separation of the adsorbed components. Flexible substrates are also expected to influence phase separation and lead to patterns different from those formed on rigid substrates. Using the Ising-type model discussed in Section 8.2.1 to study ternary mixtures on spherical and cylindrical substrates is also interesting.

Appendices

Appendix A

Constrained dynamics code

A.1 Spherical surfaces

```
for (i=0; i<N; i++)
{
for(k=0; k<3; k++)
{
old_position[k] = x[i][k];
x[i][k] += v[i][k]*dt + dt2*fold[i][k]/mass;
v_temp[i][k] = v[i][k] + dt1*fold[i][k]/mass;
}

switch(type[i]) // particles to constrain
{
case 1:
case 5:
dot_prod = old_position[0]*x[i][0] + old_position[1]*x[i][1] +
old_position[2]*x[i][2];
new_distance_from_center_sq = x[i][0]*x[i][0] + x[i][1]*x[i][1]
+ x[i][2]*x[i][2];
lambda = (dot_prod - sqrt(dot_prod*dot_prod -
d_sq*(new_distance_from_center_sq - d_sq)))/d_sq;
for(k=0; k<3; k++)
{
fold[i][k] = fold[i][k] - lambda * old_position[k]/dt/dt;
x[i][k] = x[i][k] - lambda*old_position[k];
}
}
```

```

    }
}

```

A.2 Cylindrical surfaces

```

    for (i=0; i<N; i++)
    {
        for(k=0; k<3; k++)
        {
            old_position[k] = x[i][k];
            x[i][k] += v[i][k]*dt + dt2*fold[i][k]/mass;
            v_temp[i][k] = v[i][k] + dt1*fold[i][k]/mass;
        }

        switch(type[i])
        {
            case 1:
            case 5:
                dot_product=old_position[0]*x[i][0] +old_position[2]*x[i][2];
                new_distance_from_center_sq=x[i][0]*x[i][0] +x[i][2]*x[i][2];
                lambda = (dot_product - sqrt(dot_product*dot_product -
                    d_sq*(new_distance_from_center_sq - d_sq)))/d_sq;

                fold[i][0] = fold[i][0] - lambda*old_position[0]/dt/dt;
                fold[i][2] = fold[i][2] - lambda*old_position[2]/dt/dt;

                x[i][0] = x[i][0] - lambda*old_position[0];
                x[i][2] = x[i][2] - lambda*old_position[2];
                break;
            default::
        }

        x[i][1] -= Len[1]*anint(x[i][1]*invLen[1]);
    }
}

```

A.3 Flat surfaces

```
for (i=0; i<N; i++)
{
  for(k=0; k<3; k++)
  {
    old_position[k] = x[i][k];
    x[i][k] += v[i][k]*dt + dt2*fold[i][k]/mass;
    v_temp[i][k] = v[i][k] + dt1*fold[i][k]/mass;
  }

  switch(type[i])
  {
    case 1:
    case 5:
      lambda = (x[i][2] - flat_plane_depth)/old_position[2];
      fold[i][2] = fold[i][2] - lambda * old_position[2]/dt/dt;
      x[i][2] = x[i][2] - lambda*old_position[2];
      break;
  }

  for(k=0; k<2; k++)
  {
    x[i][k] -= Len[k]*anint(x[i][k]*invL[k]);
  }
}
```


Appendix B

Bridge identification code

B.1 bridge.cpp

```
{
#include <new>
#include <cstdlib>
#include <iostream>
#include <string>
#include "bridges.h"
#include "definitions.h"

void quit(void)
{
    exit(1);
}

void bridge_identification(double interface_r1, double interface_r2,
int n_stripes, double Stripe_angle1[], double Stripe_angle2[],
double d_angle, int n_mols, MOL_ *Molecules, int& n_bridges,
BRIDGE_ *Bridges, double LBox[3], double NPC[3], int frID,
bool write_bridge, int mode)
{
    static bool firsttime = true;
    int i, j;
    static waterMolecule *waterMols;
    static cell *cells;
    static list *nlist;
```

```

static list *global_nlist;
static int numWaters;
static bool globalListGenerated = false;

if(firsttime == true)
{
    firsttime = false;

    waterMols = (waterMolecule *) calloc(
        MAX_NUMMOLECULES, sizeof(waterMolecule));
    InitializeWaterMols(waterMols);

    /* allocate cells & give them capacity */
    cells = (cell *) calloc(NCELL_TOTAL, sizeof (cell));

    for(i = 0; i < NCELL_TOTAL; i++)
    {
        cells[i].last = 0;
        cells[i].watersInThisCell = (int*) calloc(
            MAX_WATERS_PER_CELL, sizeof(int));
        for (j = 0; j < MAX_WATERS_PER_CELL; j++)
        {
            cells[i].watersInThisCell[j] = 0;
        }
    }

    /* allocate neighbor list space */
    nlist = (list*) calloc(MAX_NUMMOLECULES,
        sizeof(list));
    global_nlist = (list*) calloc(MAX_NUMMOLECULES,
        sizeof(list));
    for(i = 0; i < MAX_NUMMOLECULES; i++)
    {
        nlist[i].last = 0;
        nlist[i].neighbors = (int*) calloc(
            MAX_NEIGHBORS_PER_WATER, sizeof(int));
    }
}

```

```

        global_nlist[i].last = 0;
        global_nlist[i].neighbors = (int*) calloc(
            MAX_NEIGHBORS_PER_WATER_GLOBAL,
            sizeof(int));
    }

    init_cells(cells);
}

PopulateWaterMols(waterMols, &numWaters, n_stripes,
Stripe_angle1, Stripe_angle2, d_angle, n_mols, Molecules,
LBox, NPC);

if(frID == FIRST_FRAME || write_bridge){
    char name[20];
    sprintf(name, "stripes_\\%04d.xyz", frID);
    PrintWaterMols(waterMols, numWaters, name);
}

load(waterMols, numWaters, cells, LBox);

if(mode == APPEND_NLIST_MODE)
{
    if(frID == FIRST_FRAME)
    {
        neighbor_list(global_nlist, waterMols,
numWaters, cells, interface_r1, interface_r2,
LBox, NPC);
        globalListGenerated = true;
        make_bridges(global_nlist, waterMols,
numWaters, n_bridges, Bridges, n_mols,
Molecules, n_stripes, frID, write_bridge);
    }
    else
    {
        neighbor_list(nlist, waterMols, numWaters,
cells, interface_r1, interface_r2, LBox, NPC);
    }
}

```

```

        append_to_global_nlist(global_nlist ,
                               nlist , numWaters);
        make_bridges(global_nlist , waterMols ,
                    numWaters , n_bridges , Bridges , n_mols ,
                    Molecules , n_stripes , frID , write_bridge);
    }
}
else // i.e. if mode == GENERATE_BRIDGE_MODE
{
    if(globalListGenerated == true)
    {
        neighbor_list(nlist , waterMols , numWaters ,
                    cells , interface_r1 , interface_r2 , LBox , NPC);
        append_to_global_nlist(global_nlist ,
                               nlist , numWaters);
        make_bridges(global_nlist , waterMols ,
                    numWaters , n_bridges , Bridges , n_mols ,
                    Molecules , n_stripes , frID , write_bridge);
    }
    else
    {
        neighbor_list(nlist , waterMols , numWaters ,
                    cells , interface_r1 , interface_r2 , LBox , NPC);
        make_bridges(nlist , waterMols , numWaters ,
                    n_bridges , Bridges , n_mols , Molecules ,
                    n_stripes , frID , write_bridge);
    }
}
}

//int test()
int main()
{
    const int NUMATOMS_MH = 21;
    const int NUMATOMS_OT = 26;
    int t;

```

```

int num_frames = 20;

int i, j, num_atoms, num_molecules, d;
ATOM_ *allAtoms;
MOL_ *allMolecules;
BRIDGE_ *allBridges;

double LBox[3], invL[3];
double NPC[3];
LBox[0] = 79.208635;
LBox[1] = 79.208635;
LBox[2] = 79.208635;
for(d = 0; d < 3; d++)
{
    invL[d] = 1.0/LBox[d];
}

allMolecules = new MOL_[MAX_NUM_MOLECULES];
allBridges = new BRIDGE_[MAX_NUM_BRIDGES];
// allBridges=NULL;

FILE *fpInput;
FILE *fpOutput;
fpInput = fopen("HISTORY_GOOD_WITH_NPC", "r");

for(t = 1; t <= num_frames; t++)
{
    fscanf(fpInput, "%d", &num_atoms);
    allAtoms = new ATOM_[num_atoms];
    num_molecules = 0;
    for(i = 0; i < num_atoms; i++)
    {
        allAtoms[i].atomID = i;
        allAtoms[i].molID = num_molecules;
        fscanf(fpInput, "%s\t%f\t%f\t%f\n",
            &allAtoms[i].atomName,

```

```

&allAtoms [ i ]. Coor [ 0 ], &allAtoms [ i ]. Coor [ 1 ],
&allAtoms [ i ]. Coor [ 2 ] );

for ( d = 0 ; d < 3 ; d ++ )
{
    allAtoms [ i ]. Coor [ d ] -= LBox [ d ] * anint (
        allAtoms [ i ]. Coor [ d ] * invL [ d ] );
}

if ( ( strcmp ( allAtoms [ i ]. atomName , "S1" ) == 0 )
( strcmp ( allAtoms [ i ]. atomName , "S2" ) == 0 ) ||
( strcmp ( allAtoms [ i ]. atomName , "O2" ) == 0 ) )
{
    allMolecules [ num_molecules ]. molID =
        num_molecules ;
    if ( strcmp ( allAtoms [ i ]. atomName , "S1" )
        == 0 )
    {
        strcpy ( allMolecules [ num_molecules ].
            molName , "MH" );
        allMolecules [ num_molecules ].
            n_atoms = 1 ;
        allMolecules [ num_molecules ].
            Atoms_ = new ATOM_ [ NUM_ATOMS_MH ] ;
    }
    else if ( strcmp ( allAtoms [ i ]. atomName ,
        "S2" ) == 0 )
    {
        strcpy ( allMolecules [ num_molecules ].
            molName , "OT" );
        allMolecules [ num_molecules ].
            n_atoms = 1 ;
        allMolecules [ num_molecules ].
            Atoms_ = new ATOM_ [
                NUM_ATOMS_OT ] ;
    }
}

```

```

else if (strcmp (allAtoms [ i ]. atomName ,
                "O2") == 0)
{
    strcpy (allMolecules [ num_molecules ]
            molName, " water");
    allMolecules [ num_molecules ].
        n_atoms = 1;
    allMolecules [ num_molecules ].
        Atoms_ = new ATOM_[
            NUM_ATOMS_WATER];
}
allMolecules [ num_molecules ].
    n_bridges = 0;
allMolecules [ num_molecules ].
    BridgeID = new
        int [MAX_NUM_BRIDGES_PER_MOL];
allMolecules [ num_molecules ]. Atoms_ [0]
    = allAtoms [ i ];
}
else if (strcmp (allAtoms [ i ]. atomName , "NPC")
        == 0)
{
    NPC[0] = allAtoms [ i ]. Coord [0];
    NPC[1] = allAtoms [ i ]. Coord [1];
    NPC[2] = allAtoms [ i ]. Coord [2];
    for (d = 0; d < 3; d++)
    {
        NPC[d] -= LBox[d]* anint (NPC[d]
            *invL[d]);
    }
}
else
{
    allMolecules [ num_molecules ]. Atoms_
        [ allMolecules [ num_molecules ].
            n_atoms]= allAtoms [ i ];
}

```

```

        allMolecules[num_molecules].n_atoms++;
        if ((( strcmp( allMolecules[num_molecules]
            .molName, "OT") == 0) && (
            allMolecules[num_molecules].n_atoms ==
            NUMATOMS_OT)) || ( strcmp( allMolecules
            [num_molecules].molName, "MH") == 0) &&
            ( allMolecules[num_molecules].n_atoms ==
            NUMATOMS_MH)) || ( strcmp( allMolecules
            [num_molecules].molName, "water") == 0) &&
            ( allMolecules[num_molecules].n_atoms ==
            NUMATOMS_WATER)) )
            {
                num_molecules++;
            }
    }
}

```

```

double interface_r1 = 26.70;
double interface_r2 = 33.25;
int n_bridges = 0;
int n_stripes = 4;
double Stripe_angle1[4] = {0.00, 46.58967, 98.31935,
    150.16739};
double Stripe_angle2[4] = {29.83238, 81.46224,
    133.41094, 180.00};
double d_angle = 10.0;

```

```

if(t == num_frames)
{
    bridge_identification(interface_r1 , interface_r2 ,
        n_stripes , Stripe_angle1 , Stripe_angle2 ,
        d_angle , num_molecules , allMolecules ,
        n_bridges , allBridges , LBox, NPC, t, true ,
        GENERATE_BRIDGE_MODE);
}
else

```



```

        {
            // for cumulative
            bridge_identification(interface_r1 , interface_r2 ,
            n_stripes , Stripe_angle1 , Stripe_angle2 ,
            d_angle , num_molecules , allMolecules ,
            n_bridges , allBridges , LBox, NPC, t, true ,
            APPEND_NLIST_MODE);

            // for non-cumulative
            // bridge_identification(interface_r1 , interface_r2
            n_stripes , Stripe_angle1 , Stripe_angle2 ,
            d_angle , num_molecules , allMolecules ,
            n_bridges , allBridges , LBox, NPC, t, true ,
            GENERATE_BRIDGE_MODE);
        }
    }
    fclose(fpInput);

    delete [] allAtoms;
    delete [] allMolecules;
    delete [] allBridges;

    return 1;
}

```

B.2 bridges.h

```

{
#ifndef BRIDGES
#define BRIDGES

#define MAX_NUM_BRIDGES 50000
#define MAX_BRIDGE_LEN 10
#define MIN_BRIDGE_LEN 3
#define MAX_NUM_BRIDGES_PER_MOL 5800

```

```

struct ATOM_{
    int atomID;
    int molID;
    char atomName[10]; //S1 for the sulfur of MH
    //O1 and H1 for the oxygen and hydrogen of MH
    //O2 for the oxygen of water
    //H2 and H3 for the hydrogen of water
    double Coor[3];
};

struct MOL_{
    int molID;
    char molName[10];
    bool alcohol;
    int n_atoms;
    ATOM_ *Atoms_;
    int n_bridges;
    int *BridgeID;
};

struct BRIDGE_{
    int bridgeID;
    int BridgeEnds_molIDs[2]; //molID of the MH;
    //make sure bridgeEnds_molIDs[0]<bridgeEnds_molIDs[1]
    int n_bridgeWater;
    int *BridgeWater_MolID;
    //BridgeWater_MolID contains the molIDs of WATERS only
    //arranged in order starting with the one connecting
    // to BridgeEnds_molIDs[0]
    //and ending with the one connecting to
    //BridgeEnds_molIDs[1]
};
double LBox[3]);

void bridge_identification(double interface_r1 ,
double interface_r2 , int n_stripes ,

```

```

    double Stripe_angle1 [], double Stripe_angle2 [],
    double d_angle, int n_mols, MOL_ *Molecules,
    int& n_bridges, BRIDGE_ *Bridges,
    double LBox[3], double NPC[3], int frID,
    bool write_bridge, int mode);

    int test();

#endif
}

```

B.3 definitions.h

```

{
#ifndef DEFN
#define DEFN
#include <stdio.h>
#include <math.h>
#include <stdlib.h>
#include <string.h>

#define NBRS 27
#define NCELLX 8
#define NCELLY 8
#define NCELLZ 8
#define NCELL_TOTAL (NCELLX * NCELLY * NCELLZ)
#define PI 3.14159265359

#define PRINT_WATER 5000

#define MAX_STACK_LENGTH 10000
#define MAX_NEIGHBORS_PER_WATER 10
#define MAX_NEIGHBORS_PER_WATER_GLOBAL 50
#define MAX_WATERS_PER_CELL (1000*MAX_NUM_MOLECULES/NCELL_TOTAL)

```

```

#define MAX_NUM_MOLECULES 14000
#define NUM_ATOMS_WATER 3

#define HBOND_ANGLE 145
#define HBOND_DIST 3.5

#define APPEND_NLIST_MODE 0
#define GENERATE_BRIDGE_MODE 1
#define FIRST_FRAME 1

#define anint(x) ((x >= 0.5) ? (1.0) : (x < -0.5) ? (-1.0) : (0.0))

typedef struct _cell
{
    int *watersInThisCell; /*array of water indices in the cell*/
    int last; /*array element containing the last molecule*/
    int neighbors[NBRS]; /*nearest neighbor identities */
    int neighbor_counter;
} cell;

typedef struct _list
{
    int *neighbors; /*array of neighboring atoms/molecules*/
    int last; /*last molecule on the list*/
} list;

typedef struct _waterMolecule
{
    int type;
    int sub_typeA; // for OH groups only
    int sub_typeB; // for OH groups only
    int molID;
    double oxygen[3];
    double first_hydrogen[3];
    double second_hydrogen[3];
} waterMolecule;

```

```

typedef struct _bridge
{
    int bridge_length;
    int bridge_body[MAX_BRIDGE_LEN];
} bridge;

typedef struct _stack
{
    int length;
    int **stack_list;
} stack;

void InitializeWaterMols(waterMolecule *waterMols);

void PopulateWaterMols(waterMolecule *waterMols, int *numWaters,
    int n_stripes, double Stripe_angle1[], double Stripe_angle2[],
    double d_angle, int n_mols, MOL_ *Molecules,
    double LBox[3], double NPC[3]);

void PrintWaterMols(waterMolecule *waterMols,
    int numWaters, char *outputFileName);

void init_cells(cell* cells);

void load(waterMolecule *waterMols, int numWaters,
    cell *cells, double LBox[3]);

void neighbor_list(list *nlist, waterMolecule *waterMols,
    int numWaters, cell *cells, double interface_r1,
    double interface_r2, double LBox[3], double NPC[3]);

int HBond(double oxy1[3], double oxy2[3], double hyd[3],
    double LBox[3]);

void make_bridges(list *nlist, waterMolecule *waterMols,

```

```

        int numWaters, int& n_bridges, BRIDGE_ *Bridges,
            int n_mols, MOL_ *Molecules, int n_stripes,
            int frID, bool wrtbridge);

int check_bridge(bridge current_bridge, int end_type,
    bridge *all_bridges, int bridge_count, int sub_typeA1,
    int sub_typeA2, int sub_typeB1, int sub_typeB2,
    int n_stripes);

int AreHBondedWaters(waterMolecule first_water,
    waterMolecule second_water, double LBox[3]);

//void getFlippedBridge(bridge current_bridge, bridge flipped_bridge);

void bridge_identification(double interface_r1, double interface_r2,
    int n_stripes, double Stripe_angle1[], double Stripe_angle2[],
    double d_angle, int n_mols, MOL_ *Molecules,
    int& n_bridges, BRIDGE_ *Bridges,
    double LBox[3], double NPC[3],
    int frID, bool write_bridge, int mode);

void append_to_global_nlist(list *global_nlist, list *nlist,
    int numWaters);

#endif
}

```

Bibliography

- [1] A. Ulman, "Formation and structure of self-assembled monolayers," *Chemical Reviews*, vol. 96, no. 4, pp. 1533–1554, 1996.
- [2] J. C. Love, L. A. Estroff, J. K. Kriebel, R. G. Nuzzo, and G. M. Whitesides, "Self-assembled monolayers of thiolates on metals as a form of nanotechnology," *Chemical Reviews*, vol. 105, pp. 1103–1169, 2005.
- [3] S. D. Evans, R. Sharma, and A. Ulman, "Contact-angle stability - reorganization of monolayer surfaces," *Langmuir*, vol. 7, no. 1, pp. 156–161, 1991.
- [4] R. G. Nuzzo, L. H. Dubois, and D. L. Allara, "Fundamental-studies of microscopic wetting on organic-surfaces. 1. Formation and structural characterization of a self-consistent series of polyfunctional organic monolayers," *Journal of the American Chemical Society*, vol. 112, no. 2, pp. 558–569, 1990.
- [5] M. D. Porter, T. B. Bright, D. L. Allara, and C. E. D. Chidsey, "Spontaneously organized molecular assemblies. 4. Structural characterization of normal-alkyl thiol monolayers on gold by optical ellipsometry, infrared-spectroscopy, and electrochemistry," *Journal of the American Chemical Society*, vol. 109, no. 12, pp. 3559–3568, 1987.
- [6] J. H. Fendler, "Chemical self-assembly for electronic applications," *Chemistry of Materials*, vol. 13, no. 10, pp. 3196–3210, 2001.
- [7] P. Harder, M. Grunze, R. Dahint, G. M. Whitesides, and P. E. Laibinis, "Molecular conformation in oligo(ethylene glycol)-terminated self-assembled monolayers on gold and silver surfaces determines their ability to resist protein adsorption," *Journal of Physical Chemistry B*, vol. 102, no. 2, pp. 426–436, 1998.
- [8] P. E. Laibinis, R. G. Nuzzo, and G. M. Whitesides, "Structure of monolayers formed by coadsorption of 2 normal-alkanethiols of different chain lengths of gold and its relation to wetting," *Journal of Physical Chemistry*, vol. 96, no. 12, pp. 5097–5105, 1992.
- [9] M. Mrksich, C. S. Chen, Y. N. Xia, L. E. Dike, D. E. Ingber, and G. M. Whitesides, "Controlling cell attachment on contoured surfaces with self-assembled monolayers of alkanethiolates on gold," *Proceedings of the National Academy of Sciences of the United States of America*, vol. 93, no. 20, pp. 10775–10778, 1996.

- [10] E. Ostuni, L. Yan, and G. M. Whitesides, "The interaction of proteins and cells with self-assembled monolayers of alkanethiolates on gold and silver," *Colloids and Surfaces B-Biointerfaces*, vol. 15, no. 1, pp. 3–30, 1999.
- [11] A. M. Jackson, J. W. Myerson, and F. Stellacci, "Spontaneous assembly of subnanometre-ordered domains in the ligand shell of monolayer-protected nanoparticles," *Nature Materials*, vol. 3, no. 5, pp. 330–336, 2004.
- [12] J. J. Kuna, K. Voitchovsky, C. Singh, H. Jiang, S. Mwenifumbo, P. K. Ghorai, M. M. Stevens, S. C. Glotzer, and F. Stellacci, "The effect of nanometre-scale structure on interfacial energy," *Nature Materials*, vol. 8, no. 10, pp. 837–842, 2009.
- [13] K. Salaita, A. Amarnath, D. Maspoeh, T. B. Higgins, and C. A. Mirkin, "Spontaneous phase separation of patterned binary alkanethiol mixtures," *Journal of the American Chemical Society*, vol. 127, no. 32, pp. 11283–11287, 2005.
- [14] Y. Wang, Z. Y. Tang, X. R. Liang, L. M. Liz-Marzan, and N. A. Kotov, "SiO₂ - coated CdTe nanowires: Bristled nano centipedes," *Nano Letters*, vol. 4, no. 2, pp. 225–231, 2004.
- [15] T. Wink, S. J. vanZuilen, A. Bult, and W. P. vanBennekom, "Self-assembled monolayers for biosensors," *Analyst*, vol. 122, no. 4, pp. R43–R50, 1997.
- [16] C. D. Bain, J. Evall, and G. M. Whitesides, "Formation of monolayers by the coadsorption of thiols on gold - variation in the head group, tail group and solvent," *Journal of the American Chemical Society*, vol. 111, no. 18, pp. 7155–7164, 1989.
- [17] J. P. Folkers, P. E. Laibinis, G. M. Whitesides, and J. Deutch, "Phase-behavior of 2-component self-assembled monolayers of alkanethiols on gold," *Journal of Physical Chemistry*, vol. 98, no. 2, pp. 563–571, 1994.
- [18] P. E. Laibinis and G. M. Whitesides, "Self-assembled monolayers of n-alkanethiols on copper are barrier films that protect the metal against oxidation by air," *Journal of the American Chemical Society*, vol. 114, no. 23, pp. 9022–9028, 1992.
- [19] S. J. Stranick, A. N. Parikh, Y. T. Tao, D. L. Allara, and P. S. Weiss, "Phase-separation of mixed-composition self-assembled monolayers into nanometer-scale molecular domains," *Journal of Physical Chemistry*, vol. 98, no. 31, pp. 7636–7646, 1994.
- [20] S. J. Stranick, M. M. Kamna, K. R. Krom, A. N. Parikh, D. L. Allara, and P. S. Weiss, "Scanning-tunneling-microscopy studies of self-assembled monolayers of

- alkanethiols on gold,” *Journal of Vacuum Science and Technology B*, vol. 12, no. 3, pp. 2004–2007, 1994.
- [21] S. J. Stranick, S. V. Atre, A. N. Parikh, M. C. Wood, D. L. Allara, N. Winograd, and P. S. Weiss, “Nanometer-scale phase separation in mixed composition self-assembled monolayers,” *Nanotechnology*, vol. 7, no. 4, pp. 438–442, 1996.
- [22] C. Gentilini, P. Franchi, E. Mileo, S. Polizzi, M. Lucarini, and L. Pasquato, “Formation of patches on 3D SAMs driven by thiols with immiscible chains observed by ESR spectroscopy,” *Angewandte Chemie-International Edition*, vol. 48, no. 17, pp. 3060–3064, 2009.
- [23] N. J. Brewer and G. J. Leggett, “Chemical force microscopy of mixed self-assembled monolayers of alkanethiols on gold: Evidence for phase separation,” *Langmuir*, vol. 20, no. 10, pp. 4109–4115, 2004.
- [24] G. Binnig and H. Rohrer, “Scanning tunneling microscopy,” *IBM Journal of Research and Development*, vol. 30, no. 4, pp. 355–369, 1986.
- [25] F. J. Giessibl, “Advances in atomic force microscopy,” *Reviews of Modern Physics*, vol. 75, pp. 949–983, 2003.
- [26] S. C. Glotzer and M. J. Solomon, “Anisotropy of building blocks and their assembly into complex structures,” *Nature Materials*, vol. 6, pp. 557–562, 2007.
- [27] A. M. Jackson, Y. Hu, P. J. Silva, and F. Stellacci, “From homoligand- to mixed-ligand-monolayer-protected metal nanoparticles: A scanning tunneling microscopy investigation,” *Journal of the American Chemical Society*, vol. 128, no. 34, pp. 11135–11149, 2006.
- [28] G. A. DeVries, M. Brunnbauer, Y. Hu, A. M. Jackson, B. Long, B. T. Neltner, O. Uzun, B. H. Wunsch, and F. Stellacci, “Divalent metal nanoparticles,” *Science*, vol. 315, pp. 358–361, 2007.
- [29] A. Centrone, E. Penzo, M. Sharma, J. W. Myerson, A. M. Jackson, N. Marzari, and F. Stellacci, “The role of nanostructure in the wetting behavior of mixed-monolayer-protected metal nanoparticles,” *Proceedings of the National Academy of Sciences of the United States of America*, vol. 105, no. 29, pp. 9886–9891, 2008.
- [30] A. Verma, O. Uzun, Y. H. Hu, Y. Hu, H. S. Han, N. Watson, S. L. Chen, D. J. Irvine, and F. Stellacci, “Surface-structure-regulated cell-membrane penetration by

- monolayer-protected nanoparticles,” *Nature Materials*, vol. 7, no. 7, pp. 588–595, 2008.
- [31] Z. L. Zhang, M. A. Horsch, M. H. Lamm, and S. C. Glotzer, “Tethered nano building blocks: Toward a conceptual framework for nanoparticle self-assembly,” *Nano Letters*, vol. 3, no. 10, pp. 1341–1346, 2003.
- [32] Z. L. Zhang and S. C. Glotzer, “Self-assembly of patchy particles,” *Nano Letters*, vol. 4, no. 8, pp. 1407–1413, 2004.
- [33] R. P. Carney, G. A. DeVries, C. Dubois, H. Kim, J. Y. Kim, C. Singh, P. K. Ghorai, J. B. Tracy, R. L. Stiles, R. W. Murray, S. C. Glotzer, and F. Stellacci, “Size limitations for the formation of ordered striped nanoparticles,” *Journal of the American Chemical Society*, vol. 130, no. 3, p. 798, 2008.
- [34] J. Israelachvili, *Intermolecular and Surface Forces*. Academic London, 1992.
- [35] R. G. Larson, *The Structure and Rheology of Complex Fluids*. Oxford University Press, 1999.
- [36] E. J. Wanless and W. A. Ducker, “Organization of sodium dodecyl sulfate at the graphite-solution interface,” *Journal of Physical Chemistry*, vol. 100, no. 8, pp. 3207–3214, 1996.
- [37] C. Richard, F. Balavoine, P. Schultz, T. W. Ebbesen, and C. Mioskowski, “Supramolecular self-assembly of lipid derivatives on carbon nanotubes,” *Science*, vol. 300, no. 5620, pp. 775–778, 2003.
- [38] N. Tillman, A. Ulman, and J. F. Elman, “Oxidation of a sulfide group in self-assembled monolayer,” *Langmuir*, vol. 5, no. 4, pp. 1020–1026, 1989.
- [39] N. Tillman, A. Ulman, and T. L. Penner, “Formation of multilayers by self-assembly,” *Langmuir*, vol. 5, no. 1, pp. 101–111, 1989.
- [40] F. Schmid, C. Stadler, and D. Duchs, “Computer simulations of self-assembled monolayers,” *Journal of Physics-Condensed Matter*, vol. 13, no. 38, pp. 8653–8659, 2001.
- [41] R. G. Nuzzo, F. A. Fusco, and D. L. Allara, “Spontaneously organized molecular assemblies. 3. Preparation and properties of solution adsorbed of organic disulfides on gold surfaces,” *Journal of the American Chemical Society*, vol. 109, no. 8, pp. 2358–2368, 1987.

- [42] C. E. D. Chidsey and D. N. Loiacono, "Organosulfur monolayers on gold - structure, defects and electron-transfer kinetics," *Journal of the Electrochemical Society*, vol. 134, no. 8B, pp. C504–C504, 1987.
- [43] A. Marchenko, Z. X. Xie, J. Cousty, and L. P. Van, "Structures of self-assembled monolayer of alkanes adsorbed on Au(111) surfaces," *Surface and Interface Analysis*, vol. 30, no. 1, pp. 167–169, 2000.
- [44] T. Sawaguchi, Y. Sato, and F. Mizutani, "In situ STM imaging of individual molecules in two-component self-assembled monolayers of 3-mercaptopropionic acid and 1-decanethiol on Au(111)," *Journal of Electroanalytical chemistry*, vol. 496, no. 1-2, pp. 50–60, 2001.
- [45] T. Takami, E. Delamarche, B. Michel, C. Gerber, H. Wolf, and H. Ringsdorf, "Recognition of individual tail groups in self-assembled monolayers," *Langmuir*, vol. 11, no. 10, pp. 3876–3881, 1995.
- [46] E. Delamarche, B. Michel, C. Gerber, D. Anselmetti, H. J. Guntherodt, H. Wolf, and H. Ringsdorf, "Real-space observation of nanoscale molecular domains in self-assembled monolayers," *Langmuir*, vol. 10, no. 9, pp. 2869–2871, 1994.
- [47] D. H. Kim, J. Noh, M. Hara, and H. Lee, "An adsorption process study on the self-assembled monolayer formation of octadecanethiol chemisorbed on gold surface," *Bulletin of the Korean Chemical Society*, vol. 22, no. 3, pp. 276–280, 2001.
- [48] W. Mar and M. L. Klein, "Molecular dynamics study of the self assembled monolayer composed of $S(CH_2)_{14}CH_3$ molecules using an all atoms model," *Langmuir*, vol. 10, no. 1, pp. 188–196, 1994.
- [49] S. Vemparala, B. B. Karki, R. K. Kalia, A. Nakano, and P. Vashishta, "Large-scale molecular dynamics simulations of alkanethiol self-assembled monolayers," *Journal of Chemical Physics*, vol. 121, no. 9, pp. 4323–4330, 2004.
- [50] P. K. Ghori and S. C. Glotzer, "Molecular dynamics simulation study of self-assembled monolayers of alkanethiol surfactants on spherical gold nanoparticles," *Journal of Physical Chemistry C*, vol. 111, pp. 15857–15862, 2007.
- [51] D. Zanchet, B. D. Hall, and D. Ugarte, "Structure population in thiol-passivated gold nanoparticles," *Journal of Physical Chemistry B*, vol. 104, no. 47, pp. 11013–11018, 2000.

- [52] U. Landman and W. D. Luedtke, "Small is different: energetic, structural, thermal, and mechanical properties of passivated nanocluster assemblies," *Faraday Discussions*, vol. 125, pp. 1–22, 2004.
- [53] R. S. Ingram, M. J. Hostetler, and R. W. Murray, "Poly-hetero-omega-functionalized alkanethiolate-stabilized gold cluster compounds," *Journal of the American Chemical Society*, vol. 119, no. 39, pp. 9175–9178, 1997.
- [54] R. K. Smith, S. M. Reed, P. A. Lewis, J. D. Monnell, R. S. Clegg, K. F. Kelly, L. A. Bumm, J. E. Hutchison, and P. S. Weiss, "Phase separation within a binary self-assembled monolayer on Au{111} driven by an amide-containing alkanethiol," *Journal of Physical Chemistry B*, vol. 105, no. 6, pp. 1119–1122, 2001.
- [55] I. Szleifer and M. A. Carignano, "Tethered polymer layers: phase transitions and reduction of protein adsorption," *Macromolecular Rapid Communications*, vol. 21, no. 8, pp. 423–448, 2000.
- [56] S. T. Milner, "Polymer brushes," *Science*, vol. 251, no. 4996, pp. 905–914, 1991.
- [57] S. Minko, M. Muller, D. Usov, A. Scholl, C. Froeck, and M. Stamm, "Lateral versus perpendicular segregation in mixed polymer brushes," *Physical Review Letters*, vol. 88, no. 3, 2002.
- [58] S. T. Milner, T. A. Witten, and M. E. Cates, "Theory of the grafted polymer brush," *Macromolecules*, vol. 21, no. 8, pp. 2610–2619, 1988.
- [59] J. F. Marko and T. A. Witten, "Phase-separation in a grafted polymer layer," *Physical Review Letters*, vol. 66, no. 11, pp. 1541–1544, 1991.
- [60] J. F. Marko and T. A. Witten, "Correlations in grafted polymer layers," *Macromolecules*, vol. 25, no. 1, pp. 296–307, 1992.
- [61] A. V. Shevade, J. Zhou, M. T. Zin, and S. Y. Jiang, "Phase behavior of mixed self-assembled monolayers of alkanethiols on Au(111): A configurational-bias Monte Carlo simulation study," *Langmuir*, vol. 17, no. 24, pp. 7566–7572, 2001.
- [62] J. I. Siepmann and I. R. McDonald, "Monte-Carlo simulations of mixed monolayers," *Molecular Physics*, vol. 75, no. 2, pp. 255–259, 1992.
- [63] K. Aoki, "Theory of phase separation of binary self-assembled films," *Journal of Electroanalytical Chemistry*, vol. 513, no. 1, pp. 1–7, 2001.

- [64] W. Mizutani, T. Ishida, and H. Tokumoto, “Monte Carlo simulation of phase-separated self-assembled films,” *Applied Surface Science*, vol. 130, pp. 792–796, 1998.
- [65] P. Espanol, “Hydrodynamics from dissipative particle dynamics,” *Physical Review E*, vol. 52, no. 2, pp. 1734–1742, 1995.
- [66] P. Espanol and P. Warren, “Statistical-mechanics of dissipative particle dynamics,” *Europhysics Letters*, vol. 30, no. 4, pp. 191–196, 1995.
- [67] P. Espanol, “Dissipative particle dynamics revisited,” *ESF Simu Programme Newsletter*, vol. 4, pp. 59–77, 2002.
- [68] R. D. Groot and P. B. Warren, “Dissipative particle dynamics: Bridging the gap between atomistic and mesoscopic simulation,” *Journal of Chemical Physics*, vol. 107, no. 11, pp. 4423–4435, 1997.
- [69] R. D. Groot, “Applications of dissipative particle dynamics,” in *Novel Methods in Soft Matter Simulations*, vol. 640 of *Lecture Notes in Physics*, pp. 5–38, Springer Berlin / Heidelberg, 2004.
- [70] R. D. Groot and T. J. Madden, “Dynamic simulation of diblock copolymer microphase separation,” *Journal of Chemical Physics*, vol. 108, no. 20, pp. 8713–8724, 1998.
- [71] R. D. Groot, T. J. Madden, and D. J. Tildesley, “On the role of hydrodynamic interactions in block copolymer microphase separation,” *Journal of Chemical Physics*, vol. 110, no. 19, pp. 9739–9749, 1999.
- [72] P. J. Hoogerbrugge and J. M. V. A. Koelman, “Simulating microscopic hydrodynamic phenomena with dissipative particle dynamics,” *Europhysics Letters*, vol. 19, no. 3, pp. 155–160, 1992.
- [73] J. M. V. A. Koelman and P. J. Hoogerbrugge, “Dynamic simulations of hard-sphere suspensions under steady shear,” *Europhysics Letters*, vol. 21, no. 3, pp. 363–368, 1993.
- [74] N. Chennamsetty, H. Bock, and K. E. Gubbins, “Coarse-grained potentials from Widom’s particle insertion method,” *Molecular Physics*, vol. 103, no. 21-23, pp. 3185–3193, 2005.

- [75] J. R. Silbermann, S. H. L. Klapp, M. Schoen, N. Chennamsetty, H. Bock, and K. E. Gubbins, "Mesoscale modeling of complex binary fluid mixtures: Towards an atomistic foundation of effective potentials," *Journal of Chemical Physics*, vol. 124, no. 7, 2006.
- [76] D. Frenkel and M. Smit, *Understanding Molecular Simulation*. Academic Press, New York, 2002.
- [77] M. P. Allen and D. J. Tildesley, *Computer Simulations of Liquids*. Oxford University Press, 1991.
- [78] P. Tang, F. Qiu, H. D. Zhang, and Y. L. Yang, "Phase separation patterns for diblock copolymers on spherical surfaces: A finite volume method," *Physical Review E*, vol. 72, no. 1, 2005.
- [79] M. A. Horsch, Z. L. Zhang, C. R. Iacovella, and S. C. Glotzer, "Hydrodynamics and microphase ordering in block copolymers: Are hydrodynamics required for ordered phases with periodicity in more than one dimension?," *Journal of Chemical Physics*, vol. 121, no. 22, pp. 11455–11462, 2004.
- [80] S. Jury, P. Bladon, M. Cates, S. Krishna, M. Hagen, N. Ruddock, and P. Warren, "Simulation of amphiphilic mesophases using dissipative particle dynamics," *Physical Chemistry Chemical Physics*, vol. 1, no. 9, pp. 2051–2056, 1999.
- [81] P. Prinsen, P. B. Warren, and M. A. J. Michels, "Mesoscale simulations of surfactant dissolution and mesophase formation," *Physical Review Letters*, vol. 89, no. 14, 2002.
- [82] S. Yamamoto, Y. Maruyama, and S. Hyodo, "Dissipative particle dynamics study of spontaneous vesicle formation of amphiphilic molecules," *Journal of Chemical Physics*, vol. 116, no. 13, pp. 5842–5849, 2002.
- [83] C. M. Wijmans, B. Smit, and R. D. Groot, "Phase behavior of monomeric mixtures and polymer solutions with soft interaction potentials," *Journal of Chemical Physics*, vol. 114, no. 17, pp. 7644–7654, 2001.
- [84] A. G. Schlijper, P. J. Hoogerbrugge, and C. W. Manke, "Computer-simulation of dilute polymer-solutions with the dissipative particle dynamics method," *Journal of Rheology*, vol. 39, no. 3, pp. 567–579, 1995.
- [85] N. A. Spenley, "Scaling laws for polymers in dissipative particle dynamics," *Europhysics Letters*, vol. 49, no. 4, pp. 534–540, 2000.

- [86] W. Tschop, K. Kremer, J. Batoulis, T. Burger, and O. Hahn, "Simulation of polymer melts. I. Coarse-graining procedure for polycarbonates," *Acta Polymerica*, vol. 49, no. 2-3, pp. 61–74, 1998.
- [87] S. Pal and C. Seidel, "Dissipative particle dynamics simulations of polymer brushes: Comparison with molecular dynamics simulations," *Macromolecular Theory and Simulations*, vol. 15, no. 9, pp. 668–673, 2006.
- [88] E. S. Boek, P. V. Coveney, H. N. W. Lekkerkerker, and P. vanderSchoot, "Simulating the rheology of dense colloidal suspensions using dissipative particle dynamics," *Physical Review E*, vol. 55, no. 3, pp. 3124–3133, 1997.
- [89] E. S. Boek and P. van der Schoot, "Resolution effects in dissipative particle dynamics simulations," *International Journal of Modern Physics C*, vol. 9, no. 8, pp. 1307–1318, 1998.
- [90] E. S. Boek, P. V. Coveney, and H. N. W. Lekkerkerker, "Computer simulation of rheological phenomena in dense colloidal suspensions with dissipative particle dynamics," *Journal of Physics-Condensed Matter*, vol. 8, no. 47, pp. 9509–9512, 1996.
- [91] J. B. Gibson, K. Chen, and S. Chynoweth, "Simulation of particle adsorption onto a polymer-coated surface using the dissipative particle dynamics method," *Journal of Colloid and Interface Science*, vol. 206, no. 2, pp. 464–474, 1998.
- [92] J. B. Gibson, K. Zhang, K. Chen, S. Chynoweth, and C. W. Manke, "Simulation of colloid-polymer systems using dissipative particle dynamics," *Molecular Simulation*, vol. 23, no. 1, pp. 1–41, 1999.
- [93] S. C. C. Juan, C. Y. Hua, C. L. Chen, X. Q. Sun, and H. T. Xi, "Dissipative particle dynamics simulation of a gold nanoparticle system," *Molecular Simulation*, vol. 31, no. 4, pp. 277–282, 2005.
- [94] P. Malfreyt and D. J. Tildesley, "Dissipative particle dynamics simulations of grafted polymer chains between two walls," *Langmuir*, vol. 16, no. 10, pp. 4732–4740, 2000.
- [95] J. H. Huang, Y. M. Wang, and M. Laradji, "Flow control by smart nanofluidic channels: A dissipative particle dynamics simulation," *Macromolecules*, vol. 39, no. 16, pp. 5546–5554, 2006.
- [96] J. L. Jones, M. Lal, J. N. Ruddock, and N. A. Spenley, "Dynamics of a drop at a liquid/solid interface in simple shear fields: A mesoscopic simulation study," *Faraday Discussions*, vol. 112, no. 112, pp. 129–142, 1999.

- [97] J. A. Elliott and A. H. Windle, “A dissipative particle dynamics method for modeling the geometrical packing of filler particles in polymer composites,” *Journal of Chemical Physics*, vol. 113, no. 22, pp. 10367–10376, 2000.
- [98] I. Vattulainen, M. Karttunen, G. Besold, and J. M. Polson, “Integration schemes for dissipative particle dynamics simulations: From softly interacting systems towards hybrid models,” *Journal of Chemical Physics*, vol. 116, no. 10, pp. 3967–3979, 2002.
- [99] N. S. Martys and R. D. Mountain, “Velocity verlet algorithm for dissipative-particle-dynamics-based models of suspensions,” *Physical Review E*, vol. 59, no. 3, pp. 3733–3736, 1999.
- [100] W. K. den Otter and J. H. R. Clarke, “A new algorithm for dissipative particle dynamics,” *Europhysics Letters*, vol. 53, no. 4, pp. 426–431, 2001.
- [101] C. Singh, P. K. Ghorai, M. A. Horsch, A. M. Jackson, R. G. Larson, F. Stellacci, and S. C. Glotzer, “Entropy-mediated patterning of surfactant-coated nanoparticles and surfaces,” *Physical Review Letters*, vol. 99, no. 22, p. 226106, 2007.
- [102] W. Lu and Z. Suo, “Symmetry breaking in self-assembled monolayers on solid surfaces: Anisotropic surface stress,” *Physical Review B*, vol. 65, no. 8, 2002.
- [103] J. Tabony and D. Job, “Gravitational symmetry-breaking in microtubular dissipative structures,” *Proceedings of the National Academy of Sciences of the United States of America*, vol. 89, no. 15, pp. 6948–6952, 1992.
- [104] S. C. Glotzer and A. Coniglio, “Self-consistent solution of phase-separation with competing interactions,” *Physical Review E*, vol. 50, no. 5, pp. 4241–4244, 1994.
- [105] S. C. Glotzer, E. A. Dimarzio, and M. Muthukumar, “Reaction-controlled morphology of phase-separating mixtures,” *Physical Review Letters*, vol. 74, no. 11, pp. 2034–2037, 1995.
- [106] S. C. Glotzer, D. Stauffer, and N. Jan, “Monte-Carlo simulations of phase-separation in chemically reactive binary-mixtures,” *Physical Review Letters*, vol. 75, no. 8, pp. 1675–1675, 1995.
- [107] M. Seul and D. Andelman, “Domain shapes and patterns - the phenomenology of modulated phases,” *Science*, vol. 267, no. 5197, pp. 476–483, 1995.

- [108] D. Andelman, F. Brochard, and J. F. Joanny, "Modulated structures and competing interactions in amphiphilic monolayers," *Proceedings of the National Academy of Sciences of the United States of America*, vol. 84, no. 14, pp. 4717–4718, 1987.
- [109] S. M. Loverde, Y. S. Velichko, and M. O. de la Cruz, "Competing interactions in two dimensional coulomb systems: Surface charge heterogeneities in coassembled cationic-anionic incompatible mixtures," *Journal of Chemical Physics*, vol. 124, no. 14, p. 144702, 2006.
- [110] C. B. Muratov, "Instabilities and disorder of the domain patterns in systems with competing interactions," *Physical Review Letters*, vol. 78, pp. 3149–3152, 1997.
- [111] M. Kim, J. N. Hohman, E. I. Morin, T. A. Daniel, and P. S. Weiss, "Self-assembled monolayers of 2-Adamantanethiol on Au{111}: Control of structure and displacement," *Journal of Physical Chemistry A*, vol. 113, no. 16, pp. 3895–3903, 2009.
- [112] A. A. Dameron, L. F. Charles, and P. S. Weiss, "Structures and displacement of 1-Adamantanethiol self-assembled monolayers on Au{111}," *Journal of the American Chemical Society*, vol. 127, pp. 8697–8704, 2005.
- [113] J. N. Hohman, P. P. Zhang, E. I. Morin, P. Han, M. Kim, A. R. Kurland, P. D. McClanahan, V. P. Balema, and P. S. Weiss, "Self-assembly of carboranethiol isomers on Au{111}: Intermolecular interactions determined by molecular dipole orientations," *ACS Nano*, vol. 3, no. 3, pp. 527–536, 2009.
- [114] W. Smith and T. R. Forester, "DL_POLY_2.0: A general-purpose parallel molecular dynamics simulation package," *Journal of Molecular Graphics*, vol. 14, no. 3, pp. 136–141, 1996.
- [115] W. L. Jorgensen, J. D. Madura, and C. J. Swenson, "Optimized intermolecular potential functions for liquid hydrocarbons," *Journal of the American Chemical Society*, vol. 106, no. 22, pp. 6638–6646, 1984.
- [116] W. L. Jorgensen, D. S. Maxwell, and J. TiradoRives, "Development and testing of the OPLS all-atom force field on conformational energetics and properties of organic liquids," *Journal of the American Chemical Society*, vol. 118, no. 45, pp. 11225–11236, 1996.
- [117] S. J. Weiner, P. A. Kollman, D. A. Case, U. C. Singh, C. Ghio, G. Alagona, S. Profeta, and P. Weiner, "A new force-field for molecular mechanical simulation of nucleic-

- acids and proteins,” *Journal of the American Chemical Society*, vol. 106, no. 3, pp. 765–784, 1984.
- [118] J. P. Ryckaert, G. Ciccotti, and H. J. C. Berendsen, “Numerical-integration of cartesian equations of motion of a system with constraints - molecular-dynamics of n-alkanes,” *Journal of Computational Physics*, vol. 23, no. 3, pp. 327–341, 1977.
- [119] C. Castellano and S. C. Glotzer, “On the mechanism of pinning in phase-separating polymer blends,” *Journal of Chemical Physics*, vol. 103, no. 21, pp. 9363–9369, 1995.
- [120] A. Santos, C. Singh, and S. C. Glotzer, “Coarse-grained models of tethers for fast self-assembly simulations,” *Physical Review E*, vol. 1, no. 81, pp. 011113–1–011113–11, 2010.
- [121] C. Singh et al., “Ordered nanoscale stripes and micelles in mixed self-assembled monolayers,” *in preparation*, 2010.
- [122] H. J. Risselada and S. J. Marrink, “The molecular face of lipid rafts in model membranes,” *Proceedings of the National Academy of Sciences of the United States of America*, vol. 105, no. 45, pp. 17367–17372, 2008.
- [123] C. T. Black, K. W. Guarini, K. R. Milkove, S. M. Baker, T. P. Russell, and M. T. Tuominen, “Integration of self-assembled diblock copolymers for semiconductor capacitor fabrication,” *Applied Physics Letters*, vol. 79, no. 3, pp. 409–411, 2001.
- [124] V. Z. H. Chan, J. Hoffman, V. Y. Lee, H. Iatrou, A. Avgeropoulos, N. Hadjichristidis, R. D. Miller, and E. L. Thomas, “Ordered bicontinuous nanoporous and nanorelief ceramic films from self assembling polymer precursors,” *Science*, vol. 286, no. 5445, pp. 1716–1719, 1999.
- [125] J. Y. Cheng, C. A. Ross, V. Z. H. Chan, E. L. Thomas, R. G. H. Lammertink, and G. J. Vancso, “Formation of a cobalt magnetic dot array via block copolymer lithography,” *Advanced Materials*, vol. 13, no. 15, p. 1174, 2001.
- [126] S. Y. Chou, M. S. Wei, P. R. Krauss, and P. B. Fischer, “Single-domain magnetic pillar array of 35-nm diameter and 65-gbits/in² density for ultrahigh density quantum magnetic storage,” *Journal of Applied Physics*, vol. 76, no. 10, pp. 6673–6675, 1994.
- [127] R. R. Li, P. D. Dapkus, M. E. Thompson, W. G. Jeong, C. Harrison, P. M. Chaikin, R. A. Register, and D. H. Adamson, “Dense arrays of ordered GaAs nanostructures

- by selective area growth on substrates patterned by block copolymer lithography,” *Applied Physics Letters*, vol. 76, no. 13, pp. 1689–1691, 2000.
- [128] W. D. Volkmuth and R. H. Austin, “DNA electrophoresis in microlithographic arrays,” *Nature*, vol. 358, no. 6387, pp. 600–602, 1992.
- [129] W. D. Volkmuth, T. Duke, M. C. Wu, R. H. Austin, and A. Szabo, “DNA electrophoresis in a 2D array of posts,” *Physical Review Letters*, vol. 72, no. 13, pp. 2117–2120, 1994.
- [130] D. Weiss, M. L. Roukes, A. Menschig, P. Grambow, K. Vonklitzing, and G. Weimann, “Electron pinball and commensurate orbits in a periodic array of scatterers,” *Physical Review Letters*, vol. 66, no. 21, pp. 2790–2793, 1991.
- [131] S. O. Kim, H. H. Solak, M. P. Stoykovich, N. J. Ferrier, J. J. de Pablo, and P. F. Nealey, “Epitaxial self-assembly of block copolymers on lithographically defined nanopatterned substrates,” *Nature*, vol. 424, no. 6947, pp. 411–414, 2003.
- [132] C. Park, J. Yoon, and E. L. Thomas, “Enabling nanotechnology with self assembled block copolymer patterns,” *Polymer*, vol. 44, no. 22, pp. 6725–6760, 2003.
- [133] M. Park, C. Harrison, P. M. Chaikin, R. A. Register, and D. H. Adamson, “Block copolymer lithography: Periodic arrays of similar to 10(11) holes in 1 square centimeter,” *Science*, vol. 276, no. 5317, pp. 1401–1404, 1997.
- [134] J. W. Cahn, “On spinodal decomposition,” *Acta Metallurgica*, vol. 9, no. 9, pp. 795–801, 1961.
- [135] J. W. Cahn and J. E. Hilliard, “Spinodal decomposition - reprise,” *Acta Metallurgica*, vol. 19, no. 2, pp. 151–161, 1971.
- [136] D. K. Schwartz, “Mechanisms and kinetics of self-assembled monolayer formation,” *Annual Review of Physical Chemistry*, vol. 52, pp. 107–137, 2001.
- [137] C. Dubois and F. Stellacci, “Self-assembled monolayer of short carboxyl-terminated molecules investigated with ex situ scanning tunneling microscopy,” *Journal of Physical Chemistry C*, vol. 112, no. 19, pp. 7431–7435, 2008.
- [138] T. Geisinger, M. Muller, and K. Binder, “Symmetric diblock copolymers in thin films. I. Phase stability in self-consistent field calculations and Monte Carlo simulations,” *Journal of Chemical Physics*, vol. 111, no. 11, pp. 5241–5250, 1999.

- [139] H. P. Huinink, J. C. M. Brokken-Zijp, M. A. van Dijk, and G. J. A. Sevink, "Asymmetric block copolymers confined in a thin film," *Journal of Chemical Physics*, vol. 112, no. 5, pp. 2452–2462, 2000.
- [140] S. M. Loverde, F. J. Solis, and M. O. de la Cruz, "Charged particles on surfaces: Coexistence of dilute phases and periodic structures at interfaces," *Physical Review Letters*, vol. 98, no. 23, 2007.
- [141] S. M. Loverde and M. O. de la Cruz, "Asymmetric charge patterning on surfaces and interfaces: Formation of hexagonal domains," *Journal of Chemical Physics*, vol. 127, 2007.
- [142] C. Singh, A. M. Jackson, F. Stellacci, and S. C. Glotzer, "Exploiting substrate stress to modify nanoscale sam patterns.," *Journal of the American Chemical Society*, vol. 131, no. 45, pp. 16377–9, 2009.
- [143] C. Singh, Y. Hu, B. P. Khanal, E. Zubarev, F. Stellacci, and S. C. Glotzer, "Self-assembly of SAMs into striped patterns on nanowires and nanorods," *in preparation*, 2010.
- [144] M. Gsell, P. Jakob, and D. Menzel, "Effect of substrate strain on adsorption," *Science*, vol. 280, no. 5364, pp. 717–720, 1998.
- [145] R. V. Kukta, D. Kouris, and K. Sieradzki, "Adatoms and their relation to surface stress," *Journal of the Mechanics and Physics of Solids*, vol. 51, no. 7, pp. 1243–1266, 2003.
- [146] F. J. Solis, S. I. Stupp, and M. O. de la Cruz, "Charge induced pattern formation on surfaces: Segregation in cylindrical micelles of cationic-anionic peptide-amphiphiles," *Journal of Chemical Physics*, vol. 122, no. 5, 2005.
- [147] W. Lu and D. Kim, "Engineering nanophase self-assembly with elastic field," *Acta Metallurgica*, vol. 53, no. 13, pp. 3689–3694, 2005.
- [148] L. H. He and L. G. Huang, "Pattern formation on a stretchable substrate," *International Journal of Solids and Structures*, vol. 45, no. 22-23, pp. 5879–5889, 2008.
- [149] F. Dmitrii and F. Rosei, "Metal nanoparticles: From artificial atoms to artificial molecules," *Angewandte Chemie-International Edition*, vol. 46, no. 32, pp. 6006–6008, 2007.

- [150] Y. Hu, B. H. Wunsch, S. Sahni, and F. Stellacci, “Statistical analysis of scanning tunneling microscopy images of striped mixed monolayer protected gold nanoparticles,” *Journal of Scanning Probe Microscopy*, vol. 4, no. 1, pp. 24–35, 2009.
- [151] M. M. D. Lim, Y. S. Velichko, M. O. De la Cruz, and G. Vernizzi, “Low-radii transitions in co-assembled cationic - anionic cylindrical aggregates,” *Journal of Physical Chemistry B*, vol. 112, no. 17, pp. 5423–5427, 2008.
- [152] Y. S. Velichko and M. O. de la Cruz, “Pattern formation on the surface of cationic-anionic cylindrical aggregates,” *Physical Review E*, vol. 72, no. 4, 2005.
- [153] G. Vernizzi, K. L. Kohlstedt, and M. O. de la Cruz, “The electrostatic origin of chiral patterns on nanofibers,” *Soft Matter*, vol. 5, no. 4, pp. 736–739, 2009.
- [154] K. L. Kohlstedt, F. J. Solis, G. Vernizzi, and M. O. de la Cruz, “Spontaneous chirality via long-range electrostatic forces,” *Physical Review Letters*, vol. 99, no. 3, 2007.
- [155] K. L. Kohlstedt, G. Vernizzi, and M. O. de la Cruz, “Surface patterning of low-dimensional systems: the chirality of charged fibres,” *Journal of Physics-Condensed Matter*, vol. 21, no. 42, 2009.
- [156] K. L. Kohlstedt, G. Vernizzi, and M. O. de la Cruz, “Electrostatics and optimal arrangement of ionic triangular lattices confined to cylindrical fibers,” *Physical Review E*, vol. 80, no. 5, 2009.
- [157] H. Jiang, C. Singh, J. J. Kuna, K. Voitchovsky, F. Stellacci, and S. C. Glotzer *in preparation*, 2010.
- [158] A. B. D. Cassie and S. Baxter, “Wettability of porous surfaces,” *Transactions of the Faraday Society*, vol. 40, 1944.
- [159] P. E. Laibinis, M. A. Fox, J. P. Folkers, and G. M. Whitesides, “Comparisons of self-assembled monolayers on silver and gold - mixed monolayers derived from $HS(CH_2)_{21}X$ and $HS(CH_2)_{10}Y$ ($X, Y = -CH_3, -CH_2OH$) have similar properties.,” *Langmuir*, vol. 7, 1991.
- [160] S. Imabayashi, N. Gon, T. Sasaki, D. Hobara, and T. Kakiuchi, “Effect of nanometre-scale phase separation on wetting of binary self-assembled thiol monolayers on Au(111).,” *Langmuir*, vol. 10, 2008.
- [161] H. Bohlen, A. O. Parry, E. Diaz-Herrera, and M. Schoen, “Intrusion of fluids into nanogrooves.,” *European Physical Journal E*, vol. 25, 2008.

- [162] M. Schoen, "Fluid bridges confined between chemically nanopatterned solid substrates," *Physical Chemistry Chemical Physics*, vol. 10, 2008.
- [163] D. Wolf, P. Keblinski, S. R. Phillpot, and J. Eggebrecht, "Exact method for the simulation of coulombic systems by spherically truncated, pairwise r^{-1} summation," *Journal of Chemical Physics*, vol. 110, no. 17, pp. 8254–8282, 1999.
- [164] D. Chandler, "Interfaces and the driving force of hydrophobic assembly," *Nature*, vol. 437, pp. 640–647, 2005.
- [165] M. Kim, J. N. Hohman, E. I. Morin, T. A. Daniel, and P. S. Weiss, "Self-assembled monolayers of 2-Adamantanethiol on Au{111}: Control of structure and displacement," *Journal of Physical Chemistry A*, vol. 113, no. 16, pp. 3895–3903, 2009.
- [166] A. A. Dameron, L. F. Charles, and P. S. Weiss, "Structures and displacement of 1-Adamantanethiol self-assembled monolayers on Au{111}," *Journal of the American Chemical Society*, vol. 127, pp. 8697–8704, 2005.
- [167] J. N. Hohman, P. P. Zhang, E. I. Morin, P. Han, M. Kim, A. R. Kurland, P. D. McClanahan, V. P. Balema, and P. S. Weiss, "Self-assembly of carboranethiol isomers on Au{111}: Intermolecular interactions determined by molecular dipole orientations," *ACS Nano*, vol. 3, no. 3, pp. 527–536, 2009.
- [168] A. De Wit, P. De Kepper, K. Benyaich, G. Dewel, and P. Borckmans, "Hydrodynamical instability of spatially extended bistable chemical systems," *Chemical Engineering Science*, vol. 58, no. 21, pp. 4823–4831, 2003.
- [169] P. G. Saffman, "Viscous fingering in Hele-Shaw cells," *Journal of Fluid Mechanics*, vol. 173, pp. 73–94, 1986.
- [170] D. H. Sharp, "An overview of Rayleigh-Taylor instability," *Physica D*, vol. 12, no. 1-3, pp. 3–18, 1984.
- [171] M. Brouillette, "The Richtmyer-Meshkov instability," *Annual Review of Fluid Mechanics*, vol. 34, pp. 445–468, 2002.